Draft Manuscript for Review

Transition from plume-driven to plate-driven magmatism in the evolution of Main Ethiopian Rift

Journal:	*Journal of Petrology*
Manuscript ID	JPET-Sep-18-0118.R2
Manuscript Type:	Original Manuscript
Date Submitted by the Author:	28-Jun-2019
Complete List of Authors:	Feyissa, Dejene; Institute for Planetary Materials, Okayama University Kitagawa, Hiroshi; Institute for Planetary Matetials, Okayama University, Bizuneh, Tesfaye; Ethiopian Space Science and Technology Institute Tanaka, Ryoji; Okayama University, Institute for Study of the Earth's Interior Kabeto, Kurkura; Addis Ababa Science and Technology University Nakamura, Eizo; Okayama University, Institute for Study of the Earth's Interior
Keyword:	Ethiopian Plateau, Ethiopian Rift, Afar Depression, mantle source, mantle melting

Transition from plume-driven to plate-driven magmatism in the evolution of the Main Ethiopian Rift

Dejene Hailemariam Feyissa[1], Hiroshi Kitagawa [1*], Tesfaye Demissie Bizuneh[1, 2], Ryoji Tanaka[1], Kurkura Kabeto[1, 3†] and Eizo Nakamura[1]

[1]Pheasant Memorial Laboratory, Institute for Planetary Materials, Okayama University, Yamada 827, Misasa, Tottori 682-0193, Japan

[2]Ethiopian Space Science and Technology Institute, Addis Ababa (5 kilo)

[3]Addis Ababa Science and Technology University, Addis Ababa, Ethiopia, P.O Box 1647

[†]Deceased

*Corresponding author. Email: kitaga-h@okayama-u.ac.jp

ABSTRACT

New K-Ar ages, major and trace element concentrations, and Sr-Nd-Pb isotope data are presented for Oligocene to recent mafic volcanic rocks from the Ethiopian Plateau, the Main Ethiopian Rift (MER), and the Afar depression. Chronological and geochemical data from this study are combined with previously published data sets to reveal secular variations in magmatism throughout the entire Ethiopian volcanic region. The mafic lavas in these regions show variability in terms of silica-saturation (i.e., alkaline and sub-alkaline series) and extent of differentiation (mafic through intermediate to felsic). The *P*-*T* conditions of melting, estimated using the least differentiated basalts, reveal a secular decrease in the mantle potential temperature, from when the flood basalt magmas erupted (up to 1550 ˚C) to the time of the rift-related magmatism (<1500 ˚C). Variations in the Sr-Nd-Pb isotopic compositions of the mafic lavas can account for the involvement of multiple end-member components. The relative contributions of these end-member components vary in space and time owing to changes in the thermal condition of the asthenosphere and the thickness of the lithosphere. The evolution of the Ethiopian rift is caused by a transition from plume-driven to plate-driven mantle upwelling, although the present-day mantle beneath the MER and the Afar depression is still warmer than normal asthenosphere.

KEY WORDS: Ethiopian Plateau, Ethiopian Rift; Afar Depression; mantle source; mantle melting

INTRODUCTION

Understanding of the genesis of basaltic magmas in relation to tectonic setting is fundamental in the petrologic and geochemical disciplines. It is generally accepted that basaltic magmas are derived, to a first order, by melting of asthenospheric mantle that adiabatically upwells to the base of the lithosphere (McKenzie, 1984). Magma productivity is primarily controlled by the temperature of the melting region; thus voluminous emplacement of basalt, as in Large Igneous Provinces (LIPs), is generally attributed to melting of anomalously hot mantle (White & McKenzie, 1989; White *et al*., 2008). Compositional heterogeneity is also considered to be an important factor in enhancing magma productivity and diminishing the need for extremely high temperatures in the mantle (Korenaga, 2004; Kitagawa *et al*., 2008). The LIP basalts in intra-continental plate settings show geochemical evidence for interaction with sub-continental lithosphere, which could result in high magma production through enrichment of volatiles in the melting regions (Arndt & Christensen, 1992; Furman *et al*., 2016).

The Afar province in eastern Africa and adjacent regions is one example of a recent terrestrial LIP (Fig. 1; White & McKenzie, 1989). Magmatism in the region began with Oligocene trap formation at about 30 Ma (Jones & Rex, 1974; Hofmann *et al*., 1997; Rochette *et al*., 1998; Ukstins *et al*., 2002; Coulié *et al*., 2003; Kieffer *et al*., 2004; Prave *et al*., 2016). The ensuing rift-related magmatism has been active over the last *c*. 27–24 Myr in the Main Ethiopian Rift (MER) and Afar (WoldeGabriel *et al*., 1990; Chernet *et al*., 1998; Ukistins *et al*., 2002; Bonini *et al*., 2005; Wolfenden *et al*., 2005; Feyissa *et al*., 2017). Trap-phase magmatism is thought to be the surface manifestation of melting of actively upwelling mantle (i.e., a plume; Hart *et al*., 1989; Marty *et al*., 1996; Pik *et al*., 1998, 1999; Furman *et al*., 2006a; Beccaluva *et al*., 2009; Natali *et al*., 2016). The present-day rift magmatism is also considered to be influenced by the mantle plume (Afar mantle plume), and its thermochemical effect has been intensively discussed in petrologic, geochemical, and geophysical studies. For example, the excess temperature in the mantle has been estimated to be 100–200 ˚C by petrologic models (Ayalew & Gibson, 2009; Rooney *et al*., 2012a; Ferguson *et al*., 2013a; Pinzuti *et al*., 2013; Armitage *et al*., 2015), which are consistent with the estimates based upon seismic tomography and receiver function analysis, if the uncertainty of compositional effects is taken into account (e.g., Nyblade *et al*., 2000; Rychert *et al*., 2012; Hammond *et al*., 2013). Persistent upwelling of a buoyant mantle plume is also suggested by the geochemistry of Oligocene to Recent mafic volcanic rocks, such as the occurrence of high $^3He/^4He$ or high-T magmas throughout this period (Marty *et al*., 1996; Scarsi & Craig, 1996; Pik *et al*., 2006; Furman *et al*., 2006a; Ayalew & Gibson, 2009; Rooney *et al*., 2012a; Rogers *et al*., 2010).

Magmatism related to rifting in Ethiopia is still ongoing, and young volcanic activity (early Pleistocene, <2 Ma) occurs in the axial sectors of the MER and Afar. Numerous studies have addressed the petrogenesis of mafic magmas in these sectors in conjunction with

75 Oligocene trap-phase magmatism (e.g., Hart *et al*., 1989; Deniel *et al*., 1994; Pik *et al*., 1998,
76 1999, 2006; Kieffer *et al*., 2004; Furman *et al*., 2004, 2006a, 2016; Furman, 2007; Rooney *et*
77 *al*., 2007, 2012a, 2012b, 2013, 2014a, 2014b; Ayalew & Gibson, 2009; Beccaluva *et al*.,
78 2009; Shinjo *et al*., 2011; Natali *et al*., 2011, 2016; Nelson *et al*., 2012; Feyissa *et al*., 2017).
79 However, although temporal variation may provide important constraints on the evolution of
80 magmatism in continental rift regions, it remains uncertain how magmatic activity varied
81 with time. In particular, the relationship between the compositions of erupted magmas and
82 thermal conditions of melting regions beneath this volcanic province needs to be evaluated in
83 more detail. Recent advances in thermobarometry, calibrated using numerous data sets from
84 melting experiments, allows us to estimate the thermal condition of the melting region in the
85 mantle (e.g., Putirka *et al*., 2007; Putirka, 2008; Lee *et al*., 2009; Herzberg & Asimow, 2015).
86 Rooney *et al*. (2012a) applied this approach, and demonstrated that the upwelling of hotter-
87 than-normal mantle has been persistent beneath the Afar and MER regions since 30 Ma.
88 However, the temporal variations in the entire Ethiopian and in adjacent volcanic fields were
89 not fully examined, suggesting the need for further evaluation using data sets including
90 recently published studies (e.g., Ayalew *et al*., 2016, 2018; Rooney *et al*., 2014b; Natali *et*
91 *al*., 2016).

92 In this study, we present new K-Ar ages, whole-rock major and trace element

analyses, and Sr-Nd-Pb isotope data for mafic volcanic rocks from the Ethiopian volcanic province. Our samples include Oligocene mafic rocks from the Maychew area in the northwestern (NW) Ethiopian Plateau and Oligocene to Recent mafic rocks from the rift zones in the southern and northern MER and Afar (Fig. 1). The Maychew rocks include a peculiar type of basalt not yet reported in the NW Plateau (Rooney, 2017), that is strongly alkaline (basanite) and occurs in the basal unit of a lava succession. Such a strongly alkaline basalt provides important constraints on melting conditions and source composition during the onset of Oligocene trap magmatism. We apply thermobarometric calculations to the samples of this study and those presented in previous studies, with careful screening to select the least differentiated magma types, and attempt to constrain the thermal conditions in relation to the chemical variability of the magma source.

GEOLOGICAL BACKGROUND

Eocene to Quaternary volcanic fields are distributed in three different geological domains in Ethiopia (Fig. 1; Kazmin, 1979; Berhe *et al.*, 1987; Hart *et al.*, 1989; Ebinger & Sleep, 1998; GSE, 2005): (1) the rift-bounding plateaus (northwestern, southwestern, and southeastern), (2) the rift zones (MER) and (3) the rift junction with an associated geological depression

(Afar). The MER is subdivided into northern, central, and southern sectors, each sector is denoted as Northern MER (NMER), Central MER (CMER), and Southern MER (SMER), respectively (Hayward & Ebinger, 1996; Bonini *et al*., 2005; Corti, 2009). The Afar is also subdivided three sectors, Northern Afar, Eastern Central Afar, and Southern Afar (Hayward & Ebinger, 1996; Stab *et al*., 2015). The geological and geochronological features of each volcanic region are briefly described below.

Rift-bounding plateaus (45 Ma to 10 Ma)

Magmatism related to the formation of basalt plateaus occurred during the period from 45–10 Ma (Rooney, 2017). In the initial phase, the volcanism occurred at 45–34 Ma in southern Ethiopia and northern Kenya (Davidson & Rex, 1980; Ebinger *et al*., 1993; George *et al*., 1998). This volcanism was characterized by bimodal eruptions of basalt and rhyolite producing intercalated piles of lavas in the Yabello and Amaro areas located in the southeast of the southwestern (SW) plateau (Figs 1 and Supplementary Data S1; Amaro-Gamo sequence following Ebinger *et al*., 1993). The lowest unit of the Amaro-Gamo sequence is composed mainly of subalkaline basalts (Amaro basalts; Fig. 2b) with ages of 45–40 Ma (Ebinger *et al*., 1993, George *et al*., 1998; Yemane *et al*., 1999). The upper unit of the Amaro-Gamo sequence consists of alkaline basalts (Fig. 2b), termed Gamo basalts, which conformably overlie the Amaro basalts and have been dated at 40–34 Ma (Ebinger *et al.*, 1993; George *et al.*, 1998; Yemane *et al.*, 1999). The Eocene-Oligocene rhyolitic tuff, termed the Amaro tuff (37.0–35.5 Ma; Ebinger *et al.*, 1993; George *et al.*, 1998), is distributed widely in the Amaro-Kele and Gedeb areas (Supplementary Data Fig. S1) and composed of welded ignimbrites, commonly interbedded or overlain by pyroclastic breccias and ash-fall tephra. The second period of flood-basaltic eruptions occurred at 15–7 Ma, and produced lava piles of 200–400 m thickness overlying the Amaro-Gamo sequence in the SW plateau. These mafic rocks are termed Wollega basalts in reference to their type locality (Fig. 1) and consist of subalkaline and alkaline mafic rocks (Ayalew *et al.*, 1999; Conticelli *et al.*, 1999; Bonini *et al.*, 2005).

In the early Oligocene (*c*. 31–25 Ma), intense eruptions of basalt (i.e., flood basalt volcanism) occurred in northwest and southeast Ethiopia and western Yemen (Fig. 1; Baker *et al.*, 1996a, b; Hofmann *et al.*, 1997; Rochette *et al.*, 1998; Ukstins *et al.*, 2002; Coulié *et al.*, 2003; Kieffer *et al.*, 2004; Wolfenden *et al.*, 2005; Prave *et al.*, 2016; Rooney *et al.*, 2018), referred to as the "Oligocene Traps phase" (Rooney, 2017). In Ethiopia, the lava piles produced during this phase have thicknesses of 500–3000 m and cover an area of 600,000 km^2 (Mohr & Zanettin, 1988; Rooney, 2017). Voluminous magma production in this region is generally attributed to melting of anomalously hot mantle delivered by the Afar plume (e.g., Ebinger & Sleep, 1998; Pik *et al*., 2006; Beccaluva *et al*., 2009; Natali *et al*., 2016). Several studies have also pointed out the role of volatiles in the magma source region. These components could have enhanced magma production, and been derived either by deep devolatilization in the plume stem (e.g., Beccaluva *et al*., 2009) or by delamination of sub-continental lithosphere into the plume (e.g., Furman *et al*., 2016). The majority of Oligocene plateau basalts in Ethiopia are classified as transitional or tholeiitic series (Fig. 2), and are associated with felsic volcanic and pyroclastic rocks (30–22 Ma) in the upper part of the lava successions (Ayalew *et al*., 2002; Ukstins *et al*., 2002; Coulié *et al*., 2003; Kieffer *et al*., 2004; Prave *et al*., 2016; Rooney *et al*., 2018). The type locality of Oligocene flood basalts is the NW Ethiopian plateau, divided from the SW plateau by the Yerer-Tullu Wellel volcano-tectonic lineament (YTVL in Fig. 1; Abebe *et al*., 1998). Previous studies provide details about its stratigraphy in some regions (e.g., Adigrat, Lalibela; Hofmann *et al*., 1997; Kieffer *et al*., 2004; Fig. 1). Based on spatiotemporal relationships of the distribution and composition, Pik *et al*. (1998) sub-divided the Oligocene Trap phase basalts into: (1) low-Ti basalts (LT, with Ti/Y = 288–437 and Nb/Y = 0.1–0.41); (2) high-Ti1 basalts (HT1, with Ti/Y = 352–814 or Nb/Y = 0.52–1.1); and (3) high-Ti2 basalts (HT2, with Ti/Y = 670–885 and Nb/Y = 0.9–1.44). The LT basalts mainly occur in the western periphery of the NW Ethiopian and northern Yemen plateaus, whereas the HT1 and HT2 basalts are distributed in the eastern part of the NW plateau (e.g., Lalibela and Maychew) and the southern Yemen plateau (Fig 1; Baker *et al*., 1996a, b; Pik *et al*., 1998; Beccaluva *et al*., 2009). The samples from Maychew described here include the HT1 and HT2 varieties (Supplementary Data Text S1, Table S2 and Figs S2 and S3).

Following the emplacement of the flood basalts, a number of shield volcanoes were formed during Oligocene to Miocene times, locally creating an additional 1000 to 2000 m of relief (Berhe *et al*., 1987). The shield volcanoes show a range of eruption ages, 30–19 Ma for the northernmost Simien volcano (Coulié *et al*., 2003; Kieffer *et al*., 2004), 23–22 Ma for the Choke and Guguftu volcanoes and 11 Ma for the Guna volcano on the central NW Ethiopian plateau (Kieffer *et al*., 2004), and 25–24 Ma for the Gerba Guracha volcano in the southern part of the NW plateau (Rooney *et al*., 2014a, 2017a). Miocene volcanoes also occur on the plateau margins (i.e., rift shoulders), e.g., the 16–10 Ma old volcanic rocks in the Tarmaber-Megezez Formation at the southeastern margin of the NW plateau (e.g., Zanettin & Justin-Visentin, 1974; Zanettin *et al*., 1978; Chernet *et al*., 1998; Wolfenden *et al*., 2004).

Main Ethiopian rift (30 Ma to present)

The Getra-Kele basalts in the SMER are syn-rift alkaline rocks, distributed in the northwestern and southwestern parts of the Amaro-Yabello areas and unconformably overlying the Amaro-Gamo sequence (Supplementary Data Fig. S1). These basalts have been dated at 20–11 Ma by the K-Ar method (this study; Ebinger *et al*., 1993, 2000; George *et al*., 1998; Shinjo *et al*., 2011) and 19.8–11.9 Ma by the $^{40}Ar/^{39}Ar$ method (Yemane *et al*., 1999; Rooney, 2010). The Quaternary volcanic rocks, termed the Nech Sar basalts and Bobem trachybasalts (Ebinger *et al*., 1993) or Tosa-Sucha volcanics (George, 1999), overlie the Getra-Kele basalts. The ages of Getra-Kele basalts indicate that the volcanism followed a period of marked extension in the SMER from 19–18 Ma (Ebinger *et al*., 2000). The K-Ar ages of the Tosa-Sucha basalts range from 1.94 to 0.29 Ma (Ebinger *et al*., 1993, Shinjo *et al*., 2011; this study), and indicate Quaternary volcanic activity. This mafic volcanism produced basanite flows and accompanied eruptions of widespread ignimbrites from 1.6–0.5 Ma (Ebinger *et al*., 1993; Bonini *et al*., 2005; Corti, 2009; Rooney, 2010; Shinjo *et al*., 2011). The basanites contain mantle xenoliths consisting of anhydrous and hydrous (amphibole- and mica-bearing) spinel lherzolites (Meshesha *et al*., 2011).

Volcanic activity in the CMER and NMER has been active since 16–10 Ma, coincident with the onset of rifting (Supplementary Data Fig. S4; WoldeGabriel *et al*., 1990; Chernet *et al*., 1998; Ukstins *et al*., 2002; Wolfenden *et al*., 2004; Bonini *et al*., 2005). The Miocene volcanism is characterized by voluminous felsic rocks (e.g., 9–6 Ma Nazret Group and 4–3 Ma Butajira ignimbrite) with associated mafic volcanic rocks (e.g., Justin-Visentin *et* *al*., 1974; WoldeGabriel *et al*., 1990; Wolfenden *et al*., 2004). A riftward-younging trend of the ages of volcanic rocks has been well documented in the NMER and CMER (e.g., Morton *et al*., 1979). The rift-margin volcanic rocks yield K-Ar and $^{40}Ar/^{39}Ar$ ages of *c.* 30–10 Ma; they are variably named in reference to their type localities (WoldeGabriel *et al*., 1990; Chernet *et al*., 1998; Ukistins *et al*., 2002; Wolfenden et al., 2004; Bonini *et al*., 2005; GSE, 2005; Feyissa *et al*., 2017; see Supplementary Data Fig. S5). In ascending stratigraphic order, the mafic rock series are termed Alaje (or Alage) and Kella (Oligocene–Miocene), Tarmaber-Megezez (middle Miocene), Anchar or Guraghe (middle–late Miocene), Kessem or Nazret (late Miocene), Mursi, Bofa, and Mathabila (or Metehbila, early Pliocene). The late Miocene to Pliocene mafic volcanic rocks occur in the transition of marginal regions to axial regions in the rift, commonly associated with widespread ignimbrites. In CMER, the late Miocene to Pliocene volcanic activity also occurred in the rift embayment (Bishoftu embayment; Supplementary Data Fig. S4); e.g., Miocene Addis Ababa basalts (Morton *et al*., 1979; Chernet *et al*., 1998) and Miocene Guraghe basalts (Bonini *et al*., 2005).

Pliocene-Quaternary volcanic activity mainly occurred at monogenetic vents located in the fault belts in the MER (Figs 1, S4 and S5), e.g., Wonji Fault Belt (WFB; Mohr, 1967) and Silti-Debre Zeyit Fault Zone (SDFZ; WoldeGabriel *et al*., 1990). Off-axis vents parallel to the rift axis also occur locally, e.g., Akaki magmatic zone and Galema range in the CMER

(Rooney *et al*., 2014b; Chiasera *et al*., 2018). The WFB is a 20 km wide system of bounding faults that developed since 2 Ma and forms a structural link between the MER and Afar (Mohr, 1967; Bonini *et al*., 2005; Kier *et al*., 2015; Mazzarini *et al*., 2016). *En-echelon* segments in the WFB form individual magmatic plumbing systems, e.g., Fantale, Dofan, Boset, and Kone (Supplementary Data Fig. S4, WoldeGabriel *et al*., 1990, 1992a, b; Ebinger & Casey, 2001; Rooney *et al*., 2007, 2011). These volcanic complexes are characterized by the occurrence of mafic to felsic lavas (e.g., Boccaletti *et al*., 1999; Peccerillo *et al*., 2003; Abebe *et al*., 2007; Rooney *et al*., 2012c; Rooney *et al*., 2007, 2011, 2012c, 2014b; Corti, 2009; Giordano *et al*., 2014), resulting from the development of shallow and mature magma reservoirs (Rooney *et al*., 2007). In contrast, the SDFZ lacks the development of intense faulting and has less evolved magmatic plumbing systems (Rooney *et al*., 2007).

Afar depression (5 Ma to present)

The Afar depression is a down-faulted lowland plain bounded by uplifted basement (Danakil Range) in the north, Oligocene flood basalt plateaus in the southeast and west, and the Red Sea in the northeast (Figs. 1, S6 and S7). At its margin, rift-parallel basins are imposed on the Oligocene flood basalt piles (Wolfenden *et al*., 2005; Rooney *et al*., 2013; Corti *et al*., 2015). The Afar depression is divided into three rift systems, the Southern, Central, and Northern

Afar sectors (Hayward & Ebinger, 1996). The Central and Southern Afar are divided by a Quaternary fault zone known as Tendaho-Goba'ad Discontinuity (TGD), whereas the Central and Northern Afar are divided at 12–13 ˚N, corresponding to the landward extension of the Red Sea Rift through the Gulf of Zula. Crustal thickness varies from 16 km in Northern Afar through 25 km in Central Afar to 26 km in Southern Afar (Hayward & Ebinger, 1996). The TGD also marks an abrupt change in the rate and direction of extension. Rifting is faster in the north of the TGD (20 mm/yr) and NNE-SSW directed, whereas rifting is slower (3–8 mm/yr) and NW-SE directed in the south of the TGD, similar to that in the NMER.

The stratigraphy of the Afar depression consists of six units in the ascending order (Bosworth *et al*., 2005) of: (1) Neoproterozoic metamorphic rocks; (2) Mesozoic strata and *Early* Tertiary volcanic rocks; (3) Oligocene trap basalts (Aiba and Alaje basalts); (4) Miocene volcanic rocks; (5) Plio-Pleistocene volcanic rocks; and (6) Quaternary volcanic rocks. The Miocene volcanic units (Mabla rhyolites and Adolei-Dalha basalts) are distributed in the margin of the depression, and are dated to 23–5 Ma (e.g., Barberi *et al*., 1975; Zumbo *et al*., 1995; Audin *et al*., 2004; Stab *et al*., 2015). The Pliocene-Pleistocene mafic volcanic rocks are widely distributed in the Afar depression, and termed the Afar stratoid series (Supplementary Data Fig. S6; Barberi *et al*., 1974; Barberi & Varet, 1975; Varet, 1978; Berhe, 1986). The Quaternary volcanic rocks occur in internal grabens and marginal zones

(Chernet *et al*., 1998; Deniel *et al*., 1994; Pinzuti *et al*., 2013; Stab *et al*., 2015). They consist of basalt lava flows [Gulf basalts (Kidane *et al*., 2003) and axial range basalts, e.g., Erta'Ale and Manda Inakir], scoria cones, and some felsic rocks (Varet, 1978). According to the geological map of Stab *et al*. (2015), our samples consist of mafic rocks corresponding to the Afar stratoid basalts, Gulf basalts, and axial range basalts (Supplementary Data Fig. S6).

GEOPHYSICAL PROPERTIES

Seismic and gravity data provide constraints on the properties of the lithosphere and asthenosphere beneath the volcanic regions in this area. The lithosphere-asthenosphere boundary (LAB) lies at *c*. 60–80 km depth beneath the plateaus, and at *c*. 50 km depth beneath the MER and Afar (Dugda *et al*., 2007; Rychert *et al*., 2012; Hammond *et al*., 2013). The LAB boundary is well-defined beneath the plateau regions, whereas it is obscured beneath the rift axes due to thermal erosion of the base of the lithosphere (Rychert *et al*., 2012; Armitage *et al*., 2015). The crustal thickness beneath the eastern and western Ethiopian plateaus is estimated at 30–45 km, whereas beneath the rift it shows lateral variation, from 35 km in the SMER, through 25–30 km in the CMER, and 25 km in the NMER to 16–26 km beneath the Afar depression (Dugda *et al*., 2005; MacKenzie *et al*., 2005; Maguire *et al*., 2006; Hammond *et al*., 2011; Lavayssière *et al*., 2018).

273 Seismic tomography detects broad low-velocity anomalies in the upper mantle beneath Ethiopia, extending from the base of lithosphere to the mantle Transition Zone (e.g., Hammond *et al*., 2013; Civiero *et al*., 2015). The pronounced low-velocity zone at 75–150 km depth, aligned along the Afar and MER axial zones, is interpreted to reflect the presence of partially molten mantle (Bastow *et al*., 2008), whereas the low-velocity anomaly at greater depth is thought to be due to a weak thermal anomaly (<150 K) and hydrated mantle materials (Thompson *et al*., 2015).

SAMPLES AND ANALYTICAL METHODS

Samples analyzed in this study were collected from several volcanic fields in the Ethiopian volcanic provinces including the MER (NMER and SMER), Afar, and the NW Plateau (Supplementary DatA Figs S1, S2, S4–S7). These fields are the same or close to the fields investigated in previous studies [e.g., Plateau region by Beccaluva *et al*. (2009), Afar by Barrat *et al*. (1998), NMER by Furman *et al*. (2006a), and SMER by George & Rogers (2002)]. We therefore integrate our new data sets with the existing data and provide an update of geochemical information about Ethiopian volcanism. The geodetic coordinates and altitude of sampling locations were obtained using GPS (Global Positioning System), or estimated from maps. Efforts were made to sample the least altered rocks for geochemical and geochronological analyses. The geochronological and other geochemical work was performed at the Pheasant Memorial Laboratory, Institute for Planetary Materials, Okayama University at Misasa, Japan (see Nakamura *et al*., 2003). Details of analytical methods are given in the Supplementary Data Text S2.

RESULTS

K-Ar ages and petrography

K-Ar dating was used to constrain the age of mafic volcanic rocks from the NW Plateau (n = 11), SMER (n = 10), NMER (n = 13), and the Afar Depression (n = 19); the results of these analyses are summarized in Table 2. Samples were selected to represent the spatial, stratigraphic, and chemical diversities in each region (Supplementary Data Figs S1, S2, S4 and S7). Our data are combined with previously published ages to reconstruct the volcanic history of these regions. Careful comparison was also made between our ages and published ones, in particular $^{40}Ar/^{39}Ar$ dates to confirm the reliability of our dates. Below, we summarize the geochronological data, together with petrographic features (Supplementary Data Table S1), of basaltic rocks from the individual volcanic regions.

Rift-bounding plateau basalts from Maychew

Eleven K-Ar ages were determined for mafic rocks from the lava successions in the Maychew area (Figs 1 and S2). We defined six volcanic units, referred to as the sequences 1, 2, 3, 4, 5 and 6 in ascending stratigraphic order (see details in Supplementary Data Text S1). The majority of them yield K-Ar ages of 28 Ma, irrespective of stratigraphic unit (Table 2 and Supplementary Data Fig. S2). The younger ages (25–21 Ma) for some samples are inconsistent with their stratigraphic positions (BK06, TS12, TS35, TS43 and TS45). Although there are no systematic differences in the extents of alteration between samples showing two age populations (28 and 25–21 Ma), including loss on ignition and petrographic texture, the younger ages are considered to be inaccurate as a result of post-eruptive processes. Recent precise and more reliable $^{40}Ar/^{39}Ar$ ages for basalts in the other regions on the NW Ethiopian Plateau suggest that the trap-phase magmatism occurred between 31–25 Ma (e.g., Hofmann *et al*., 1997; Ukstins *et al*., 2002; Coulié *et al*., 2003). We therefore consider that the volcanism in Maychew likely occurred at 28 Ma or older (*c.* 30 Ma).

The HT2 basanites (sequence 1) are aphyric with microphenocrysts of clinopyroxene. The HT2 and HT1 alkaline basalts (sequences 2–6) are porphyritic with clinopyroxene and olivine as major phenocryst phases. Occasionally, they show sub-ophitic to doleritic textures. In the upper stratigraphic units (sequences 4–6), mafic rocks include plagioclase-phyric basalts (HT1 type). The relationship among magma types, petrographic features and stratigraphic positions is similar to that observed in the other regions of the NW Ethiopian Plateau (Pik *et al.*, 1998; Beccaluva *et al.*, 2009; Natali *et al.*, 2016; Krans *et al.*, 2018; Rooney *et al.*, 2018).

Getra-Kele basalts in SMER

Six basaltic samples from Getra-Kele yield ages of 16.4–10.8 Ma (Table 2 and Supplementary Data Fig. S1). With the published K-Ar and $^{40}Ar/^{39}Ar$ ages (WoldeGabriel *et al.*, 1991; Ebinger *et al.*, 1993, 2000; George *et al.*, 1998; Rooney, 2010; Shinjo *et al.*, 2011), the eruptions of Getra-Kele mafic rocks are likely to have occurred from 20–11 Ma, coinciding with the northward propagation of the SMER (Ebinger *et al.*, 1993, 2000; George *et al.*, 1998; Bonini *et al.*, 2005). The Getra-Kele mafic rocks are commonly porphyritic, consisting of euhedral to subhedral phenocrysts of olivine, plagioclase, augite, and opaque minerals (Supplementary Data Table S1). The groundmass shows a pilotaxitic texture consisting of plagioclase, olivine, clinopyroxene, and Fe-Ti-oxides.

Tosa-Sucha basalts in SMER

Four basalts from lavas or volcanic cones in the Arba Minch area yield ages of 1.26–0.56 Ma

(Table 2 and Supplementary Data Fig. S1), consistent with K-Ar dates of 1.34–0.68 Ma by Ebinger *et al*. (1993). Shinjo *et al*. (2011) also obtained comparable K-Ar ages of 1.94–0.29 Ma for mafic volcanic rocks in the south of Yabello. The Quaternary age is consistent with the volcanic morphology and occurrence of these mafic rocks overlying the Amaro and Gamo basalts (Ebinger *et al*., 1993). The Tosa-Sucha mafic rocks are porphyritic with phenocrysts mostly of plagioclase (20–42 vol.%), olivine (2–11 vol.%), and augite (up to 4 vol.%) (Supplementary Data Table S1). Plagioclase crystals are euhedral and 0.5–3 mm in size. Olivine and augite exhibit subhedral, rounded shapes (0.5–1.5 mm). Abundant plagioclase crystals are considered to be xenocrysts, based on their zoning patterns and resorption textures (Rooney, 2010). The groundmass is composed of feldspars, olivine, clinopyroxene, and Fe-Ti oxides.

Syn-rift basalts from NMER

Feyissa *et al*. (2017) referred to the late Oligocene to early Pliocene mafic volcanic rocks from the NMER as Mathabila basalts. These mafic rocks are commonly subdivided into six major formations: Alage, Tarmaber-Megezez, Nazret-Afar, Cholalo-Bishoftu, and the Quaternary Formations (GSE, 2005; Supplementary Data Fig. S5). The oldest rocks are distributed in the western escarpment of the NMER, and dated at 27–25 Ma (DBZ-22 and

DBZ-30; Table 2). Considering their localities (Supplementary Data Fig. S5), these basalts are equivalent to the Alage basalts. The ages obtained in this study is consistent with the existing K-Ar and $^{40}Ar/^{39}Ar$ ages for Alage basalts or intercalated pyroclastic rocks (Chernet *et al*., 1998; Ukstins *et al*., 2002; Supplementary Data Fig. S4). Two samples, DBZ-8 and DH-429, collected in the east of Debre Birhan (Supplementary Data Figs S4 and S5), yield ages of 20–15 Ma. Based on the ages and localities, they are classified as Tarmaber-Megezez basalts (GSE, 2005). Similar ages (19.8–10.0 Ma) were obtained by the $^{40}Ar/^{39}Ar$ method for this formation (basalt and associated ignimbrites: Ukstins *et al*., 2002; Wolfenden *et al*., 2004).

The K-Ar ages of mafic rocks from the rift floors (n = 7) fall within the range 6.5–2.7 Ma, consistent with the eruptive products of the Miocene-Pliocene Nazret Series and the overlying Pliocene Formations, i.e., the Bofa and Bishoftu basalts (Chernet *et al*., 1998). These samples were collected in regions surrounding the Fantale-Dofan magmatic segment (Supplementary Data Figs S4 and S5), and the ages obtained here are consistent with the $^{40}Ar/^{39}Ar$ ages (7–2 Ma) for intercalated ignimbrites (WoldeGabriel *et al*., 1992a; Chernet *et al*., 1998; Wolfenden *et al*., 2004). We refer to these basalts as Nazret series.

Two basalts from Fantale volcano yield ages of 0.24 and 0.20 Ma (DHDH-4 and DBAG-115). These ages are consistent with a fission-track age of 0.17 ± 0.04 Ma for a welded tuff in the caldera of this volcano (Williams *et al*., 2004) and also fall within the range of an explosive volcanic pulse (0.32–0.17 Ma) in the NMER and CMER (Peccerillo *et al*., 2003; Hutchison *et al*., 2016; Siegburg *et al*., 2018). We refer to these basalts as Quaternary Fantale basalts.

Mafic rocks in the NMER show similar petrographic features, irrespective of eruption ages. They are porphyritic with a phenocryst assemblage of plagioclase (*c.* 14 vol%), olivine (2–12 vol%), and rare clinopyroxene (2–3 vol%). An exception are the mineral modes of the older mafic lavas with ages of 25 and 15 Ma (Alage and Tarmaber-Megezez series, respectively). These rocks are highly porphyritic with 20–25 vol% plagioclase phenocrysts (Supplementary Data Table S1). Groundmasses of all rocks are composed of olivine, clinopyroxene, feldspars, and Fe-Ti oxides, with dark interstitial glass.

Afar basalts

The K-Ar ages of nineteen mafic samples range from 4.5 to 0.1 Ma (Table 2 and Supplementary Data Fig. S7). Our results are consistent with existing K-Ar and $^{40}Ar/^{39}Ar$ ages (5.4 to <0.1 Ma) for mafic volcanic rocks from the Pliocene and Quaternary formations in this region (Zumbo *et al*., 1995; Manighetti *et al*., 1998; Kidane *et al*., 2003; Lahitte *et al*., 2003; Audin *et al*., 2004; Daoud *et al*., 2010; Ferguson *et al*., 2013b; Stab *et al*., 2015).

Following Stab *et al*. (2015), our samples are subdivided into stratoid basalts, Gulf basalts, and Afar axial range basalts in ascending stratigraphic order (Supplementary Data Fig. S6).

Our K-Ar ages for the Afar stratoid basalts range from 4.50 to 1.18 Ma (n = 17). Combined with previous geochronological studies (Supplementary Data Fig. S7), the majority of ages for the stratoid series fall within the range 4.0–1.1 Ma, as suggested by Stab *et al*. (2015). Among the stratoid series, the rocks in the west and southwest of the TGD tend to have older ages (4.5–2.7 Ma) than those in the east and northeast of the TGD (2.3–1 Ma). The ages of the stratoid series also show different spatial variations within these two regions. In the north of the TGD, ages become older from the axial range towards the northeast or southwest, consistent with NNE-SSW directed rifting (Hayward & Ebinger, 1996). In the south of the TGD, *ages* become older towards the northwest of the rift axis, consistent with NW-SE directed extension.

The K-Ar age of 0.79 Ma obtained for a basalt (DHA-17) from the Tendaho Graben corresponds to that of Gulf basalts (1.1–0.6 Ma) of Lahitte *et al*. (2003), Kidane *et al*. (2003) and Daoud *et al*. (2010), whereas the age of 0.12 Ma for basalt DHA-1 is consistent with the existing K-Ar and $^{40}Ar/^{39}Ar$ dates for the axial range basalts (< 0.6 Ma; Manighetti *et al*., 1998; Kidane *et al*., 2003; Lahitte *et al*., 2003; Audin *et al*., 2004; Ferguson *et al*., 2013b).

The Afar mafic rocks are mostly aphyric and vesicular (up to 30 vol. % vesicles). A few samples are porphyritic, consisting of phenocrysts of plagioclase (28 vol. %), olivine (up to 11 vol. %) and clinopyroxene (5 vol. %, except one sample with 31 vol. %; Supplementary Data Table S1). Some olivines are altered to iddingsite. Rocks without olivine phenocrysts tend to have relatively fine-grained groundmasses composed of olivine, clinopyroxene, plagioclase, and Fe-Ti oxides. Zeolites, silica, and carbonate are also found in some vesicles and interstitial parts of the groundmass in some rocks.

Major element compositions

The Ethiopian volcanic rocks studied here are classified as basanite, picro-basalt, basalt, basaltic andesite, trachybasalt or basaltic trachyandesite (Fig. 2; Le Bas *et al*., 1986), and as belonging to either the alkaline or the sub-alkaline rock series (Irvine & Baragar, 1971). The Oligocene mafic rocks in Maychew include basanites (classified into HT2) from the lowest sequence (Figs 2a and S3). These basanites show a strong deficiency of SiO_2, quite different from the other HT2 mafic rocks from the NW Plateau which have a sub-alkaline affinity (Figs 2a and S3; Pik *et al*., 1998, 1999; Kieffer *et al*., 2004; Beccaluva *et al*., 2009; Natali *et al*., 2011, 2016). To our knowledge, the silica-deficient HT suite is found only in Oligocene mafic rocks in the Yemen Plateau (Baker *et al*., 1996a; Beccaluva *et al*., 2009; Natali *et al*., 2016) and from a Miocene shield volcano, Gerba Guracha (25–24 Ma), in the western

434 Ethiopian Plateau (Rooney *et al*., 2014a, 2017a). Compositions of the Maychew HT1 group largely overlap with the other HT1 rocks in the NW Ethiopian and Yemen Plateaus, and are more alkaline than the LT samples. Mafic volcanic rocks from Wollega in the SW Plateau (15–7 Ma; Ayalew *et al*., 1999; Conticelli *et al*., 1999) have higher Na_2O + K_2O abundances than the LT-type mafic rocks from the NW Plateau. Mafic rocks from the SMER (Miocene Getra-Kele and Quaternary Tosa-Sucha) are classified into alkaline series (Fig. 2b), consistent with data obtained in previous studies (Yemane *et al*., 1999; George & Rogers, 2002; Rooney, 2010; Shinjo *et al*., 2011). These rocks have similar alkali enrichment to the Eocene Gamo basalts (Yemane *et al*., 1999; George & Rogers, 2002). Mafic rocks from the NMER and Afar *province* include both alkaline and sub-alkaline series, irrespective of eruption ages (Figs 2d, e); sub-alkaline rocks are dominant in the Afar region. These features are consistent with those reported in previous studies (Deniel *et al*., 1994; Wolde, 1996; Barrat *et al*., 1998; Boccaletti *et al*., 1999; Furman *et al*., 2006a; Daoud *et al*., 2010; Rooney *et al*., 2012b; Pinzuti *et al*., 2013; Giordana *et al*., 2014; Ayalew *et al*., 2016, 2018; Alene *et al*., 2017). Quaternary mafic volcanic rocks in the CMER also show transitional compositions between the alkaline and sub-alkaline series (Fig. 2c; Boccaletti *et al*., 1999; Rooney *et al*., 2007, 2011, 2014b; Rooney, 2010; Giordana *et al*., 2014; Ayalew *et al*., 2016; Tadesse *et al*., 2019). CMER mafic rocks from three Quaternary magmatic zones, the WFB, SDFZ, and

Akaki segments, have composition overlapping with each other (Gasparon *et al*., 1993; Wolde, 1996; Rooney, 2010; Rooney *et al*., 2005, 2007, 2014b; Ayalew *et al*., 2016). The composition of Miocene Addis Ababa basalts from the Bishoftu embayment largely overlap with mafic rocks from the SDFZ and Akaki (Wolde, 1996; Furman *et al*., 2006a).

In this study, we define mafic rocks as those with SiO_2 and MgO concentrations of 42–54 wt % and 20–2 wt %, respectively (Figs 3 and S8a). The Maychew HT2 basanites in the lowest sequence have the highest TiO_2 (*c.* 6 wt %) and FeO^T (total Fe as FeO; *c.* 19 wt %) among the studied mafic rocks, as well as the existing data sets for Ethiopian volcanic rocks. These basanites are also different from the other HT suites in the NW Ethiopian Plateau in terms of their low SiO_2 (*c.* 41–43 wt %) and high CaO (*c.* 15 wt %). Such features are similar to those of the HT basanites and picro-basalts in the Yemen Plateau (Baker *et al*., 1996b; Natali *et al*., 2016) and the Oligocene HT mafic rocks from the Gerba Guracha shield volcano in the southern part of the NW Plateau (except for their high P_2O_5; Rooney *et al*., 2014a, 2017a). Major element abundances of Maychew HT1 samples are similar to those of other HT1 mafic rocks from the NW Plateau (Pik *et al*., 1998; Beccaluva *et al*., 2009; Natali *et al*., 2016) and the Yemen Plateau (Baker *et al*., 1996b; Natali *et al*., 2016). Miocene Wollega basalts from the SW Ethiopian Plateau have major element compositions that largely overlap with those of LT mafic rocks in the NW Plateau, except for their higher Na_2O, K_2O

470 and P_2O_5 abundances.

471 Abundances of major elements in Miocene Getra-Kele and Quaternary Tosa-Sucha mafic rocks largely overlap with each other, except for FeO^T and MnO (Figs 3 and S8b). These oxides are more abundant in Miocene Getra-Kele mafic rocks than in Quaternary Tosa-Sucha mafic rocks. Rooney (2010) also found a similar relationship for Miocene (Chencha, Fe-rich) and Quaternary (Arba Minch, Fe-poor) mafic rocks from the vicinity of the Amaro-Yabello area in the SMER. Eocene Gamo basalts show significant overlaps with Miocene Getra-Kele samples, except for TiO_2, whereas Eocene Amaro basalts show the highest abundances of SiO_2 and the lowest abundances of TiO_2 and Na_2O at a given MgO among the Eocene–recent mafic rocks in this region (Yemane *et al*., 1999; George & Rogers, 2002; Rooney, 2010; Shinjo *et al*., 2011).

481 Major element abundances of Quaternary mafic rocks from the CMER (Rooney *et al*., 2007; 2014b) are similar to those of the SMER (Supplementary Data Fig. S8c). Abundances of Na_2O for CMER rocks are slightly lower than those for Tosa-Sucha mafic rocks, and thus CMER rocks are classified as transitional rock series (Fig. 2). Rocks from the WFB and SDFZ show significant differences in abundances of CaO, Na_2O and K_2O at a given MgO, and Akaki mafic rocks exhibit intermediate compositions between those of the WFB and SDFZ. Compositions of Miocene Addis Ababa basalts largely overlap with these Quaternary

mafic rocks (Furman *et al*., 2006a).

Mafic rocks in the NMER have major element compositions similar to those in the CMER (Figs 3 and S8d). Our data are consistent with the existing data sets for mafic rocks in adjacent regions (e.g., Boccaletti *et al*., 1999; Furman *et al*., 2006a; Giordana *et al*., 2014). The older mafic rocks (*Oligocene* Alage and Miocene Tarmaber-Megezez series) have higher TiO_2 and K_2O at a given MgO than the younger mafic rocks (Miocene-Quaternary). Our data for the Quaternary Fantale magmatic segment falls within the ranges of the existing data sets for this segment and the other Quaternary magmatic segments in the NMER (Dofan, Kone, and Boset; Furman *et al*., 2006a; Giordana *et al*., 2014; Ayalew *et al*., 2016).

Major element compositions of the stratoid, Gulf, and axial range series in the Afar region largely overlap with each other (Figs 3 and S8e). Our data are essentially consistent with the existing data for mafic rocks collected from the entire Afar province, including Djibouti (Deniel *et al*., 1994; Barrat *et al*., 1998, 2003; Daoud *et al*., 2010; Pinzuti *et al*., 2013; Ayalew *et al*., 2016; Alene *et al*., 2017). The literature data for the Gulf basalt is that for mafic rocks in the vicinity of the Gulf of Tadjoura in Djibouti (Deniel *et al*., 1994; Daoud *et al*., 2010), which have a more mafic composition (MgO > 9 wt %) than our samples from the Tendaho Graben (MgO of *c.* 7 wt %).

Trace element compositions

Nickel and Cr concentrations in the studied volcanic rocks show wide variations ([Cr] to *c.* 1700 ppm and [Ni] to *c.* 940 ppm), and a monotonous decrease with decreasing MgO (Figs 4 and S9a). Variations of these elements in the Maychew HT1 and HT2 groups largely overlap with each other, as do HT1 and HT2 in the other regions on the NW Ethiopian Plateau (Pik *et al*., 1998, 1999; Kieffer *et al*., 2004; Beccaluva *et al*., 2009; Natali *et al*., 2016). Abundances of Sr, Zr, Nb and Ba in Maychew HT2 basanites are significantly higher than those of the other HT2 rocks in the NW Ethiopian Plateau. The high-Ti mafic rocks from the Gerba Guracha shield volcano also show similar enrichment patterns for these elements (Rooney *et al*., 2014a, 2017a; see Supplementary Data Fig. S10). Abundances of moderately incompatible elements (e.g., Y and Yb) are similar between Maychew HT1 and HT2, as well as the other LT, HT1, and HT2 groups. The Wollega basalts from the SW Plateau (Ayalew *et al*., 1999) display trace element compositions overlapping with HT1 and HT2 rocks.

The SMER mafic rocks show similar trace element compositions within different sequential units (Figs 4 and S9b), except for the sub-alkaline Amaro basalts (Yemane *et al*., 1999; George & Rogers, 2002). Our data for the Getra-Kele and Tosa-Sucha mafic rocks show variations consistent with the existing data for these rocks (Yemane *et al*., 1999; George & Rogers, 2002; Rooney, 2010; Shinjo *et al*., 2011). The NMER mafic rocks of this study show smaller variations in trace element compositions, due to the lack of data for highly magnesian rocks. Our data for Quaternary rocks from the Fantale segment fall within the range of data sets for this and the other magmatic segments in the literature (Dofan, Kone, Boset; Boccaletti *et al*., 1999; Furman *et al*., 2006a; Giordana *et al*., 2014; Ayalew *et al*., 2016). Afar mafic rocks also show trace element variations similar to those of NMER mafic rocks. Our data for three groups of Afar rocks, stratoid series, Gulf basalt, and axial range series, show greater overlap with each other, and fall within the range of literature data sets (Deniel *et al*., 1994; Barrat *et al*., 1998, 2003; Daoud *et al*., 2010; Ayalew *et al*., 2016; Alene *et al*., 2017).

Mafic rocks with MgO > 6 wt % from different regions in Ethiopian volcanic fields show variable extents of incompatible trace element enrichment (Figs 5 and S10–S12). The Maychew HT2 plateau samples show higher Nb and Ta abundances relative to U and K (Fig. 5a). The $(La/Yb)_N$ ratios of Maychew HT2 samples are 7.7–24 (subscript N denotes chondrite-normalized abundance), comparable to the other HT2 rocks from the Ethiopian and Yemen Plateaus (8.7–24), and higher than those of the HT1 samples in this region (4.7–10) and the other HT1 (6.1–14) and LT (1.0–3.9) basalts from the NW Ethiopian Plateau (Supplementary Data Fig. S11a; data sources are the same as in Fig. 5). Strong enrichments of Nb, Ta, and LREE in Maychew HT2 samples are similar to high-Ti mafic rocks from the

Gerba Guracha shield volcano [$(La/Yb)_N$ = 18–32; Rooney *et al.*, 2017a; Supplementary Data Fig. S12a]. These two rock types show similar depletion of K (Fig. S10). The Wollega basalts from the SW Plateau (Ayalew *et al.*, 1999) display LREE abundance similar to HT1 rocks, but HREE abundance similar to LT samples from the NW Ethiopian Plateau [$(La/Yb)_N$ = 6.0–10].

Among the mafic rocks from the SMER, the subalkaline Amaro basalts have the lowest abundances of incompatible elements and low LREE/HREE ratios [Figs 5b and S11b; $(La/Yb)_N$ = 1.9–6.0 (George & Rogers, 2002)]. Irrespective of eruption age, the other SMER mafic rocks (Eocene Gamo, Miocene Getra-Kele, and Quaternary Tosa-Sucha) show similar trace element patterns (George & Rogers, 2002; Shinjo *et al.*, 2011). The $(La/Yb)_N$ ratios of the Gamo, Getra-Kele, and Tosa-Sucha rocks are 7.2-7.6, 7.3-21, and 9.0-17, showing strong overlap with each other [Figs 5b and S11b; George & Rogers (2002); Shinjo *et al.* (2011); this study].

The NMER rocks show similar incompatible trace element and REE abundance patterns, irrespective of eruption age (Figs 5c and S11c). The older rocks (Alage and Tarmaber-Megezez series) have higher abundances of these elements, due to their differentiated nature (rocks with MgO 4-6 wt % are included in these plots). The younger mafic rocks analyzed in this study (Nazret series and Fantale segment) show trace element abundance patterns consistent with previous studies (Wolde, 1996; Boccaletti *et al*., 1999; Furman *et al*., 2006a; Rooney *et al*., 2012b; Ayalew *et al*., 2018). The $(La/Yb)_N$ ratios of NMER mafic rocks are 4.1-14. The existing data for mafic rocks from the CMER and the Addis Ababa region (Bishoftu embayment) show variations in $(La/Yb)_N$ ratios of 5.1-14 (Fig. S12b; Gasparon *et al*., 1993; Wolde, 1996; Furman *et al*., 2006a; Rooney, 2010; Rooney *et al*., 2005, 2007, 2014b; Giordana *et al*., 2014; Ayalew *et al*., 2016; Tadesse *et al*., 2019), similar to the variations observed in NMER mafic rocks.

Trace element abundance patterns for Afar mafic rocks are similar to those of NMER mafic rocks (Fig. 5d). The $(La/Yb)_N$ ratios of these rocks range from 3.4 to 6.8, consistent with the existing data sets (2.6–7.1; Deniel *et al*., 1994; Barrat *et al*., 2003). An exception are samples from axial-range series in Manda Hararo (Barrat *et al*., 2003) and from Gulf basalts in the vicinity of the Gulf of Tadjoura in Djibouti (Deniel *et al*., 1994; Daoud *et al*., 2010, see localities in Supplementary Data Figs S6 and S7 and REE patterns in Fig. S11d). These mafic rocks have lower $(La/Yb)_N$ ratios of 0.69-1.3, similar to those reported for submarine ridge-axis basalts in the Gulf of Tadjoura (Barrat *et al*., 1990, 1993). Overall, our data confirm the northward decreasing trend of $(La/Yb)_N$ ratios in mafic rocks from the MER and Afar axial regions, as pointed out by Furman *et al*. (2006a), Rooney *et al*. (2011), and Ayalew *et al*. (2016).

Sr-Nd-Pb isotope compositions

Maychew HT1 and HT2 samples have isotopic compositions largely overlapping with each other, and mostly fall within the range of the existing data for Oligocene HT mafic rocks in the NW Ethiopian and Yemen Plateaus (Figs 6a and S13; Baker *et al*., 1996b; Pik *et al*., 1998, 1999; Kieffer *et al*., 2004; Natali *et al*., 2011, 2016). The Maychew HT2 basanites have the most radiogenic Pb isotopic compositions [$(^{206}Pb/^{204}Pb)_i$ = 19.20-19.26] among the HT2 rocks in the NW Ethiopian Plateau. Strongly alkaline rocks (basanites, foidites and tephrites) in the Gerba Guracha volcano in the NW Ethiopian Plateau have more radiogenic Pb isotopic compositions than the Maychew HT2 samples [$(^{206}Pb/^{204}Pb)_i$ of *c*. 20; Rooney *et al*. (2017)]. The Wollega basalts from the SW Plateau (Ayalew *et al*., 1999) have lower $(^{87}Sr/^{86}Sr)_i$ ratios and more radiogenic Pb isotope compositions than the Oligocene Plateau mafic rocks, and their isotopic features are similar to those of SMER mafic rocks (Getra-Kele and Tosa-Sucha).

The Sr-Nd-Pb isotopic compositions of the Getra-Kele and Tosa-Sucha mafic rocks from the SMER largely overlap with each other (this study; George & Rogers, 2002; Rooney, 2010; Shinjo *et al*., 2011), and significantly differ from those of the Eocene Amaro and Gamo basalts (George & Rogers, 2002). The Getra-Kele and Tosa-Sucha mafic rocks are characterized by radiogenic Pb isotopic compositions [$(^{206}Pb/^{204}Pb)_i$ >19] and lower

$(^{87}Sr/^{86}Sr)_i$ ratios (=0.703–0.704). Such features are akin to those of Miocene-Quaternary mafic rocks from the Turkana Depression, south of the SMER (Fig. 6b; Furman *et al*., 2004, 2006b). Among the NMER mafic lavas, the Oligocene Alage basalts and Miocene Tarmaber-Megezez mafic rocks have lower $(^{143}Nd/^{144}Nd)_i$ and higher $(^{87}Sr/^{86}Sr)_i$ ratios than those of the younger (Miocene to Quaternary) mafic rocks. In particular, two Alage (DBZ-22 and DBZ-30) and one Tarmaber-Megezez (DH-429) rock show highly radiogenic $(^{87}Sr/^{86}Sr)_i$ ratios of 0.7051–0.7068 (Feyissa *et al*., 2017). They are also characterized by higher SiO_2 abundances (> 50 wt %), lower $(^{206}Pb/^{204}Pb)_i$ ratios, and higher $(^{207}Pb/^{204}Pb)_i$ and $(^{208}Pb/^{204}Pb)_i$ ratios at a given $(^{206}Pb/^{204}Pb)_i$ (Figs 6c and S13). The Sr-Nd-Pb isotopic compositions of the Miocene–Quaternary CMER mafic rocks (Fig. S14) largely overlap with those of the Miocene–Quaternary NMER mafic rocks (Gasparon *et al*., 1993; Furman *et al*., 2006a; Rooney *et al*., 2012b; Giordana *et al*., 2014; Ayalew *et al*., 2016).

The Sr, Nd and Pb isotopic compositions of Afar mafic rocks partly overlap with those of NMER mafic rocks (except for Oligocene–Miocene rocks) and extend to more radiogenic Nd and less radiogenic Sr compositions (Figs 6d and S13). Overall, the Afar mafic rocks have lower $^{207}Pb/^{204}Pb$ ratios at a given $^{206}Pb/^{204}Pb$ than the NMER mafic rocks, and are thus similar to basalts from the Red Sea (Dupré *et al*., 1988; Volker *et al*., 1993, 1997). The axial range series in Djibouti and Etra 'Ale (Deniel *et al*., 1994; Barrat *et al*., 1998) have

613 more radiogenic Pb isotope compositions [($^{206}Pb/^{204}Pb)_i > 19$] than this series of mafic rocks
614 in the western part of the central Afar region (this study). In contrast, Sr and Nd isotopic
615 compositions do not show such lateral variations within the axial range series. The Sr-Nd-Pb
616 isotopic compositions of the stratoid series and Gulf basalts largely overlap (this study;
617 Deniel *et al*., 1994; Barrat *et al*., 1998; Daoud *et al*., 2010; Alene *et al*., 2017).
618

619 **Spatial and temporal variations in elemental and isotopic compositions**

620 Previous studies have revealed spatial variations in the geochemical characteristics of mafic
621 rocks in the Ethiopian volcanic province (e.g., Furman *et al*., 2006a; Rooney, 2010; Rooney
622 *et al*., 2012b; Ayalew *et al*., 2016). Here, we integrate our data sets with the existing data to
623 provide an up-to-date the view of spatio-temporal variations in the volcanism of this region.

624 Latitudinal variations in $(K/Nb)_N$, $(La/Sm)_N$, $(Sm/Yb)_N$ $(^{87}Sr/^{86}Sr)_i$, $(^{143}Nd/^{144}Nd)_i$ and
625 $(^{206}Pb/^{204}Pb)_i$ for the mafic volcanic rocks (MgO > 6 wt %) from rift zones (MER and Afar)
626 are shown in Fig. 7 (subscript N denotes primitive mantle normalized abundance). The
627 $(La/Sm)_N$ ratio broadly decreases from the SMER through CMER and NMER to the Afar
628 province, whereas $(Sm/Yb)_N$ does not show any systematic change. A small positive peak in
629 $(La/Sm)_N$ is found at 9 ˚N, coincident with high $(K/Nb)_N$ and $(^{87}Sr/^{86}Sr)_i$ as well as a high
630 $^3He/^4He$ peak on a northward increasing trend reported by Pik *et al*. (2006) and Rooney *et al*.

(2012b). Our compilation also reveals that $(^{143}Nd/^{144}Nd)_i$ and $(^{206}Pb/^{204}Pb)_i$ show a concave pattern with peaks or troughs at 9 °N. We note that the LAB boundary beneath the rift has a steep dip there (Kendall *et al*., 2005; Keir *et al*., 2015). In Afar, $(La/Sm)_N$ and $(Sm/Yb)_N$ are highly variable due to the occurrence of LREE- and MREE-depleted basalts (Barrat *et al*., 1993, 2003; Daoud *et al*., 2010).

The NW Plateau mafic rocks show large variations in $(K/Nb)_N$ of 0.04-3.9 and $(Sm/Yb)_N$ of 1.4-7.1. These variations are significantly larger than those found in MER and Afar mafic rocks [$(K/Nb)_N$ = 0.20-3.1 and $(Sm/Yb)_N$ = 0.82-4.5] (Supplementary Data Fig. S15). Among the Oligocene mafic rocks in the NW Ethiopian Plateau, the HT2 type has the highest $(La/Sm)_N$ and $(Sm/Yb)_N$, whereas the LT type has the lowest values of these ratios (Pik *et al*., 1998, 1999; Kieffer *et al*., 2004; Beccaluva *et al*., 2009). Given the spatial distributions of LT, HT1 and HT2 (Pik *et al*., 1998; see Fig. 1), $(K/Nb)_N$ increases and $(La/Sm)_N$ and $(Sm/Yb)_N$ decrease from south to north. The $(^{87}Sr/^{86}Sr)_i$ and $(^{206}Pb/^{204}Pb)_i$ isotopic compositions also show a decrease from south to north, whereas $(^{143}Nd/^{144}Nd)_i$ does not show a clear latitudinal variation. The Wollega basalts from the SW Plateau have $(K/Nb)_N$, $(La/Sm)_N$ and $(^{206}Pb/^{204}Pb)_i$ comparable to those of HT2 mafic rocks in the NW Plateau, whereas their $(Sm/Yb)_N$, $(^{87}Sr/^{86}Sr)_i$ and $(^{143}Nd/^{144}Nd)_i$ are comparable to those of LT mafic rocks (Ayalew *et al*., 1999). Overall, the latitudinal variations in $(La/Sm)_N$ and

$(Sm/Yb)_N$ of mafic rocks from the Plateau (Oligocene–Miocene) and rift (Oligocene to Recent) are concordant with each other (Pik *et al*., 2006; Rooney *et al*., 2012b; Ayalew *et al*., 2016).

DISCUSSION

Origin of geochemical variation

Fractional crystallization

The majority of the mafic rocks for which data are presented in this study are differentiated (Figs 3, 4, S8 and S9), with low concentrations of MgO (<8 wt %), low Ni (<200 ppm), and low Cr (<400 ppm). Concentrations of MgO, CaO, Ni, and Cr show positive correlations, suggesting that variations in major and trace element compositions are controlled primarily by fractional crystallization of mafic phases (olivine, clinopyroxene, and spinel). Plagioclase is considered to play a minor role in producing the elemental variation, based on petrographic and major and trace element characteristics; a lack of clear linear correlations of Al_2O_3 and Sr with MgO (Supplementary Data Figs S8 and S9), the lack of negative Eu and Sr anomalies in trace element abundance patterns (Figs 5, S10 and S11), and the sparse occurrence of plagioclase phenocrysts (Supplementary Data Table S1). These features in our samples are consistent with existing data for other Ethiopian mafic rocks (Figs 5 and S8–12).

To examine phase assemblages and extents of fractional crystallization, the major element compositions of the Ethiopian mafic volcanic rocks are expressed as normative minerals and compared with the compositions of melts produced in fractional crystallization experiments (Thompson *et al*., 2001; Supplementary Data Fig. S16). In the normative tetrahedron, the cotectic saturation of olivine + pyroxene + plagioclase at 1 atm forms a curved line (cotectic boundary), which with increasing pressure shifts to the olivine apex of the tetrahedron (Thompson *et al*., 2001). Most mafic rocks plot below the 1-atm cotectic boundary and form broad arrays subparallel to this line. This variation is interpreted as fractionation at various pressures with a phase assemblage of olivine during early differentiation, then clinopyroxene (cpx) + olivine, in both alkaline and subalkaline magma suites. Subsequently, orthopyroxene begins to crystallize with plagioclase in subalkaline magmas, and melt compositions become more siliceous. This expected phase assemblage has been confirmed by thermodynamic modeling of mafic-felsic magmatic evolution in the MER (e.g., Peccerillo *et al*., 2003; Rooney *et al*., 2012c; Feyissa *et al*., 2017). However, we also note that trace element and isotope compositions within each volcanic region vary significantly, and thus that processes other than fractional crystallization must also be involved (Fig. 8). Below, we discuss other possible mechanisms for the production of the observed compositional variations, including crustal assimilation, variable melting conditions, and mixing of different magma sources.

Crustal contamination

Mantle-derived basaltic magmas have temperatures higher than the solidus of crustal materials of intermediate to felsic composition (<1000 ˚C; Grove *et al*., 1988). Consequently, the magmas may have reacted to some extent with crustal materials during their ascent to the surface (Baker *et al*., 1996b; Rogers *et al*., 2000; Peccerillo *et al*., 2003; Rooney *et al*., 2005, 2007; Rooney *et al*., 2012c). Since Plateau and rift-escarpment regions have thicker continental lithosphere than that beneath the rift-floor (Dugda *et al*., 2007), a greater extent of crustal assimilation is anticipated in the former. Crustal materials, mainly consisting of evolved igneous rocks (intermediate to felsic intrusives), are expected to have high abundances of incompatible elements (Rudnick & Gao, 2003). Element ratios such as La/Nb, Ba/La, and Ce/Pb and isotope ratios such as $^{87}Sr/^{86}Sr$ and $^{206}Pb/^{204}Pb$ can be useful tracers to detect crustal input to mantle-derived magmas due to the large differences in these ratios between magmas and crustal lithologies (Stewart & Rogers, 1996; Meshesha & Shinjo, 2008; Shinjo *et al*., 2011; Rooney *et al*., 2005; Rooney, 2017). The low-Mg LT suite in the NW Ethiopian Plateau (MgO <6 wt %) has higher Ba/La ratios than mantle-derived oceanic basalts [mid-ocean ridge basalts (MORB) or ocean island basalts (OIB) after Willbold &

Stracke (2006); Fig. 8], suggesting that the geochemistry of differentiated LT rocks is affected by crustal contamination (Pik *et al*., 1998, 1999; Kieffer *et al*., 2004; Beccaluva *et al*., 2009). In contrast, HT1 and HT2 mafic rocks from the NW Plateau and Wollega basalts from the SW Plateau have Ba/La ratios mostly falling within the range of OIB and MORB, suggesting minor roles for crustal assimilation during their magmatic evolution. Some mafic rocks from the NMER show geochemical characteristics suggestive of crustal assimilation; they are characterized by high SiO_2 abundance and high Ba/La and $(^{87}Sr/^{86}Sr)_i$ (Figs 6 and 8). Below, the effect of crustal assimilation in these NMER rocks are discussed.

Crustal assimilation cools the magma and leads to crystallization, whereas the latent heat of fractional crystallization promotes assimilation. Such a positive feedback is referred to as AFC (assimilation combined with fractional crystallization; DePaolo, 1981). AFC is considered to result in co-variation of element abundance (dominantly by crystallization) and isotopic compositions (by mixing of crust and magma). In plots of $(^{87}Sr/^{86}Sr)_i$ *vs* SiO_2 (Fig. 8), the differentiated NMER rocks (with SiO_2 > 50 wt % or MgO < 6 wt %) exhibit higher $(^{87}Sr/^{86}Sr)_i$, suggesting the influence of crustal materials (e.g., Pan-African crust: Stewart & Rogers, 2002; Shinjo *et al*., 2011; Rooney, 2017) in the petrogenesis of these rocks. We exclude low-MgO NMER rocks (MgO < 6 wt %) in the following discussions about melting processes and source characteristics. The other SMER and Afar volcanic rocks do not show such correlations (Fig. 8), suggesting that the role of crustal assimilation in these mafic rocks was insignificant; a conclusion consistent with previous studies (e.g., Furman *et al*., 2006a; Rooney *et al*., 2005).

Melting conditions

Since the mantle is compressible, its temperature varies with pressure to conserve heat content along the adiabatic gradient. It is therefore useful to have a conceptual reference, known as "mantle potential temperature" (T_p), which represents the temperature of solid mantle expanded to atmospheric pressure (McKenzie & Bickle, 1988). To estimate T_p for the Ethiopian magmatism, we applied the geothermobarometry approaches of Putrika (2008), Lee *et al*. (2009) and Herzberg & Asimow (2015).

Data for mafic rocks used for this evaluation are from this study and previous studies (Gasparon *et al*., 1993; Deniel *et al*., 1994; Baker *et al*., 1996b; Wolde, 1996; Barrat *et al*., 1998, 2003; Pik *et al*., 1998, 1999; Ayalew *et al*., 1999, 2016, 2018; George & Rogers, 2002; Kieffer *et al*., 2004; Rooney *et al*., 2005, 2014b; Furman *et al*., 2006a; Beccaluva *et al*., 2009; Daoud *et al*., 2010; Natali *et al*., 2011, 2016; Shinjo *et al*., 2011; Alene *et al*., 2017; Tadesse *et al*., 2019) and filtered to exclude rocks with liquidus phases other than olivine. On major element plots (Supplementary Data Fig. S8), CaO generally shows an increase to MgO of *c*. 8

wt %, then it decreases with decreasing MgO. This variation is interpreted as a result of participation of clinopyroxene in crystallization (e.g., Rooney *et al*., 2007; Rooney, 2010; Pinzuti *et al*., 2013). We therefore used data for mafic rocks with MgO > 8.5 wt %. Highly magnesian rocks (MgO > 15 wt %) were avoided as they likely contain accumulated phases which were not equilibrated with the melt. Details of the thermobarometric modeling are described in Supplementary Data Text S3.

Results of *P*-*T* estimates are summarized in Supplementary Data Table S4 and Fig. S17 [including calculated primary magma composition equilibrated with mantle (Fo_{89}) and mantle potential temperature (T_p) using an adiabatic gradient of 18 K GPa^{-1} (McKenzie & Bickle, 1988; Katz *et al*., 2003), or the gradients of Herzberg & Asimow (2015)]. Melting *T* and *P* estimated using the methods of Putirka (2008), Lee *et al*. (2009), and Herzberg & Asimow (2015) are generally consistent with each other, ±50 ˚C and ±1 GPa (mostly < 0.5 GPa), in the ranges Supplementary Data 1300–1600 ˚C and 1–3 GPa, respectively. Exceptions are thermobarometric estimates for the Maychew basanites ($n = 2$) from this study (Supplementary Data Fig. S17). The large discrepancy for *P* (hence *T* by error propagation from *P*) for basanites (3 GPa by the Putirka (2008) algorithm and 6 GPa by the Lee *et al*. (2009) algorithm) is probably due to inaccuracy of the Lee *et al*. thermobarometry in this case, which is not applicable to SiO_2-deficient magmas formed in the garnet-stability field

(Till, 2017).

The Maychew rocks yield T_p of 1400–1550 ˚C (Fig. 9a) which is significantly higher than the ambient mantle [1340 ˚C; Cottrell & Kelley (2011)]. In particular, the HT2 basanites from the lower Maychew section show the highest T_p range found in the HT series in previous studies (1600 ˚C: Rooney *et al*., 2012a; Beccaluva *et al*., 2009; Rogers *et al*., 2010; Natali *et al*., 2016). We also reaffirm the gradation of T_p in the mantle for the production of HT1 and HT2 (1400–1600 ˚C) to LT (1350–1400 ˚C) proposed by Natali *et al*. (2016), who ascribed this variation to thermal zonation in the Afar mantle plume at 30 Ma, with integration of their earlier model (Beccaluva *et al*., 2009) and He-Sr-Nd-Pb isotope data. The calculated T_p for the mantle beneath the SW Plateau (Wollega; 11 Ma) is 1380 ˚C, similar to that for LT rocks from the NW Plateau, and also consistent with T_p determined through a REE inversion model (*c.* 1375 ˚C; Ayalew & Gibson, 2009) for Miocene SW Plateau rocks (15-Ma Shewa to the northeast of Addis Ababa; Fig. 1).

The Miocene to Quaternary mafic rocks from the SMER, CMER, NMER and Afar yield T_p values mostly falling within the range of 1350–1500 ˚C (Fig. 9b). The obtained values are consistent with those of previous studies (1260–1490 ˚C; Rooney *et al*., 2012a; Ayalew & Gibson, 2009; Ferguson *et al*., 2013a; Pinzuti *et al*., 2013; Armitage *et al*., 2015). Lateral variation in T_p along the MER-Afar region are less clear (Fig. 9b), but show a slight

775 increase from the CMER and NMER to the south (SMER) and to the north (Afar), as
776 suggested by Rooney *et al*. (2012a).

777 The maximum T_p > 1500 ˚C is consistent with melting of adiabatically upwelling
778 mantle for the genesis of the Plateau mafic rocks (Beccaluva *et al*., 2009; Rogers *et al*., 2010;
779 Rooney *et al*., 2012a; Natali *et al*., 2016). Anomalously hot mantle began to melt at a greater
780 depth, probably in the garnet stability field (*P* > 3.3 GPa, depth > 100 km; Walter *et al*.,
781 1995). In addition, the thick lithosphere beneath the Plateau may have acted as a lid on the
782 upwelling mantle, resulting in preferential sampling of melts from the deeper mantle (Ellam,
783 1992). By contrast, the shallower lithosphere beneath the MER and Afar region may have led
784 to preferential tapping of magmas from shallower regions of the upwelling mantle. To
785 substantiate this inference, we apply a melting model and examine the role of a garnet-
786 bearing source during magma production. Since garnet preferentially hosts the heavy REE
787 (Johnson, 1998), melting of the source leaving garnet in the residue leads to elevated
788 LREE/HREE (La/Yb) and MREE/HREE (Gd/Yb or Dy/Yb; Fig. 10) in the partial melts.
789 Clinopyroxene is also known as a possible phase to fractionate these elements (Blundy *et al*.,
790 1998). However, it is unlikely that this phase plays a major role in REE fractionation. The
791 "garnet-like" REE partitioning of clinopyroxene occurs only in small-degree melts at shallow
792 depths (*F* <5% and *P* <1.5 GPa, where *F* and *P* denote melting degree and pressure; Blundy

et al., 1998); such conditions are distinctly different from those estimated for the Ethiopian mafic rocks (Supplementary Data Fig. S17 and Table S4). We thus consider that a melting model involving garnet-bearing mantle is appropriate to examine the causes of LREE/HREE and MREE/HREE variations. Superimposed on the plot in Fig. 10 are calculated curves for partial melting of lherzolite in garnet-bearing and garnet-free assemblages (see details regarding the modeling in the caption of Fig. 10). The HT2 mafic rocks have the highest Dy/Yb ratios among the Oligocene Plateau volcanic rocks, and are inferred to contain a greater contribution of melts from mantle in the garnet stability field. Differences in LREE enrichment within the HT2 series are attributed to various extents of melting (*F*); 1–2% for basanite and 3–7% for basalt and picrite. The LT series have lower La/Sm and Dy/Yb ratios and can be explained by a larger extent of melting in the spinel stability field, consistent with the lower T_p estimates for these samples (Beccaluva *et al*., 2009; Natali *et al*., 2016).

The MER and Afar mafic rocks show larger contributions of melts formed in the spinel stability field. These mafic rocks, however, may have contributions from melts from garnet-bearing sources, inferred from elevated Dy/Yb ratios relative to spinel lherzolite melts calculated by our modeling. This inference is consistent with the REE models of Ferguson *et al*. (2013a) and Pinzuti *et al*. (2013). Since T_p is essentially constant among the MER mafic rocks (Fig. 9b), LREE enrichment in the SMER mafic rocks (Figs. 7) is largely due to the geochemistry of the magma sources rather than LREE/HREE fractionation during partial melting (George & Rogers, 2002). As a possible origin of this source, localized lithosphere enriched by metasomatism has been proposed (Furman & Graham, 1999; George & Rogers, 2002; Rooney, 2010).

Evolution of Ethiopian magmatism: interplay between melting conditions and source composition

Previous studies have identified multiple end-member components in the genesis of mafic magmas in Ethiopia and adjacent regions (e.g., Marty *et al*., 1996; Pik *et al*., 1999, 2006; Rogers *et al*., 2000; George & Rogers, 2002; Furman *et al*., 2006a; Rooney *et al*., 2012b). Pik *et al*. (1999) first identified four end-member components for Oligocene Plateau magmatism. Subsequently, Meshesha & Shinjo (2008) identified five end-member components for Oligocene to Recent magmatism across the entire region in Ethiopia. Since then, numerous isotope data have been published (e.g., Shinjo *et al*., 2011; Rooney *et al*., 2012b, 2014a; Natali *et al*., 2016; Ayalew *et al*., 2016, 2018; Alene *et al*., 2017). Here we examine the end-member compositions proposed by Meshesha & Shinjo (2008) using data from the present study and complied from the recent literature.

We used principal component analysis (PCA) to inspect the geometries of the data on

829 the plot. Details about the method are outlined in Supplementary Data Text S4; PCA score
830 plots are given in Supplementary Data Fig. S18 in which the mantle end-member components
831 of Meshesha & Shinjo (2008) are projected. The PCA outputs demonstrate that these end-
832 member components explain the variability of Sr-Nd-Pb isotope data sets well, including
833 those presented in the more recent studies, and in this study. It is noted that this evaluation
834 does not include $^{3}He/^{4}He$ data, as was done by Meshesha & Shinjo (2008). Based on the Sr-
835 Nd-Pb isotopic compositions of high-$^{3}He/^{4}He$ lavas (Marty *et al*., 1996; Pik *et al*., 2006),
836 Meshesha & Shinjo (2008) defined an additional end-member component (their C4, and its
837 subtype C4'), and we used this composition to examine the effect of this source.

838 Meshesha & Shinjo (2008) inferred the origin of five end-member components as:
839 C1, recycled gabbro in the Afar plume (in the Oligocene); C2, enriched lithospheric materials
840 beneath the SMER (or lithosphere metasomatized by C2-dominated melts); C3, EM-1-like
841 recycled crustal material in the Afar plume; C4, crust-mantle hybrid rocks from the lower
842 mantle [essentially identical to the "C" component of Hanan & Graham (1996) or "FOZO" of
843 Stracke *et al*. (2005)]; C5, unpolluted upper mantle (Schilling *et al*., 1992). Furman (2007)
844 and Rooney *et al*. (2014a, 2017a) argued for an origin of C2 as a 'metasome' within
845 lithosphere formed by reaction with asthenosphere-derived melts. Ayalew *et al*. (2016) also
846 suggested a similar scenario for the C3 isotopic signature; the EM1-like isotopic signature of

this source is preserved as veins in the lithosphere, presumably formed by infiltration of asthenosphere-derived melts into the lithosphere. Based on these inferences, the fusibility, i.e., how easy it is to be melted, is roughly estimated as C2 = C3 > C4 > C1 > C5. Thus, to a first order, contributions of C1 (Oligocene) or C5 (Miocene to recent) relative to the other end-member component are interpreted to reflect the dominance of a refractory source domain in the melting process.

When more than three end-member components are involved in mixing, the relative mass fraction of them cannot be solved mathematically (e.g., Schilling *et al*., 1992). Instead, we use the PCA score as a proxy for the relative contribution from a specific end-member component. For Oligocene magmas, Meshesha & Shinjo (2008) suggested that C1 is the most depleted, hence considered to be the most refractory source. From the location of C1 in isotope correlation space, its contribution can be seen as a positive score of PC1 (first principal component; Supplementary Data Fig. S18). Figure 11 shows a clear negative correlation between the PC1 score and $(La/Sm)_N$ ratio. Such a relationship can be interpreted as reflecting different averaging of melts sampled from a heterogeneous mantle consisting of materials with different fusibilities (e.g., Stracke *et al*., 2003). The HT2 rocks represent melts sampled preferentially from a fusible source in the deep melting region, whereas LT mafic rocks represent melts sampled preferentially from a refractory source (C1) in the shallower melting region (Fig. 12a). This inference is consistent with Pik *et al*. (1998), Furman *et al*. (2006a), Beccaluva *et al*. (2009), and Natali *et al*. (2016). A Maychew HT2 sample from the basal section (TR1V3) is one of the deepest melts sampled during Oligocene trap magmatism (estimated to have segregated at a pressure of 3 GPa; Supplementary Data Fig. S17), and its isotopic composition is similar to C4' of Meshesha & Shinjo (2008) (see also Figs 6 and S13). Meshesha & Shinjo (2008) argued that C4' observed in the Quaternary Afar basalts would have evolved from C4 over time. Instead, our data for HT2 basanites suggests that the composition of this end-member component did not change over time. To advance the knowledge of the evolution of this magma source, further studies on Maychew basanites, including $^3He/^4He$ analysis, are necessary.

In the subsequent period (<30 Ma), volcanic activity coincided with rifting, and magma production was driven by adiabatic decompression of asthenospheric mantle through plate divergence (e.g., Deniel *et al*., 1994; Rooney *et al*., 2007, 2013; Rooney, 2010; Ayalew & Gibson, 2009; Pinzuti *et al*., 2013; Feyissa *et al*., 2017; Ayalew *et al*., 2018). Previous studies have documented temporal and spatial changes in the melting regime associated with the development of the rift system; deeper melting occurred in regions of incipient rift zones such as Oligocene–Miocene rift axes and the Quaternary SDFZ, whereas shallow melting occurred in the regions of axial and mature rift zones (e.g., Rooney, 2010; Ferguson *et al*., 2013a; Feyissa *et al*., 2017; Ayalew *et al*., 2018).

The Miocene to Recent mafic rocks in the MER have contributions from the C2 and C3 end-member components of Meshesha & Shinjo (2008) (Figs 6, S13, and S14). The C2 end-member component mainly contributed to mafic rocks from the SEMR and Turkana region (Furman *et al*., 2004, 2006b; Shinjo *et al*., 2011), whereas the C3 component mainly contributed to the CMER and NMER mafic rocks (Furman *et al*., 2006a; Ayalew *et al*., 2016). The C2 end-member component is characterized by radiogenic Pb isotopic compositions, and the C3 end-member component is clearly defined by higher $^{87}Sr/^{86}Sr$ (Fig. 6). The compositions of these end-member components of Meshesha & Shinjo (2008) are located on the lower extension of PC1 and PC2 in PCA score plots (Supplementary Data Fig. S18; PC1 and PC2 denote first and second principal components). The contribution of the C2 end-member component (represented as a negative PC1 score) and $(La/Sm)_N$ ratio show a correlation, as seen in Oligocene Plateau mafic rocks. The decreasing effect of this end-member component in mafic rocks along the MER from south to north could be related to shallow melting of more refractory source (C5). The southward increase in LAB depth is documented as along-strike depth variation of a mid-lithosphere reflector (Maguire *et al*., 2006; Keir *et al*., 2015). We suggest that thick lithosphere may act as an obstruction to the upwelling asthenospheric flow to shallower depths (Fig. 12b), resulting in preferential sampling of melt from fusible sources. Lateral changes in the lithospheric structure (e.g., dip of its base; Kendall *et al*., 2005; Keir *et al*., 2015) may also enhance melt extraction and produce melt from refractory sources, as observed in the NMER at 9 ˚N (Fig. 7). The presence of two different fusible sources (C2 and C3) must be an intrinsic feature in the mantle beneath the MER, and may be attributed to a difference in phase assemblages in these sources, depending on the conditions of their formation [e.g., amphibole- *vs* phlogopite-bearing assemblage: Furman (2007); Rooney *et al*. (2017)].

Temporal and spatial variations of basalt compositions in Oligocene to Recent Ethiopian magmatism require changes in the relative contributions of multiple end-member components in the mantle. Correlations between major and trace element and isotopic compositions suggest that melting integrated chemically-variable melts formed across a range of pressures. Secular and lateral changes in magma compositions are probably due to changes in the melting regime related to the influence of the Afar plume in space and time (Furman *et al*., 2006a; Rooney, 2010; Rooney *et al*., 2012b; Ayalew *et al*., 2016). The ongoing rifting in Ethiopia may represent the transition from a plume-driven to a plate-driven setting for the upwelling of asthenospheric mantle.

918 **CONCLUSIONS**

919 Geochronological and geochemical results from this study are combined with existing data
920 and yield constraints on petrologic processes and magma sources for Ethiopian magmatism
921 since 30 Ma. The conclusions of this study are as follows.

922 • The K-Ar ages of this study are essentially consistent with the existing K-Ar and
923 $^{40}Ar/^{39}Ar$ ages. The ages range from *c*. 30 Ma to Recent (*c*. 0.1 Ma), and represent
924 volcanism transitional from an Oligocene trap phase to a Miocene to Recent rift-
925 related phase.

926 • Maychew basanites record the highest range of mantle potential temperature among
927 Oligocene Plateau rocks (T_p = *c*. 1600 ˚C), and are considered to be the melting
928 product of the starting Afar plume head. Oligocene to Recent mafic rocks from the
929 MER and Afar regions yield lower T_p (1500–1340 ˚C), suggesting a decrease in T_p by
930 100–260 ˚C in the post trap-phase magmatism.

931 • Our new Sr-Nd-Pb isotope data for Plateau and rift-related mafic lavas reaffirm the
932 involvement of the end-member source components defined by Meshesha & Shinjo
933 (2008). Temporal and spatial changes in lava geochemistry can be explained by
934 changes in the relative contributions these end-member components.

935 • Relative contributions of these end-member components are primarily attributed to

change in sampling of melts derived from a heterogeneous mantle, as related to the thermal condition of the asthenosphere (for Oligocene magmatism) and the thickness of the lithosphere (for MER magmatism).

- The ongoing rifting in Ethiopia may represent a transitional phase from a plume-driven to a plate-driven setting of magmatism.

ACKNOWLEDGEMENTS

We are grateful to Gray E. Bebout and Tyrone O. Rooney for discussion and improving the manuscript. We would also like to thank Tazue Nogi for help in K-Ar analysis. All members of the Pheasant Memorial Laboratory are thanked for their constructive discussion, technical support, and encouragement. Tanya Furman and two anonymous reviewers are acknowledged for their constructive review of the manuscript and Georg Zellmer is thanked for editorial handling. This study was supported by the MEXT (Ministry of Education, Culture, Sports, Science and Technology). We appreciate the Geological Survey of Ethiopia (GSE), in particular the Basic Geoscience Mapping Core Processes for their comprehensive support during the fieldwork. Figures were prepared using GMT (Wessel *et al*., 2013) and R (R Core Team, 2019).

SUPPLEMENTARY DATA

Supplementary data are available at Journal of Petrology online.

REFERENCES

Abebe, T., Mazzarini, F., Innocenti, F. & Manetti, P. (1998). The Yerer-Tullu Wellel volcanotectonic lineament: A transtensional structure in central Ethiopia and the associated magmatic activity. Journal of African Earth Sciences, 26(1), 135-150, doi: 10.1016/S0899-5362(97)00141-3.

Abebe, B., Acocella, V., Korme, T. & Ayalew, D. (2007). Quaternary faulting and volcanism in the Main Ethiopian Rift. Journal of African Earth Sciences, 48(2-3), 115-124, doi: 10.1016/j.jafrearsci.2006.10.005.

Alene, M., Hart, W. K., Saylor, B. Z., Deino, A., Mertzman, S., Haile-Selassie, Y. & Gibert, L. B. (2017). Geochemistry of Woranso–Mille Pliocene basalts from west-central Afar, Ethiopia: Implications for mantle source characteristics and rift evolution. Lithos, 282, 187-200, doi: 10.1016/j.lithos.2017.03.005.

Armitage, J. J., Ferguson, D. J., Goes, S., Hammond, J. O., Calais, E., Rychert, C. A. & Harmon, N. (2015). Upper mantle temperature and the onset of extension and break-up in Afar, Africa. Earth and Planetary Science Letters, 418, 78-90, doi:

10.1016/j.epsl.2015.02.039.

Arndt, N. T., & Christensen, U. (1992). The role of lithospheric mantle in continental flood volcanism: thermal and geochemical constraints. Journal of Geophysical Research: Solid Earth, 97(B7), 10967-10981, doi: 10.1029/92JB00564.

Audin, L., Quidelleur, X., Coulié, E., Courtillot, V., Gilder, S., Manighetti, I., Gillot, P.-Y., Tapponnier, P. & Kidane, T. (2004). Palaeomagnetism and K-Ar and $^{40}Ar/^{39}Ar$ ages in the Ali Sabieh area (Republic of Djibouti and Ethiopia): constraints on the mechanism of Aden ridge propagation into southeastern Afar during the last 10 Myr. Geophysical Journal International, 158(1), 327-345, doi: 10.1111/j.1365-246X.2004.02286.x.

Ayalew, D., Yirgu, G. & Pik, R. (1999). Geochemical and isotopic (Sr, Nd and Pb) characteristics of volcanic rocks from southwestern Ethiopia. Journal of African Earth Sciences, 29(2), 381-391, doi: 10.1016/S0899-5362(99)00104-9.

Ayalew, D., Barbey, P., Marty, B., Reisberg, L., Yirgu, G. & Pik, R. (2002). Source, genesis, and timing of giant ignimbrite deposits associated with Ethiopian continental flood basalts. Geochimica et Cosmochimica Acta, 66(8), 1429-1448, doi: 10.1016/S0016-7037(01)00834-1.

Ayalew, D. & Gibson, S. A. (2009). Head-to-tail transition of the Afar mantle plume:

Geochemical evidence from a Miocene bimodal basalt–rhyolite succession in the Ethiopian Large Igneous Province. Lithos, 112(3-4), 461-476, doi: 10.1016/j.lithos.2009.04.005.

Ayalew, D., Jung, S., Romer, R. L., Kersten, F., Pfänder, J. A. & Garbe-Schönberg, D. (2016). Petrogenesis and origin of modern Ethiopian rift basalts: Constraints from isotope and trace element geochemistry. Lithos, 258, 1-14, doi: 10.1016/j.lithos.2016.04.001.

Ayalew, D., Jung, S., Romer, R. L. & Garbe-Schönberg, D. (2018). Trace element systematics and Nd, Sr and Pb isotopes of Pliocene flood basalt magmas (Ethiopian rift): A case for Afar plume-lithosphere interaction. Chemical Geology, 493, 172-188, doi: 10.1016/j.chemgeo.2018.05.037.

Baker, J., Snee, L. & Menzies, M. (1996a). A brief Oligocene period of flood volcanism in Yemen: implications for the duration and rate of continental flood volcanism at the Afro-Arabian triple junction. Earth and Planetary Science Letters, 138(1-4), 39-55, doi: 10.1016/0012-821X(95)00229-6.

Baker, J. A., Thirlwall, M. F. & Menzies, M. A. (1996b). Sr-Nd-Pb isotopic and trace element evidence for crustal contamination of plume-derived flood basalts: Oligocene flood volcanism in western Yemen. Geochimica et Cosmochimica Acta, 60(14), 2559-2581, doi: 10.1016/0016-7037(96)00105-6.

Barberi, F., Bonatti, E., Marinelli, G. & Varet, J. (1974). Transverse tectonics during the split of a continent: data from the Afar rift. Tectonophysics, 23(1-2), 17-29, doi: 10.1016/0040-1951(74)90108-5.

Barberi, F. & Varet, J. (1975). Nature of the Afar crust: a discussion. In: Pilger, A. & Rösler, A. (Eds.), *Afar depression of Ethiopia*, Proceedings of an International Symposium on the Afar Region and Related Rift Problems, Bad Bergzabern, F. R. Germany, April 1–6, vol. 1, E. Schweizerbart'sche Verlagsbunchhandlung, Stuttgart, pp. 375–378.

Barberi, F. Santacroce, R. & Varet, J. (1975). Structural evolution of the Afar triple junction, In: Pilger, A. & Rösler, A. (Eds.), *Afar depression of Ethiopia*, Proceedings of an International Symposium on the Afar Region and Related Rift Problems, Bad Bergzabern, F. R. Germany, April 1–6, vol. 1, E. Schweizerbart'sche Verlagsbunchhandlung, Stuttgart, pp. 38–54.

Barrat, J. A., Jahn, B. M., Joron, J. L., Auvray, B. & Hamdi, H. (1990). Mantle heterogeneity in northeastern Africa: evidence from Nd isotopic compositions and hygromagmaphile element geochemistry of basaltic rocks from the Gulf of Tadjoura and southern Red Sea regions. Earth and Planetary Science Letters, 101(2-4), 233-247, doi: 10.1016/0012-821X(90)90156-R.

Barrat, J. A., Jahn, B. M., Fourcade, S. & Joron, J. L. (1993). Magma genesis in an ongoing rifting zone: The Tadjoura Gulf (Afar area). Geochimica et cosmochimica acta, 57(10), 2291-2302, doi: 10.1016/0016-7037(93)90570-M.

Barrat, J. A., Fourcade, S., Jahn, B. M., Cheminée, J. L. & Capdevila, R. (1998). Isotope (Sr, Nd, Pb, O) and trace-element geochemistry of volcanics from the Erta'Ale range (Ethiopia). Journal of Volcanology and Geothermal Research, 80(1-2), 85-100, doi: 10.1016/S0377-0273(97)00016-4.

Barrat, J. A., Joron, J. L., Taylor, R. N., Fourcade, S., Nesbitt, R. W. & Jahn, B. M. (2003). Geochemistry of basalts from Manda Hararo, Ethiopia: LREE-depleted basalts in Central Afar. Lithos, 69(1-2), 1-13, doi: 10.1016/S0024-4937(03)00044-6.

Bastow, I. D., Nyblade, A. A., Stuart, G. W., Rooney, T. O. & Benoit, M. H. (2008). Upper mantle seismic structure beneath the Ethiopian hot spot: Rifting at the edge of the African low-velocity anomaly. Geochemistry Geophysics Geosystems, 9(12), Q12022, doi: 10.1029/2008GC002107.

Beccaluva, L., Bianchini, G., Natali, C. & Siena, F. (2009). Continental flood basalts and mantle plumes: a case study of the Northern Ethiopian Plateau. Journal of Petrology, 50(7), 1377-1403, doi: 10.1093/petrology/egp024.

Berhe, S. M. (1986). Geologic and geochronologic constraints on the evolution of the Red

Sea-Gulf of Aden and Afar Depression. Journal of African Earth Sciences (1983), 5(2), 101-117, doi: 10.1016/0899-5362(86)90001-1.

Berhe, S. M., Desta, B., Nicoletti, M. & Teferra, M. (1987). Geology, geochronology and geodynamic implications of the Cenozoic magmatic province in W and SE Ethiopia. Journal of the Geological Society, 144(2), 213-226, doi: 10.1144/gsjgs.144.2.0213.

Blundy, J. D., Robinson, J. A. C. & Wood, B. J. (1998). Heavy REE are compatible in clinopyroxene on the spinel lherzolite solidus. Earth and Planetary Science Letters, 160(3-4), 493-504, doi: 10.1016/S0012-821X(98)00106-X.

Boccaletti, M., Mazzuoli, R., Bonini, M., Trua, T. & Abebe, B. (1999). Plio-Quaternary volcanotectonic activity in the northern sector of the Main Ethiopian Rift: relationships with oblique rifting. Journal of African Earth Sciences, 29(4), 679-698, doi: 10.1016/S0899-5362(99)00124-4.

Bonini, M., Corti, G., Innocenti, F., Manetti, P., Mazzarini, F., Abebe, T. & Pecskay, Z. (2005). Evolution of the Main Ethiopian Rift in the frame of Afar and Kenya rifts propagation. Tectonics, 24(1), TC1007, doi: 10.1029/2004TC001680.

Bosworth, W., Huchon, P. & McClay, K. (2005). The Red Sea and Gulf of Aden basins. Journal of African Earth Sciences, 43(1-3), 334-378, doi: 10.1016/j.jafrearsci.2005.07.020.

Boynton, W. V. (1983). Cosmochemistry of the rare earth elements: Meteorite studies. In: Henderson, P. (Ed.) Rare earth element geochemistry, 63–114, New York, Elsevier, doi: 10.1016/B978-0-444-42148-7.50008-3.

Chernet, T., Hart, W. K., Aronson, J. L. & Walter, R. C. (1998). New age constraints on the timing of volcanism and tectonism in the northern Main Ethiopian Rift–southern Afar transition zone (Ethiopia). Journal of Volcanology and Geothermal Research, 80(3-4), 267-280, doi: 10.1016/S0377-0273(97)00035-8.

Chiasera, B., Rooney, T. O., Girard, G., Yirgu, G., Grosfils, E., Ayalew, D., Mohr, P., Zimbelman, J. R. and Ramsey, M. S., (2018). Magmatically assisted off-rift extension—The case for broadly distributed strain accommodation. Geosphere, 14(4), 1544–1563, doi: 10.1130/GES01615.1.

Civiero, C., Hammond, J. O. S., Goes, S., Fishwick, S., Ahmed, A., Ayele, A., Doubre, C., Goitom, B., Keir, D., Kendall, J.-M., Leroy, S., Ogubazghi, G., Rümpker, G. & Stuart, G. W. (2015), Multiple mantle upwellings in the transition zone beneath the northern East-Africa Rift system from relative P-wave travel-time tomography, Geochemistry Geophysics Geosystems, 16, 2949–2968, doi: 10.1002/2015GC005948.

Conticelli, S., Sintoni, M. F., Abebe, T., Mazzarini, F., & Manetti, P. (1999). Petrology and geochemistry of ultramafic xenoliths and host lavas from the Ethiopian Volcanic

Province: An insight into the upper mantle under eastern Africa. Acta Vulcanologica, 11, 143-160.

Corti, G. (2009). Continental rift evolution: from rift initiation to incipient break-up in the Main Ethiopian Rift, East Africa. Earth-science reviews, 96(1-2), 1-53, doi: 10.1016/j.earscirev.2009.06.005.

Corti, G., Bastow, I. D., Keir, D., Pagli, C. & Baker, E. (2015), Rift-related morphology of the Afar Depression, In: P. Billi (Ed.)., Landscapes and Landforms of Ethiopia, World Geomorphological Landscapes, doi: 10.1007/978-94-017-8026-1_15, Sprinfer Science Business Media Dordrecht 2-15.

Cottrell, E. & Kelley, K. A. (2011). The oxidation state of Fe in MORB glasses and the oxygen fugacity of the upper mantle. Earth and Planetary Science Letters, 305(3-4), 270-282, doi: 10.1016/j.epsl.2011.03.014.

Coulié, E., Quidelleur, X., Gillot, P. Y., Courtillot, V., Lefèvre, J. C. & Chiesa, S. (2003). Comparative K–Ar and Ar/Ar dating of Ethiopian and Yemenite Oligocene volcanism: implications for timing and duration of the Ethiopian traps. Earth and Planetary Science Letters, 206(3-4), 477-492, doi: 10.1016/S0012-821X(02)01089-0.

Dalton, C. A., Langmuir, C. H. & Gale, A. (2014). Geophysical and geochemical evidence for deep temperature variations beneath mid-ocean ridges. Science, 344(6179), 80-83, doi: 10.1126/science.1249466.

Daoud, M. A., Maury, R. C., Barrat, J.-A., Talyor, R. N., Gall, B. L., Guillou, H., Cotton, J. & Rolet, J. (2010). A LREE-depleted component in the Afar plume: Further evidence from Quaternary Djibouti basalts, Lithos, 114(3-4), 327-336, doi: 10.1016/j.lithos.2009.09.008.

Davidson, A. & Rex, D. C. (1980). Age of volcanism and rifting in southwestern Ethiopia. Nature, 283(5748), 657, doi: 10.1038/283657a0.

Deniel, C., Vidal, P., Coulon, C., Vellutini, P. J. & Piguet, P. (1994). Temporal evolution of mantle sources during continental rifting: the volcanism of Djibouti (Afar). Journal of Geophysical Research: Solid Earth, 99(B2), 2853-2869, doi: 10.1029/93JB02576.

DePaolo, D. J. (1981). Trace element and isotopic effects of combined wallrock assimilation and fractional crystallization. Earth and Planetary Science Letters, 53(2), 189–202, doi: 10.1016/0012-821X(81)90153-9.

Dugda, M. T., Nyblade, A. A., Julia, J., Langston, C. A., Ammon, C. J. and Simiyu, S. (2005). Crustal structure in Ethiopia and Kenya from receiver function analysis: Implications for rift development in eastern Africa. Journal of Geophysical Research: Solid Earth, 110(B1), B01303, doi:10.1029/2004JB003065.

Dugda, M. T., Nyblade, A. A., & Julia, J. (2007). Thin lithosphere beneath the Ethiopian Plateau revealed by a joint inversion of Rayleigh wave group velocities and receiver functions. Journal of Geophysical Research: Solid Earth, 112(B8), B08305, doi: 10.1029/2006JB004918.

Dupré, B., Blanc, G., Boulègue, J. & Allègre, C. J. (1988). Metal remobilization at a spreading centre studied using lead isotopes. Nature, 333(6169), 165, doi: 10.1038/333165a0.

Ebinger, C. J., Yemane, T., WoldeGabriel, G., Aronson, J. L. & Walter, R. C. (1993). Late Eocene–Recent volcanism and faulting in the southern main Ethiopian rift. Journal of the Geological Society, 150(1), 99-108, doi: 10.1144/gsjgs.150.1.0099.

Ebinger, C. J. & Sleep, N. H. (1998). Cenozoic magmatism throughout east Africa resulting from impact of a single plume. Nature, 395(6704), 788-791, doi: 10.1038/27417.

Ebinger, C. J., Yemane, T., Harding, D. J., Tesfaye, S., Kelley, S. & Rex, D. C. (2000). Rift deflection, migration, and propagation: Link of the Ethiopian and Eastern rifts, Africa, Geological Society of America Bulletin, 112(2), 163-176, doi: 10.1130/0016-7606(2000)112<163:RDMAPL>2.0.CO;2.

Ebinger, C.J. & Casey, M. (2001). Continental breakup in magmatic provinces: An Ethiopian example. Geology, 29(6), 527-530, doi: 10.1130/0091-

7613(2001)029<0527:CBIMPA>2.0.CO;2.

Ellam, R. M. (1992). Lithospheric thickness as a control on basalt geochemistry. Geology, 20(2), 153-156, doi: 10.1130/0091-7613(1992)020<0153:LTAACO>2.3.CO;2.

Ferguson, D. J., Maclennan, J., Bastow, I. D., Pyle, D. M., Jones, S. M., Keir, D., Blundy, J. D., Plank, T. & Yirgu, G. (2013a). Melting during late-stage rifting in Afar is hot and deep. Nature, 499(7456), 70-73, doi: 10.1038/nature12292.

Ferguson, D. J., Calvert, A. T., Pyle, D. M., Blundy, J. D., Yigru, G. & Wright, T. J. (2013b), Constraining timescales of focused magmatic accretion and extension in the Afar crust using lava geochronology, Nature Communications, 4(1416), doi: 10.1038/ncomms2410.

Feyissa, D. H., Shinjo, R., Kitagawa, H., Meshesha D. & Nakamura, E. (2017). Petrologic and geochemical characterization of rift-related magmatism at the northernmost Main Ethiopian Rift: Implications for plume-lithosphere interaction and the evolution of rift mantle sources. Lithos, 282, 240-261, doi: 10.1016/j.lithos.2017.03.011.

Fram, M. S., Lesher, C. E. & Volpe, A. M. (1998). Mantle melting systematics: transition from continental to oceanic volcanism on the southeast Greenland margin. In Saunders, A. D., Larsen, H. C. & Wise, S. W. (Eds.), Proceedings of the Ocean Drilling Program, Scientific Results, 152, pp. 373-386, doi:

10.2973/odp.proc.sr.152.236.1998.

Furman, T. & Graham, D. (1999). Erosion of lithospheric mantle beneath the East African Rift system: geochemical evidence from the Kivu volcanic province, Lithos, 48(1–4), 237–262, doi: 10.1016/S0024-4937(99)00031-6.

Furman, T., Bryce, J. G., Karson, J. & Iotti, A. (2004). East African Rift System (EARS) plume structure: insights from Quaternary mafic lavas of Turkana, Kenya. Journal of Petrology, 45(5), 1069-1088, doi: 10.1093/petrology/egh004.

Furman, T., Bryce, J., Rooney, T., Hanan, B., Yirgu, G. & Ayalew, D. (2006a). Heads and tails: 30 million years of the Afar plume. Geological Society, London, Special Publications, 259(1), 95-119, doi: 10.1144/GSL.SP.2006.259.01.09.

Furman, T., Kaleta, K. M., Bryce, J. G., & Hanan, B. B. (2006b). Tertiary mafic lavas of Turkana, Kenya: constraints on East African plume structure and the occurrence of high-μ volcanism in Africa. Journal of Petrology, 47(6), 1221-1244, doi: 10.1093/petrology/egl009.

Furman, T. (2007). Geochemistry of East African Rift basalts: an overview. Journal of African Earth Sciences, 48(2-3), 147-160, doi: 10.1016/j.jafrearsci.2006.06.009.

Furman, T., Nelson, W. R. & Elkins-Tanton, L. T. (2016). Evolution of the East African rift: Drip magmatism, lithospheric thinning and mafic volcanism. Geochimica et

Cosmochimica Acta, 185, 418-434, doi: 10.1016/j.gca.2016.03.024.

Gasparon, M., Innocenti, F., Manetti, P., Peccerillo, A. & Tsegaye, A. (1993). Genesis of the Pliocene to Recent bimodal mafic-felsic volcanism in the Debre Zeyt area, central Ethiopia: Volcanological and geochemical constraints. Journal of African Earth Sciences (and the Middle East), 17(2), 145-165, doi: 10.1016/0899-5362(93)90032-L.

George, R., Rogers, N., & Kelley, S. (1998). Earliest magmatism in Ethiopia: Evidence for two mantle plumes in one flood basalt province. Geology, 26(10), 923-926, doi: 10.1130/0091-7613(1998)026<0923:EMIEEF>2.3.CO;2.

George, R. (1999). The petrogenesis of Plio-Pleistocene alkaline volcanic rocks from the Tosa Sucha region, Arba Minch, southern main Ethiopian rift. Acta Vulcanologica, 11, 121-131.

George, R. & Rogers, N. (2002). Plume dynamics beneath the African plate inferred from the geochemistry of the Tertiary basalts of southern Ethiopia. Contributions to Mineralogy and Petrology, 144(3), 286-304, doi: 10.1007/s00410-002-0396-z.

Giordano, F., D'Antonio, M., Civetta, L., Tonarini, S., Orsi, G., Ayalew, D., Yirgu, G., Dell'Erba, F., Di Vito, M. A. & Isaia, R. (2014). Genesis and evolution of mafic and felsic magmas at Quaternary volcanoes within the Main Ethiopian Rift: Insights from Gedemsa and Fanta'Ale complexes. Lithos, 188, 130-144, doi:

10.1016/j.lithos.2013.08.008.

Grove, T. L., Kinzler, R. J., Baker, M. B., Donnelly-Nolan, J. M. & Lesher, C. E. (1988). Assimilation of granite by basaltic magma at Burnt Lava flow, Medicine Lake volcano, northern California: decoupling of heat and mass transfer. Contributions to Mineralogy and Petrology, 99(3), 320-343, doi: 10.1007/BF00375365.

GSE (2005), Geological Map of Ethiopia, Ethiopian Ministry of Mines, Geological Survey of Ethiopia (GSE).

Hammond, J. O., Kendall, J. M., Stuart, G. W., Keir, D., Ebinger, C., Ayele, A., & Belachew, M. (2011). The nature of the crust beneath the Afar triple junction: Evidence from receiver functions. Geochemistry Geophysics Geosystems, 12(12), Q12004, doi: 10.1029/2011GC003738.

Hammond, J. O. S., Kendall, J.-M., Stuart, G. W., Ebinger, C. J., Bastow, I. D., Keir, D., Ayele, A., Belachew, M., Goitom, B., Ogubazghi, G. & Wright, T. J. (2013). Mantle upwelling and initiation of rift segmentation beneath the Afar Depression. Geology, 41(6), 635-638, doi: 10.1130/G33925.1.

Hanan, B. B. & Graham, D. W. (1996). Lead and helium isotope evidence from oceanic basalts for a common deep source of mantle plumes. Science, 272(5264), 991-995, doi: 10.1126/science.272.5264.991.

Hart, W. K., WoldeGabriel, G., Walter, R. C. & Mertzman, S. A. (1989). Basaltic volcanism in Ethiopia: constraints on continental rifting and mantle interactions. Journal of Geophysical Research: Solid Earth, 94(B6), 7731-7748, doi: 10.1029/JB094iB06p07731.

Hayward, N. J. & Ebinger, C. J. (1996). Variations in the along-axis segmentation of the Afar Rift system. Tectonics, 15(2), 244-257, doi: 10.1029/95TC02292.

Herzberg, C. & Asimow, P. D. (2015). PRIMELT3 MEGA.XLSM software for primary magma calculation: peridotite primary magma MgO contents from the liquidus to the solidus. Geochemistry Geophysics Geosystems, 16(2), 563–578, doi: 10.1002/2014GC005631.

Hofmann, C., Courtillot, V., Feraud, G., Rochette, P., Yirgu, G., Ketefo, E. & Pik, R. (1997). Timing of the Ethiopian flood basalt event and implications for plume birth and global change. Nature, 389(6653), 838-841, doi: 10.1038/39853.

Hutchison, W., Fusillo, R., Pyle, D. M., Mather, T. A., Blundy, J. D., Biggs, J., Yigru, G., Cohen, B. E., Brooker, R. A., Barford, D. N. & Calvert, A. T. (2016), A pulse of mid-Pleistocene rift volcanism in Ethiopia at the dawn of modern humans, Nature communications, 7(13192), doi: 10.1038/ncomms13192.

Irvine, T. N. J., & Baragar, W. R. A. (1971). A guide to the chemical classification of the common volcanic rocks. Canadian journal of earth sciences, 8(5), 523-548, doi: 10.1139/e71-055.

JICA (2012). The study on groundwater resources assessment in the Rift Valley lakes basin in the Federal Democratic Republic of Ethiopia. Japan International Cooperation Agency (JICA), Kokusai Kogyo, Co. Ltd. [with supplementary documents "Geological map of Konso-Yabelo area" (http://open_jicareport.jica.go.jp/pdf/12066361_06.pdf) and "Geological map of Arba Minch-Agre Marryam area" (http://open_jicareport.jica.go.jp/pdf/12066395_09.pdf)].

Johnson, K. T. (1998). Experimental determination of partition coefficients for rare earth and high-field-strength elements between clinopyroxene, garnet, and basaltic melt at high pressures. Contributions to Mineralogy and Petrology, 133(1-2), 60-68, doi: 10.1007/s004100050437.

Jones, P. W. & Rex, D. C. (1974). New dates from the Ethiopian plateau volcanics. Nature, 252(5480), 218, doi: 10.1038/252218a0.

Justin-Visentin, E., Nicoletti, M., Tolomeo, L. & Zanettin, B. (1974), Miocene and Pliocene volcanic rocks of the Addis Ababa-Bebre Berhan area (Ethiopia). Geo-petrographic and radiometric study, Bulletin Volcanologique, 38(1), 237–253, doi:

10.1007/BF02599406.

Katz, R. F., Spiegelman, M. & Langmuir, C. H. (2003). A new parameterization of hydrous mantle melting. Geochemistry Geophysics Geosystems, 4(9), 1073, doi:10.1029/2002GC000433.

Kazmin, V. (1979). Stratigraphy and correlation of Cenozoic volcanic rocks in Ethiopia. Reports of Ethiopian Institute of Geological Survey, 106, 1-26.

Kelemen, P. B., Yogodzinski, G. M. & Scholl, D. W. (2003). Along-strike variation in lavas of the Aleutian island arc: Implications for the genesis of high Mg# andesite and the continental crust. In Eiler, J. (Ed.) Inside the subduction factory, Geophysical Monograph, 138, 223-276, doi: 10.1029/138GM11.

Kendall, J. M., Stuart, G. W., Ebinger, C. J., Bastow, I. D. & Keir, D. (2005). Magma-assisted rifting in Ethiopia. Nature, 433(7022), 146-148, doi: 10.1038/nature03161.

Kidane, T., Courtillot, V., Manighetti, I., Audin, L., Lahitte, P., Quidelleur, X., Gillot, P.-Y., Gallet, Y., Carlut, J. & Haile, T. (2003), New paleomagnetic and geochronological results from Ethiopian Afar: Block rotations linked to rift overlap and propagation and determination of a ~2 Ma reference pole for stable Africa, Journal of Geophysical Research, 108(B2), 2102, doi: 10.1029/2001JB000645.

Kieffer, B., Arndt, N., Lapierre, H., Bastien, F., Bosch, D., Pecher, A., Yirgu, G., Ayalew, D., Weis, D., Jerram, D.A., Keller, F. & Meugniot, C. (2004). Flood and shield basalts from Ethiopia: magmas from the African superswell. Journal of Petrology, 45(4), 793–834, doi: 10.1093/petrology/egg112.

Keir, D., Bastow, I. D., Corti, G., Mazzarini, F. & Rooney, T. O. (2015). The origin of along-rift variations in faulting and magmatism in the Ethiopian Rift. Tectonics, 34(3), 464-477, doi: 10.1002/2014TC003698.

Kitagawa, H., Kobayashi, K., Makishima, A. & Nakamura, E. (2008). Multiple pulses of the mantle plume: evidence from Tertiary Icelandic lavas. Journal of Petrology, 49(7), 1365-1396, doi: 10.1093/petrology/egn029.

Korenaga, J. (2004). Mantle mixing and continental breakup magmatism. Earth and Planetary Science Letters, 218(3-4), 463-473, doi: 10.1016/S0012-821X(03)00674-5.

Krans, S. R., Rooney, T. O., Kappelman, J., Yirgu, G. & Ayalew, D. (2018). From initiation to termination: a petrostratigraphic tour of the Ethiopian Low-Ti Flood Basalt Province. Contributions to Mineralogy and Petrology, 173(5), 37, doi: 10.1007/s00410-018-1460-7.

Lahitte, P., Gillot, P. Y. & Courtillot, V. (2003). Silicic central volcanoes as precursors to rift propagation: the Afar case. Earth and Planetary Science Letters, 207(1-4), 103-116, doi: 10.1016/S0012-821X(02)01130-5.

Lavayssière, A., Rychert, C., Harmon, N., Keir, D., Hammond, J. O. S., Kendall, J.-M., Doubre, C. & Leroy, S. (2018), Imaging lithospheric discontinuities beneath the northern East African Rift using S-to-P receiver functions, Geochemistry Geophysics Geosystems, 19, 4048–4062, doi: 10.1029/2018GC007463.

Le Bas, M. J., Le Maitre, R. W., Streckeisen, A., Zanettin, B. & IUGS Subcommission on the Systematics of Igneous Rocks. (1986). A chemical classification of volcanic rocks based on the total alkali-silica diagram. Journal of petrology, 27(3), 745-750, doi: 10.1093/petrology/27.3.745.

Lee, C. T. A., Luffi, P., Plank, T., Dalton, H. & Leeman, W. P. (2009). Constraints on the depths and temperatures of basaltic magma generation on Earth and other terrestrial planets using new thermobarometers for mafic magmas. Earth and Planetary Science Letters, 279(1-2), 20-33, doi: 10.1016/j.epsl.2008.12.020.

Mackenzie, G. D., Thybo, H., & Maguire, P. K. H. (2005). Crustal velocity structure across the Main Ethiopian Rift: results from two-dimensional wide-angle seismic modelling. Geophysical Journal International, 162(3), 994-1006, doi: 10.1111/j.1365-246X.2005.02710.x.

Maguire, P. K. H., Keller, G. R., Klemperer, S. L., Mackenzie, G. D., Keranen, K., Harder, S., O’Reilly, B., Thybo, H., Asfaw, L., Khan, M. A. & Amha, M. (2006). Crustal structure of the northern Main Ethiopian Rift from the EAGLE controlled-source survey; a snapshot of incipient lithospheric break-up. In Yigru, G., Ebinger, C. J., & Maguire, P. K. H. (Eds.) The Afar Volcanic Province within the East African Rift System, Geological Society of London, Special Publications, 259, 269-291, doi: 10.1144/GSL.SP.2006.259.01.21.

Manighetti, I., Tapponnier, P., Gillot, P. Y., Jacques, E., Courtillot, V., Armijo, R., Ruegg, J. C. & King, G. (1998). Propagation of rifting along the Arabia - Somalia plate boundary: Into Afar. Journal of Geophysical Research: Solid Earth, 103(B3), 4947-4974, doi: 10.1029/97JB02758.

Marty, B., Pik, R. & Gezahegn, Y. (1996). Helium isotopic variations in Ethiopian plume lavas: nature of magmatic sources and limit on lower mantle contribution. Earth and Planetary Science Letters, 144(1-2), 223-237, doi: 10.1016/0012-821X(96)00158-6.

Mazzarini, F., Le Corvec, N., Isola, I. & Favalli, M. (2016), Volcanic field elongation, vent distribution, and tectonic evolution of a continental rift: The Main Ethiopian Rift example, Geosphere, 12(3), 706–720, doi: 10.1130/GES01193.1.

McDonough, W. F. & Sun, S.-s. (1995). The composition of the Earth. Chemical Geology, 120(3-4), 223-253, doi: 10.1016/0009-2541(94)00140-4.

McKenzie, D. (1984). The generation and compaction of partially molten rock. Journal of

Petrology, 25(3), 713-765, doi: 10.1093/petrology/25.3.713.

McKenzie, D. & Bickle, M. J. (1988). The volume and composition of melt generated by extension of the lithosphere, Journal of Petrology, 29(3), 625-679, doi: 10.1093/petrology/29.3.625

Meshesha, D. & Shinjo, R. (2008). Rethinking geochemical feature of the Afar and Kenya mantle plumes and geodynamic implications. Journal of Geophysical Research, 113, B09209, doi:10.1029/2007JB005549.

Meshesha, D., Shinjo, R., Matsumura, R. & Chekol, T. (2011), Metasomatized lithospheric mantle beneath Turkana depression in southern Ethiopia (the East Africa Rift): geochemical and Sr-Nd-Pb isotopic characteristics. Contributions to Mineralogy and Petrology, 162, 889–907, doi: 10.1007/s00410-011-0630-7.

Mohr, P. A. (1967). Major volcano–tectonic lineament in the Ethiopian rift system. Nature, 213(5077), 664-665, doi: 10.1038/213664a0.

Mohr, P. & Zanettin, B. (1988). The Ethiopian Flood Basalt Province. In McDougall, J. D. (Eds.) Continental Flood Basalts. Petrology and Structural Geology, vol 3. Springer, Dordrecht, pp. 63–110, doi: 10.1007/978-94-015-7805-9_3.

Morton, W. H., Rex, D. C., Mitchell, J. G. & Mohr, P. (1979). Riftward younging of volcanic units in the Addis Ababa region, Ethiopian rift valley. Nature, 280(5720), 284-288, doi: 10.1038/280284a0.

Nakamura, E., Makishima, A., Moriguti, T., Kobayashi, K., Sakaguchi, C., Yokoyama, T., Tanaka, R., Kuritani, T & Takei, H. (2003). Comprehensive geochemical analyses of small amounts (< 100 mg) of extraterrestrial samples for the analytical competition related to the sample return mission MUSES-C. The Institute of Space and Astronautical Science report. SP, 16, 49-101.

Natali, C., Beccaluva, L., Bianchini, G. & Siena, F. (2011). Rhyolites associated to Ethiopian CFB: clues for initial rifting at the Afar plume axis. Earth and Planetary Science Letters, 312(1-2), 59-68, doi: 10.1016/j.epsl.2011.09.059.

Natali, C., Beccaluva, L., Bianchini, G., Ellam, R. M., Savo, A., Siena, F. & Stuart, F. M. (2016). High-MgO lavas associated to CFB as indicators of plume-related thermochemical effects: the case of ultra-titaniferous picrite–basalt from the Northern Ethiopian–Yemeni Plateau. Gondwana Research, 34, 29-48, doi: 10.1016/j.gr.2016.02.009.

Nelson, W. R., Furman, T., van Keken, P. E., Shirey, S. B. & Hanan, B. B. (2012). Os-Hf isotopic insight into mantle plume dynamics beneath the East African Rift System. Chemical Geology, 320, 66-79, doi: 10.1016/j.chemgeo.2012.05.020.

Nyblade, A. A., Knox, R. P. & Gurrola, H. (2000). Mantle transition zone thickness beneath

Afar: implications for the origin of the Afar hotspot. Geophysical Journal International, 142(2), 615-619, doi: 10.1046/j.1365-246x.2000.00179.x.

Peccerillo, A., Barberio, M. R., Yirgu, G., Ayalew, D., Barbieri, M. & Wu, T. W. (2003). Relationships between mafic and peralkaline silicic magmatism in continental rift settings: a petrological, geochemical and isotopic study of the Gedemsa volcano, central Ethiopian rift. Journal of Petrology, 44(11), 2003-2032, doi: 10.1093/petrology/egg068.

Pik, R., Deniel, C., Coulon, C., Yirgu, G., Hofmann, C. & Ayalew, D. (1998). The northwestern Ethiopian Plateau flood basalts: classification and spatial distribution of magma types. Journal of Volcanology and Geothermal Research, 81(1-2), 91-111, doi: 10.1016/S0377-0273(97)00073-5.

Pik, R., Deniel, C., Coulon, C., Yirgu, G. & Marty, B. (1999). Isotopic and trace element signatures of Ethiopian flood basalts: evidence for plume–lithosphere interactions. Geochimica et Cosmochimica Acta, 63(15), 2263-2279, doi: 10.1016/S0016-7037(99)00141-6.

Pik, R., Marty, B. & Hilton, D. R. (2006). How many mantle plumes in Africa? The geochemical point of view. Chemical Geology, 226(3-4), 100-114, doi: 10.1016/j.chemgeo.2005.09.016.

Pinzuti, P., Humler, E., Manighetti, I. & Gaudemer, Y. (2013). Petrological constraints on melt generation beneath the Asal Rift (Djibouti) using Quaternary basalts. Geochemistry Geophysics Geosystems, 14(8), 2932-2953, doi: 10.1002/ggge.20187.

Prave, A. R., Bates, C. R., Donaldson, C. H., Toland, H., Condon, D. J., Mark, D. & Raub, T. D. (2016). Geology and geochronology of the Tana Basin, Ethiopia: LIP volcanism, super eruptions and Eocene–Oligocene environmental change. Earth and Planetary Science Letters, 443, 1-8, doi: 10.1016/j.epsl.2016.03.009.

Putirka, K. D., Perfit, M., Ryerson, F. J. & Jackson, M. G. (2007). Ambient and excess mantle temperatures, olivine thermometry, and active vs. passive upwelling. Chemical Geology, 241(3-4), 177-206, doi: 10.1016/j.chemgeo.2007.01.014.

Putirka, K. D. (2008). Thermometers and barometers for volcanic systems. In Putirka, K. D. & Tepley III, F. J. (Eds) Minerals, Inclusions and Volcanic Processes, Reviews in Mineralogy and Geochemistry, 69(1), 61-120, Mineralogical Society of America and Geochemical Society, doi: 10.2138/rmg.2008.69.3.

R Core Team (2019). R: A language and environment for statistical computing. R Foundation for Statistical Computing, Vienna, Austria (https://www.R-project.org/).

Robinson, J. A. C., Wood, B. J. & Blundy, J. D. (1998). The beginning of melting of fertile and depleted peridotite at 1.5 GPa. Earth and Planetary Science Letters, 155(1-2), 97-

111, doi: 10.1016/S0012-821X(97)00162-3.

Rochette, P., Tamrat, E., Féraud, G., Pik, R., Courtillot, V., Ketefo, E., Coulon, C., Hofmann, C., Vandamme, D. & Yirgu, G. (1998). Magnetostratigraphy and timing of the Oligocene Ethiopian traps. Earth and Planetary Science Letters, 164(3-4), 497-510, doi: 10.1016/S0012-821X(98)00241-6.

Rogers, N., Macdonald, R., Fitton, J. G., George, R., Smith, M. & Barreiro, B. (2000). Two mantle plumes beneath the East African rift system: Sr, Nd and Pb isotope evidence from Kenya Rift basalts. Earth and Planetary Science Letters, 176(3-4), 387-400, doi: 10.1016/S0012-821X(00)00012-1.

Rogers, N. W., Davies, M. K., Parkinson, I. J. & Yirgu, G. (2010). Osmium isotopes and Fe/Mn ratios in Ti-rich picritic basalts from the Ethiopian flood basalt province: No evidence for core contribution to the Afar plume. Earth and Planetary Science Letters, 296(3-4), 413-422, doi: 10.1016/j.epsl.2010.05.027.

Rooney, T. O., Furman, T., Yirgu, G. & Ayalew, D. (2005). Structure of the Ethiopian lithosphere: Xenolith evidence in the Main Ethiopian Rift. Geochimica et Cosmochimica Acta, 69(15), 3889-3910, doi: 10.1016/j.gca.2005.03.043.

Rooney, T., Furman, T., Bastow, I., Ayalew, D. & Yirgu, G. (2007). Lithospheric modification during crustal extension in the Main Ethiopian Rift. Journal of

Geophysical Research: Solid Earth, 112(B10), B10201, doi:10.1029/2006JB004916.

Rooney, T. O. (2010). Geochemical evidence of lithospheric thinning in the southern Main Ethiopian Rift. Lithos, 117(1-4), 33-48, doi: 10.1016/j.lithos.2010.02.002.

Rooney, T. O., Bastow, I. & Keir, D. (2011), Insights into extensional processes during magma assisted rifting: Evidence from aligned scoria cones, Journal of Volcanology and Geothermal Research, 201, 83–96, doi: 10.1016/j.jvolgeores.2010.07.019.

Rooney, T. O., Herzberg, C. & Bastow, I. D. (2012a). Elevated mantle temperature beneath East Africa. Geology, 40(1), 27-30, doi: 10.1130/G32382.1.

Rooney, T. O., Hanan, B. B., Graham, D. W., Furman, T., Blichert-Toft, J. & Schilling, J.-G. (2012b). Upper mantle pollution during Afar plume–continental rift interaction. Journal of Petrology, 53(2), 365-389, doi: 10.1093/petrology/egr065.

Rooney, T. O., Hart, W. K., Hall, C. M., Ayalew, D., Ghiorso, M. S., Hidalgo, P., & Yirgu, G. (2012c). Peralkaline magma evolution and the tephra record in the Ethiopian Rift. Contributions to Mineralogy and Petrology, 164(3), 407-426, doi: 10.1007/s00410-012-0744-6.

Rooney, T. O., Mohr, P., Dosso, L. & Hall, C. (2013). Geochemical evidence of mantle reservoir evolution during progressive rifting along the western Afar margin. Geochimica et Cosmochimica Acta, 102, 65-88, doi: 10.1016/j.gca.2012.08.019.

Rooney, T. O., Nelson, W. R., Dosso, L., Furman, T. & Hanan, B. (2014a). The role of continental lithosphere metasomes in the production of HIMU-like magmatism on the northeast African and Arabian plates. Geology, 42(5), 419-422, doi: 10.1130/G35216.1.

Rooney, T. O., Bastow, I., Keir, D., Mazzarini, F., Movsesian, E., Grosfils, E. B., Zimbelman, J. R., Ramsey, M. S., Ayalew, D. & Yirgu, G. (2014b), The protracted development of focused magmatic intrusion during continental rifting, Tectonics, 33, 875–897, doi: 10.1002/2013TC003514.

Rooney, T. O. (2017). The Cenozoic magmatism of East-Africa: Part I—flood basalts and pulsed magmatism. Lithos, 286, 264-301, doi: 10.1016/j.lithos.2017.05.014.

Rooney, T. O., Nelson, W. R., Ayalew, D., Hanan, B., Yirgu, G., & Kappelman, J. (2017). Melting the lithosphere: Metasomes as a source for mantle-derived magmas. Earth and Planetary Science Letters, 461, 105-118, doi: 10.1016/j.epsl.2016.12.010.

Rooney, T. O., Krans, S. R., Mège, D., Arnaud, N., Korme, T., Kappelman, J. & Yirgu, G. (2018), Constraining the magmatic plumbing system in a zoned continental flood basalt province, Geochemistry Geophysics Geosystems, 19, 3917-3944, doi: 10.1029/2018GC007724.

Rudnick, R. L. & Gao, S. (2003). Composition of the continental crust. In Heinrich D., Holland, D. & Turekian, K. K. (Eds.) Treatise on Geochemistry, 3, 659, pp. 1–64, Elsevier, doi: 10.1016/B0-08-043751-6/03016-4.

Rychert, C. A., Hammond, J. O. S., Harmon, N., Kendall, J.M., Keir, D., Ebinger, C., Bastow, I.D., Ayele, A., Belachew, M. & Stuart, G. (2012). Volcanism in the Afar Rift sustained by decompression melting with minimal plume influence. Nature Geoscience, 5(6), 406-409, doi: 10.1038/ngeo1455.

Sarafian, E., Gaetani, G. A., Hauri, E. H. & Sarafian, A. R. (2017). Experimental constraints on the damp peridotite solidus and oceanic mantle potential temperature. Science, 355(6328), 942-945, doi: 10.1126/science.aaj2165.

Scarsi, P. & Craig, H. (1996). Helium isotope ratios in Ethiopian Rift basalts. Earth and Planetary Science Letters, 144(3-4), 505-516, doi: 10.1016/S0012-821X(96)00185-9.

Schilling, J.-G., Kingsley, R. H., Hanan, B. B. & McCully, B. L. (1992). Nd-Sr-Pb isotopic variations along the Gulf of Aden: Evidence for Afar mantle plume - continental lithosphere interaction. Journal of Geophysical Research: Solid Earth, 97(B7), 10927-10966, doi: 10.1029/92JB00415.

Shinjo, R., Chekol, T., Meshesha, D., Itaya, Y. & Tatsumi, Y. (2011), Geochemistry and geochronology of the mafic lavas from the southern Ethiopia rift (the East African Rift System): assessment of models on magma sources, plume-lithosphere interaction and plume evolution, Contributions to Mineralogy and Petrology, 162, 209-230, doi: 10.1007/s00410-010-0591-2.

Siegburg, M., Gernon, T. M., Bull, J. M., Kier, D., Barfod, D. N., Taylor, R. N., Abede, B. & Ayele, A. (2018), Geological evolution of the Boset-Bercha Volcanic Complex, Main Ethiopian Rift: ^{40}Ar/^{39}Ar evidence for episodic Pleistocene to Holocene volcanism, Journal of Volcanology and Geothermal Research, 351, 115-133, doi: 10.1016/j.jvolgeores.2017.12.014.

Stab, M., Bellahsen, N., Pik, R., Quidelleur, X., Ayalew, D. & Leroy, S. (2015). Modes of rifting in magma-rich settings: Tectono-magmatic evolution of Central Afar, Tectonics, 35(1), 2-38, doi:10.1002/2015TC003893.

Stewart, K. & Rogers, N. (1996). Mantle plume and lithosphere contributions to basalts from southern Ethiopia. Earth and Planetary Science Letters, 139(1-2), 195-211, doi: 10.1016/0012-821X(96)00015-5.

Stracke, A., Zindler, A., Salters, V. J. M., McKenzie, D., Blichert-Toft, J., Albarède, F. & Grönvold, K. (2003). Theistareykir revisited. Geochemistry Geophysics Geosystems, 4(2), 8507, doi: 10.1029/2001GC000201.

Stracke, A., Hofmann, A. W., & Hart, S. R. (2005). FOZO, HIMU, and the rest of the mantle zoo. Geochemistry Geophysics Geosystems, 6(5), Q05007, doi: 10.1029/2004GC000824.

Tadesse, A. Z., Ayalew, D., Pik, R., Yigru, G. & Fontijn, K. (2019). Magmatic evolution of the Boku volcanic complex, Main Ethiopian Rift, Journal of African Earth Sciences, 149, 109-130, doi: 10.1016/j.jafrearsci.2018.08.003.

Thompson, R. N., Gibson, S. A., Dickin, A. P. & Smith, P. D. (2001). Early Cretaceous basalt and picrate dykes of the Southern Etendeka region, NW Namibia: Windows into the role of the Tristan mantle plume in Paraná–Etendeka magmatism, Journal of Petrology, 42(11), 2049–2081, doi: 10.1093/petrology/42.11.2049.

Thompson, D. A., Hammond, J. O., Kendall, J. M., Stuart, G. W., Helffrich, G. R., Keir, D., Ayele, A. & Goitom, B. (2015). Hydrous upwelling across the mantle transition zone beneath the Afar Triple Junction. Geochemistry Geophysics Geosystems, 16(3), 834–846, doi: 10.1002/2014GC005648.

Till, C. B. (2017). A review and update of mantle thermobarometry for primitive arc magmas. American Mineralogist, 102(5), 931-947, doi: 10.2138/am-2017-5783.

Ukstins, I. A., Renne, P. R., Wolfenden, E., Baker, J., Ayalew, D. & Menzies, M. (2002). Matching conjugate volcanic rifted margins: ^{40}Ar/^{39}Ar chrono-stratigraphy of pre-and syn-rift bimodal flood volcanism in Ethiopia and Yemen. Earth and Planetary Science

Letters, 198(3-4), 289-306, doi: 10.1016/S0012-821X(02)00525-3.

Varet, J. (1978). Geology of central and southern Afar (Ethiopia and Djibouti Republic), pp. 124, Centre National de la Recherche Scientifique (CNRS), Paris.

Volker, F., McColloch, M. T. & Altherr, R. (1993). Submarine basalts from the Red Sea: new Pb, Sr, and Nd isotopic data, Geophysical Research Letters, 20(10), 927-930, doi: 10.1029/93GL00050.

Volker, F. Altherr, R., Jochum, K. P. & McCulloch, M. T. (1997). Quaternary volcanic activity of the southern Red Sea: new data and assessment of models on magma sources and Afar plume-lithosphere interaction, Tectonophysics, 278(1–4), 15-29, doi: 10.1016/S0040-1951(97)00092-9.

Walter, M. J., Sisson, T. W. & Presnall, D. C. (1995). A mass proportion method for calculating melting reactions and application to melting of model upper mantle lherzolite. Earth and Planetary Science Letters, 135(1-4), 77-90, doi: 10.1016/0012-821X(95)00148-6.

Wessel, P., Smith, W. H., Scharroo, R., Luis, J. & Wobbe, F. (2013). Generic Mapping Tools: Improved version released. Eos, Transactions American Geophysical Union, 94(45), 409–410, doi: 10.1002/2013EO450001.

White, R. S., Smith, L. K., Roberts, A. W., Christie, P. A. F. & Kusznir, N. J. (2008). Lower-crustal intrusion on the North Atlantic continental margin. Nature, 452(7186), 460-464, doi: 10.1038/nature06687.

White, R. & McKenzie, D. (1989). Magmatism at rift zones: the generation of volcanic continental margins and flood basalts. Journal of Geophysical Research: Solid Earth, 94(B6), 7685-7729, doi: 10.1029/JB094iB06p07685.

Willbold, M. & Stracke, A. (2006). Trace element composition of mantle end-members: Implications for recycling of oceanic and upper and lower continental crust, Geochemistry Geophysics Geosystems, 7(4), Q04004, doi: 10.1029/2005GC001005.

Williams, F. M., Williams, M. A. J. & Aumento, F. (2004), Tensional fissures and crustal extension rates in the northern part of the Main Ethiopian Rift, Journal of African Earth Sciences, 38(2), 183-197, doi: 10.1016/j.jafrearsci.2003.10.007.

Wolde, B. (1996). Spatial and temporal variations in the compositions of upper Miocene to recent basic lavas in the northern Main Ethiopian rift: implications for the causes of Cenozoic magmatism in Ethiopia, Geologische Rundaschau, 85, 380-389, doi: 10.1007/BF02422243.

WoldeGabriel, G., Aronson, J. L. & Walter, R. C. (1990). Geology, geochronology, and rift basin development in the central sector of the Main Ethiopia Rift. Geological Society of America Bulletin, 102(4), 439-458, doi: 10.1130/0016-

7606(1990)102<0439:GGARBD>2.3.CO;2.

WoldeGabriel, G., Yemane, T., Suwa, G., White, T. & Asfaw, B. (1991). Age of volcanism and rifting in the Burji-Soyoma area, Amaro Horst, southern Main Ethiopian rift: Geo-and biochronologic data. Journal of African Earth Sciences (and the Middle East), 13(3-4), 437-447, doi: 10.1016/0899-5362(91)90107-A.

WoldeGabriel, G., Walter, R. C., Aronson, J. L. & Hart, W. K. (1992a). Geochronology and distribution of silicic volcanic rocks of Plio-Pleistocene age from the central sector of the Main Ethiopian Rift. Quaternary International, 13-14, 69-76, doi: 10.1016/1040-6182(92)90011-P.

WoldeGabriel, G., White, T., Suwa, G., Semaw, S., Beyene, Y., Asfaw, B., & Walter, R. (1992b). Kesem-Kebena: a newly discovered paleoanthropological research area in Ethiopia. Journal of Field Archaeology, 19(4), 471-493, doi: 10.2307/530428.

Wolfenden, E., Ebinger, C., Yirgu, G., Deino, A. & Ayalew, D. (2004). Evolution of the northern Main Ethiopian rift: birth of a triple junction. Earth and Planetary Science Letters, 224(1-2), 213-228, doi: 10.1016/j.epsl.2004.04.022.

Wolfenden, E., Ebinger, C., Yirgu, G., Renne, P. R. & Kelley, S. P. (2005). Evolution of a volcanic rifted margin: Southern Red Sea, Ethiopia. Geological Society of America Bulletin, 117(7-8), 846-864, doi: 10.1130/B25516.1.

Yemane, T., WoldeGabriel, G., Tesfaye, S., Berhe, S. M., Durary, S., Ebingher, C. & Kelley, S. (1999). Temporal and geochemical characteristics of Tertiary volcanic rocks and tectonic history in the southern Main Ethiopian Rift and the adjacent volcanic fields. Acta Vulcanologica, 11, 99–120.

Zanettin, B. & Justin-Visentin, E. (1974). The volcanic succession in central Ethiopia: the volcanics of the western Afar and Ethiopian rift margins. Memoirs of the Institute of Geology and Mineralogy, University of Padova, 31, 1-19.

Zanettin, B., Justin-Visentin, E. & Piccirillo, E. M. (1978). Volcanic succession, tectonics and magmatology in central Ethiopia. Atti e Memorie Accademia Patavina di Scienze Lettere ed Arti, 90(Parte II): 5–19

Zindler, A., & Hart, S. (1986). Chemical geodynamics. Annual Review of Earth and Planetary Sciences, 14(1), 493-571, doi: 10.1146/annurev.ea.14.050186.002425.

Zumbo, V., Féraud, G., Vellutini, P., Piguet, P. & Vincent, J. (1995), First $^{40}Ar/^{39}Ar$ dating on Early Pliocene to Plio-Pleistocene magmatic events of the Afar – Republic of Djibouti, Journal of Volcanology and Geothermal Research, 65(3-4), 281-295, doi: 10.1016/0377-0273(94)00107-R.

FIGURE CAPTIONS

Figure 1. Geological map of the Horn of Africa and the southwestern Arabian Peninsula showing the distribution of volcanic rocks erupted from 45 Ma to Recent (Hayward & Ebinger, 1996; Rooney, 2017). The border of low-Ti (LT) and high-Ti (HT) sub-provinces in the NW Plateau is after Pik *et al*. (1998) and that in Yemen is after Beccaluva *et al*. (2009). Abbreviations are as follows: MER, Main Ethiopian Rift; WFB, Wonji Fault Belt (a Quaternary bounding fault belt; Mohr, 1967); YTVL, Yerer-Tullu Wellel volcanotectonic lineament (a reactivated Precambrian suture zone; Abebe *et al*., 1998). The inset map shows the location of the Ethiopian volcanic province. The base maps were created using Generic Mapping Tools (Wessel *et al*., 2013).

Figure 2. Total alkali-silica (TAS) diagrams. Nomenclature of volcanic rocks after Le Bas *et al*. (1986). The alkaline-subalkaline divide is from Irvine & Baragar (1971). (a) Oligocene flood basalts from the Maychew area at the eastern margin of the NW Ethiopian Plateau in comparison with mafic rocks from the rift-bounding plateaus in Ethiopia and Yemen. The classification of Plateau mafic rocks [LT (low-Ti type), HT1 (high-Ti1) and HT2 (high-Ti2 type)] is after Pik *et al*. (1998). Data for Oligocne mafic rocks from other regions in NW Ethiopia are from Pik *et al*. (1998, 1999), Kieffer *et al*. (2004), Beccaluva *et al*. (2009), and Natali *et al*. (2011, 2016). Data for Oligicene Yemen Plateau basalts (HT1 and HT2 types;

1580 Baker *et al*., 1996b) and Miocene SW Ethiopian basalts (Wollega basalt; Ayalew *et al*., 1999;
1581 Conticelli *et al*., 1999) are shown as compositional fields enclosed by lines. Data for the
1582 Oligocene–Miocene shield volcanoes [Simien (30 Ma and 19 Ma), Choke (22 Ma), Guguftu
1583 (23 Ma), and Gerba Guracha (25–24 Ma)] are from Keiffer *et al*. (2004) and Rooney *et al*.
1584 (2014a, 2017a). (b) Mafic–intermediate rocks from the southern Main Ethiopian Rift (SMER;
1585 Miocene Getra-Kele and Quatenary Tosa-Sucha mafic rocks) in comparison with literature
1586 data for mafic rocks from the SMER and surrounding regions. Data sources are as follows:
1587 Amaro-Gamo basalts (Eocene), Yemane *et al*. (1999) and George & Rogers (2002); Getra-
1588 Kele (Miocene), George & Rogers (2002), Rooney (2010) and Shinjo *et al*. (2011); Tosa-
1589 sucha (Quaternary), Rooney (2010) and Shinjo *et al*. (2011). (c) Mafic–intermediate rocks
1590 from the central Main Ethiopian Rift (CMER) and adjacent regions, reported in the literature.
1591 Data sources: SDFZ (Silti-Debre Zeyit Fault Zone), Gasparon *et al*. (1993), Wolde (1996),
1592 Rooney *et al*. (2005) and Rooney (2010); WFB (Wonji Fault Belt), Boccaletti *et al*. (1999),
1593 Rooney *et al*. (2007), Rooney (2010), Giordana *et al*. (2014), Ayalew *et al*. (2016) and
1594 Tadesse *et al*. (2019); Akaki magmatic zone, Wolde (1996) and Rooney *et al*. (2014b);
1595 Miocene Addis Ababa basalts from the Bishoftu embayment, Wolde (1996) and Furman *et*
1596 *al*. (2006a). (d) Oligocene–Recent mafic rocks from the northern Main Ethiopian Rift
1597 (NMER) and its escarpments. Data sources for Miocene-Plio/Pleistocene rocks (Nazret

series) are from Wolde *et al*. (1996), Boccaletti *et al*. (1999), Furman *et al*. (2006a) and Ayalew *et al*. (2018). Data sources for Quaternary mafic rocks from rift floor and magmatic segments (Dofan, Fantale, Kone, Boset, enclosed by line) are from Wolde (1996), Boccaletti *et al*. (1999), Furman *et al*. (2006a), Rooney *et al*. (2012b), Giordana *et al*. (2014) and Ayalew *et al*. (2016). (e) Mafic rocks from the Afar region. The classification of Pliocene to Recent volcanic rocks (stratoid, 4–1.1 Ma; Gulf basalt, 1.1–0.6 Ma; axial range, <0.6 Ma) is after Stab *et al*. (2015). Compositional variations in the literature data are shown as fields enclosed by lines: stratoid series, Deniel *et al*., (1994) and Alene *et al*. (2017); Gulf basalts, Deniel *et al.* (1994); axial range series, Deniel *et al*. (1994), Barrat *et al*. (1998, 2003), Daoud *et al*. (2010) and Pinzuti *et al*. (2013). All data in Figs 2(a)–(e) are normalized to a 100% volatile-free basis.

Figure 3. Concentrations of SiO_2, TiO_2 and FeO^T (total Fe as FeO) in mafic volcanic rocks plotted against MgO concentration (in wt %). Sources of literature data are the same as in Fig. 2. Variations of all major element concentrations are shown in Supplementary Data Fig. S8.

Figure 4. Concentrations of Ni, Nb and Y (in ppm) in mafic volcanic rocks plotted against MgO concentration (in wt %). Sources of literature data are the same as in Fig. 2. Variations

1616 of the other trace element concentrations (Cr, Rb, Sr, Zr, La and Nd) are shown with Ni, Nb,
1617 and Yb in Supplementary Data Fig. S9.

1618

1619 **Figure 5.** Primitive mantle-normalized incompatible trace element diagrams for Ethiopian
1620 mafic volcanic rocks (MgO > 6 wt %, except for Oligocene and Miocene NMER mafic rocks
1621 and Afar axial-range series with MgO = 4–6 wt %): (a) Oligocene–Miocene mafic rocks from
1622 the rift-bounding plateaus; (b) Eocene–Quaternary mafic rocks in the SMER; (c) Oligocene–
1623 Quaternary mafic rocks in the NMER; (d) Pliocene–Quaternary mafic rocks from Afar.
1624 Element abundances of the primitive (upper) mantle (PUM) for normalization are from
1625 McDonough & Sun (1995). Data for mafic rocks from previous studies are shown for
1626 comparison: LT, HT1, and HT2 mafic rocks in the NW Ethiopian Plateau from Pik *et al.*
1627 (1998, 1999), Kieffer *et al.* (2004), Beccaluva *et al.* (2009), and Natali *et al.* (2011, 2016);
1628 HT1 and HT2 mafic rocks in the Yemen Plateau from Baker *et al.* (1996b); Wollega mafic
1629 rocks in the SW Plateau from Ayalew *et al.* (1999); Amaro and Gamo basalts in southern
1630 Ethiopia from Yemane *et al.* (1999) and George & Rogers (2002); Getra-Kele and Tosa-
1631 Sucha mafic rocks in the SMER from Yemane *et al.* (1999), George & Rogers (2002),
1632 Rooney (2010) and Shinjo *et al.* (2011); Miocene to Quaternary mafic rocks in the NMER
1633 (Nazret and Afar stratoid series) from Boccaletti *et al.* (1999), Furman *et al.* (2006a) and
1634 Ayalew *et al.* (2018); Quaternary mafic rocks in rift floor and magmatic segments along the

WFB from Wolde (1996), Boccaletti *et al*. (1999), Furman *et al*. (2006a), Rooney *et al*. (2012b) and Ayalew *et al*. (2016); Afar mafic rocks (stratoid, Gulf basalt, axial range series) from Deniel *et al*. (1994), Barrat *et al*. (1998, 2003), Daoud *et al*. (2010) and Alene *et al*. (2017).

Figure 6. Sr-Nd-Pb isotope compositions of the Ethiopian mafic volcanic rocks (MgO > 6 wt %, except for Oligocene and Miocene NMER mafic rocks and Afar axial-range series with MgO = 4–6 wt %): (a) Maychew HT1 and HT2 in comparison with the Oligocene–Miocene flood basalts in the other regions of the Ethiopian and Yemen Plateaus and the shield volcanoes on the plateaus (Baker *et al*.; 1996b ; Pik *et al*., 1998, 1999; Ayalew *et al*., 1999; Kieffer *et al*., 2004; Natali *et al*., 2011, 2016; Rooney *et al*., 2014a); (b) Miocene Getra-Kele and Quaternary Tosa-Sucha mafic rocks in comparison with the existing data sets for these rocks (George & Rogers, 2002; Rooney, 2010; Shinjo *et al*., 2011), Eocene Amaro and Gamo basalts (George & Rogers, 2002), and Miocene–Quaternary Turkana mafic rocks (Furman *et al*., 2004, 2006b). (c) Oligocene–Quaternary mafic rocks in the NMER in comparison with the existing data sets for these rocks and adjacent regions (Furman *et al*. 2006a; Rooney *et al*., 2012b; Ayalew *et al*., 2016, 2018). (d) Afar stratoid series, Gulf basalts, and axial range mafic rocks, in comparison with the existing data sets for these mafic rocks [shown by gray

colored symbols with the same shapes as the samples from this study; data sources are Deniel *et al*. (1994), Barrat *et al*. (1998, 2003), Daoud *et al*. (2010), Ayalew *et al*. (2016) and Alene *et al*. (2017)]. In all plots, the compositions of seafloor basalts from the Red Sea (Dupré *et al*., 1998; Volker *et al*., 1993, 1997) and the Gulf of Aden (West Sheba Ridge; Schilling *et al*., 1992) are shown for comparison (gray shaded fields). Literature data are normalized using reference standard materials with the values obtained in this study. The mantle end-member components of DMM, EM1, EM2, and HIMU are from Zindler & Hart (1986), and FOZO from Stracke *et al*. (2005). The end-member components postulated for the sources of the Ethiopian mafic volcanic rocks are also shown for reference [C1, C2, C3, C4, C4' and C5 from Meshesha & Shinjo (2008); PAL (Pan-African lithospheric material) from Rooney (2017)].

Figure 7. Latitudinal variations of $(K/Nb)_N$, $(La/Sm)_N$, $(Sm/Yb)_N$, $(^{87}Sr/^{86}Sr)_i$, $(^{143}Nd/^{144}Nd)_i$ and $(^{206}Pb/^{204}Pb)_i$ for mafic lavas in the MER and Afar. Subscript N denotes element abundances of samples normalized to those of primitive mantle for K/Nb (Sun & McDonough, 1989) and those of chondrite for La/Sm and Sm/Yb (Boynton, 1983). Large and small symbols denote data obtained in this study and those from the literature, respectively. Sources for literature data are the same as in Figs 2–6.

1672 **Figure 8.** Variation of MgO *versus* Ba/La and ($^{87}Sr/^{86}Sr$)$_i$ for Ethiopian volcanic rocks.
1673 Sources of literature data are the same as in Figs 2–6. The range of Ba/La ratios for MORB
1674 and OIB is from Willbold & Stracke (2006), and the range of ($^{87}Sr/^{86}Sr$)$_i$ values for Pan-
1675 African crustal materials (0.710 or higher) is from Stewart & Rogers (2002) and Shinjo *et al.*
1676 (2011).

1677

1678 **Figure 9.** Latitudinal variations in mantle potential temperature (T_p) estimated from primitive
1679 mafic rocks (MgO > 8.5 wt %) using the method of Putirka (2008): (a) Oligocene to Miocene
1680 magmatism in the rift-bounding plateaus; (b) Miocene to Quaternary magmatism in the MER.
1681 The literature data for mafic volcanic rocks used for calculation are from Gasparon *et al.*
1682 (1993), Deniel *et al.* (1994), Wolde (1996), Pik *et al.* (1998, 1999), Ayalew *et al.* (1999, 2016,
1683 2018), George & Rogers (2002), Barrat *et al.* (1998, 2003), Kieffer *et al.* (2004), Rooney *et*
1684 *al.* (2005, 2014b), Furman *et al.* (2006a), Beccaluva *et al.* (2009), Rooney (2010), Natali *et al.*
1685 (2011, 2016), Daoud *et al.* (2010), Shinjo *et al.* (2011), Alene *et al.* (2017), Tadesse *et al.*
1686 (2019); see Supplementary Data Table S4 [in which calculated compositions of primary
1687 magmas and the estimated T_p by the methods of Lee *et al.* (2009) and Herzberg & Asimow
1688 (2015) are also shown]. The T_p estimated by Rooney *et al.* (2012a) for the Oligocene Plateau
1689 mafic rocks and Miocene to Recent mafic rocks from the MER and Afar are shown for

comparison. The ambient mantle temperature of 1338 ˚C is from Cottrell & Kelley (2011), which is used for estimation of excess mantle temperature (ΔT_p).

Figure 10. Variation of $(La/Sm)_N$ and $(Dy/Yb)_N$ for Ethiopian mafic volcanic rocks (MgO > 6 wt %, except for Oligocene–Miocene NMER rocks with MgO >4 wt %). Subscript N for these ratios denotes normalization to abundances of these elements in chondrite (Boynton, 1983). Trajectories of melt composition with various extents of melting under spinel and garnet stability conditions are calculated using non-modal batch partial melting (Shaw, 1970) with the following variables: (1) primitive mantle of McDonough & Sun (1995) as the magma source; (2) source mineral modes under spinel and garnet stability conditions from Robinson *et al*. (1998) and Fram *et al*. (1998), respectively; (3) partition coefficients compiled by Kelemen *et al*. (2003). The extent of melting is shown as dots on the curves (1 to 20% in 1% increments), and the melts formed under the same melting extents in garnet and spinel stability conditions are connected by broken lines.

Figure 11. Variation of $(La/Sm)_N$ and the score of principal component 1 (PC1) for Pb-isotope correlation for Ethiopian mafic volcanic rocks (MgO > 6 wt %). The subscript N for La/Sm denotes chondrite normalization (Boynton, 1983). PC1 is calculated for the $^{206}Pb/^{204}Pb$-$^{207}Pb/^{204}Pb$-$^{208}Pb/^{204}Pb$ correlation (Supplementary Data Fig. S18), and regarded as a proxy of the contribution from the mantle end-member component C2 of Meshesha &

Shinjo (2008; see Figs 6 and 13). The negative correlation of $(La/Sm)_N$ with the score of PC1 suggests that sampling of melts from isotopically distinct end-member components is not a random process, rather it occurs systematically as a function of pressure and temperature (i.e., melting degree). Fusible and isotopically enriched C2 would have been sampled preferentially by small-degree partial melts formed at deeper levels in the mantle, and more refractory sources (C1 and C5) are dominant in melts formed by larger extent of melting at shallower depths.

Figure 12. (a) Schematic model for the generation of Oligocene flood basalts [modified after Beccaluva *et al*. (2009) and Natali *et al*. (2016) with data for Maychew mafic rocks from this study]. The Afar mantle plume impinged on the base of lithosphere. The isothermal contours are estimated from thermobarometric calculations in this study, and essentially consistent with those by Natali *et al*. (2016). The Maychew HT2 mafic rocks yield the estimate of highest pressure and temperature condition of melting among the Oligocene flood basalts, and place constraints on the mantle potential temperature of the plume core (T_p > 1500 ˚C). The Maychew HT2 rocks have a greater contribution from the C4 or C4' end-member components of Meshesha & Shinjo (2008), suggesting that this end-member component may have been distributed as streaks or blobs within the plume in the Oligocene. (b) Schematic model for the generation of magmas in the MER from Oligocene to Recent times. Along-rift

variation in crustal thickness is from Dugda *et al*. (2005). The asthenospheric mantle beneath the MER includes fusible streaks or blobs [C2 and C3 end-member components of Meshesha & Shinjo (2008)] in matrix of a refractory component [C5 of Meshesha & Shinjo (2008)]. Deep melting in the region with thicker crust (SMER and off-rift of CMER) preferentially samples melts from the C2 or C3 domains. Shallow melting in the region with thinner crust (NMER and Afar) samples melt from a refractory domain (C5). See text for a full discussion.

Table 1. Isotopic data for mafic volcanic rocks from Maychew in NW Plateau, Getra-Kele and Tosa-Sucha in SMER, NMER, and Afar

Sample	Latitude	Longitude	*Age (Ma)	$^{87}Sr/^{86}Sr$	$^{143}Nd/^{144}Nd$	$^{206}Pb/^{204}Pb$	$^{207}Pb/^{204}Pb$	$^{208}Pb/^{204}Pb$	$(^{87}Sr/^{86}Sr)_i$	$(^{143}Nd/^{144}Nd)_i$	ε_{Ndi}	$(^{206}Pb/^{204}Pb)_i$	$(^{207}Pb/^{204}Pb)_i$	$(^{208}Pb/^{204}Pb)_i$
Maychew (NW Plateau)														
HT2 basalt														
MH12A	12°47'N	39°35'E	*30*	0.703610	0.512869	19.378	15.640	39.512	0.703584	0.512847	4.86	19.255	15.635	39.334
MH12B	12°47'N	39°35'E	*30*	0.703662	0.512851	19.344	15.652	39.555	0.703607	0.512830	4.52	19.261	15.648	39.413
MH11B	12°47'N	39°35'E	*30*	0.703797	0.512912	18.319	15.568	38.610	0.703784	0.512885	5.60	18.222	15.563	38.504
MH14	12°47'N	39°35'E	*30*	0.703879	0.512984	18.812	15.564	38.552	0.703761	0.512958	7.01	18.689	15.558	38.418
MH15	12°47'N	39°35'E	*30*	0.703855	0.512964	19.034	15.593	38.929	0.703814	0.512938	6.63	18.947	15.589	38.826
TR3V23	12°50'N	39°34'E	30	0.703535	0.512912	19.257	15.614	39.256	0.703472	0.512891	5.71	19.148	15.609	39.102
MA1905	12°52'N	39°33'E	**28.3**	0.703878	0.512927	18.776	15.560	38.149	0.703831	0.512902	5.92	18.681	15.556	38.055
MA1907	12°52'N	39°33'E	*30*	0.703918	0.512930	18.939	15.570	38.452	0.703850	0.512905	5.98	18.795	15.563	38.285
BK01	12°46'N	39°31'E	**27.8**	0.703674	0.512867	19.299	15.640	39.443	0.703602	0.512846	4.84	19.216	15.637	39.311
BK02	12°46'N	39°31'E	*30*	0.703678	0.512856	19.270	15.643	39.416	0.703635	0.512834	4.60	19.204	15.640	39.285
TR1V3	12°46'N	39°31'E	*29*	0.703577	0.512916	19.379	15.655	39.608	0.703549	0.512896	5.80	19.259	15.650	39.444
TR1V38	12°46'N	39°31'E	*29*	0.703554	0.512973	18.795	15.558	38.514	0.703528	0.512947	6.81	18.726	15.554	38.414
BK07	12°50'N	39°30'E	*29*	0.704273	0.512937	18.844	15.568	38.546	0.704266	0.512912	6.12	18.747	15.564	38.432
TS06	12°52'N	39°30'E	*29*	0.703979	0.512942	19.045	15.592	38.986	0.703956	0.512915	6.19	18.929	15.586	38.848
HT1 basalt														
MA06A	12°50'N	39°34'E	**28.0**	0.705073	0.512816	18.502	15.550	38.509	0.705017	0.512791	3.73	18.445	15.547	38.428
MA08	12°50'N	39°34'E	*28*	0.704591	0.512900	18.618	15.552	38.367	0.704554	0.512875	5.38	18.557	15.549	38.294
MA01	12°50'N	39°34'E	*28*	0.703512	0.512914	18.887	15.555	38.895	0.703476	0.512889	5.62	18.784	15.550	38.772
MA02A	12°50'N	39°34'E	*28*	0.703715	0.512931	18.947	15.563	38.958	0.703700	0.512907	5.97	18.841	15.558	38.830
MA1810c	12°52'N	39°33'E	*29*	0.704209	0.512943	18.593	15.554	38.465	0.704170	0.512918	6.24	18.533	15.551	38.388
MA1810a	12°52'N	39°33'E	*29*	0.704488	0.512898	18.538	15.548	38.416	0.704426	0.512873	5.35	18.472	15.545	38.340
A3	12°52'N	39°33'E	*29*	0.703594	0.512917	18.533	15.550	38.527	0.703538	0.512891	5.71	18.433	15.546	38.414
A5	12°52'N	39°33'E	**27.9**	0.704091	0.512964	18.906	15.576	38.660	0.704069	0.512938	6.64	18.823	15.572	38.568
A2	12°52'N	39°33'E	*28*	–	–	18.602	15.554	38.211	–	–	–	18.522	15.550	38.124
MA1815	12°52'N	39°33'E	*28*	0.704100	0.512949	18.597	15.554	38.202	0.704055	0.512923	6.32	18.506	15.550	38.104
I2S3	12°52'N	39°33'E	*28*	0.703541	0.512832	18.938	15.560	38.941	0.703474	0.512807	4.03	18.846	15.555	38.848
BK10	12°46'N	39°31'E	*30*	0.703721	0.512922	18.600	15.553	38.343	0.703699	0.512896	5.80	18.511	15.549	38.240
BK06	12°50'N	39°30'E	*29*	0.704690	0.512911	–	–	–	0.704656	0.512886	5.61	–	–	–
TS03	12°52'N	39°30'E	*30*	0.704204	0.512985	–	–	–	0.704166	0.512959	7.05	–	–	–

TS12	12°52'N	39°30'E	*28*	0.703803	0.512905	18.403	15.541	38.033	0.703762	0.512880	5.47	18.334	15.537	37.963
TS13	12°52'N	39°30'E	*28*	0.704159	0.512922	18.638	15.556	38.150	0.704079	0.512897	5.81	18.560	15.552	38.076
TS16	12°52'N	39°30'E	*28*	0.704933	0.512826	18.532	15.545	38.456	0.704875	0.512801	3.92	18.472	15.543	38.380
B2	12°52'N	39°30'E	*28*	0.703566	0.512917	18.825	15.555	38.805	0.703529	0.512893	5.69	18.724	15.551	38.682
TS36	12°52'N	39°30'E	*28*	0.703878	0.512894	18.415	15.558	38.235	0.703836	0.512868	5.22	18.353	15.555	38.164
TS41	12°52'N	39°30'E	*28*	0.703813	0.512953	18.931	15.572	38.640	0.703769	0.512926	6.34	18.841	15.568	38.546
TS44	12°52'N	39°30'E	*28*	0.704065	0.512915	19.157	15.584	38.677	0.704027	0.512888	5.61	19.067	15.580	38.588
TS45	12°52'N	39°30'E	*28*	0.703766	0.512929	19.039	15.573	38.748	0.703736	0.512902	5.88	18.938	15.569	38.642
TS46	12°52'N	39°30'E	*28*	0.703994	0.513003	19.045	15.570	38.746	0.703894	0.512976	7.32	18.963	15.566	38.649
TS35	12°52'N	39°30'E	*28*	0.704244	0.512866	18.867	15.568	38.393	0.704161	0.512841	4.69	18.779	15.564	38.308
TS39	12°52'N	39°30'E	*28*	0.704065	0.512864	18.597	15.560	38.154	0.704039	0.512838	4.62	18.528	15.557	38.082
TS40	12°52'N	39°30'E	*28*	0.703956	0.512883	18.809	15.565	38.544	0.703898	0.512857	5.01	18.726	15.561	38.456
TS42	12°52'N	39°30'E	*28*	0.703828	0.512933	–	–	–	0.703771	0.512906	5.95	–	–	–
Getra-Kele (SMER)														
TD-1815	5°00'30"N	37°45'56"E	**11.0**	–	–	19.604	15.632	39.385	–	–	–	19.554	15.630	39.320
TD-1816A	5°01'11"N	37°44'47"E	*11*	0.702969	0.512895	19.662	15.632	39.422	0.702950	0.512887	5.14	19.603	15.629	39.342
TD-1816B	5°01'11"N	37°44'47"E	*11*	–	–	19.660	15.632	39.420	–	–	–	19.600	15.629	39.340
TD-1817	5°42'56"N	37°42'56"E	**11.3**	0.703012	0.512901	19.793	15.681	39.601	0.702998	0.512891	5.22	19.752	15.679	39.543
TD-1825	5°50'32"N	37°54'04"E	**10.8**	0.703075	0.512881	19.553	15.639	39.339	0.703055	0.512872	4.84	19.515	15.637	39.287
TD-1826A	5°50'32"N	37°54'04"E	**16.4**	0.703061	0.512879	19.677	15.646	39.422	0.703032	0.512868	4.89	19.613	15.643	39.330
TD-1826B	5°50'32"N	37°54'04"E	**16.4**	0.703062	0.512882	19.700	15.652	39.458	0.703032	0.512871	4.96	19.632	15.648	39.361
TD-1833	5°37'58"N	37°37'26"E	**12.2**	0.703401	0.512797	19.081	15.630	39.088	0.703378	0.512788	3.23	19.036	15.628	39.021
Tosa-Sucha (SMER)														
TD-1836	5°59'32"N	37°32'23"E	**0.58**	0.703415	0.512858	19.029	15.609	39.041	0.703414	0.512857	4.29	19.027	15.609	39.037
TD-1837A	5°59'37"N	37°32'21"E	**0.56**	0.703299	0.512878	19.250	15.625	39.225	0.703297	0.512878	4.69	19.249	15.625	39.221
TD-1838	5°58'17"N	37°35'29"E	*0.56*	0.703317	0.512867	19.142	15.622	39.148	0.703315	0.512867	4.47	19.140	15.622	39.143
TD-1839	5°58'06"N	37°36'00"E	**0.57**	0.703376	0.512851	19.103	15.618	39.123	0.703374	0.512850	4.16	19.101	15.618	39.119
TD-1841	5°58'04"N	37°39'12"E	*1.2*	0.703200	0.512826	19.933	15.660	39.728	0.703198	0.512826	3.69	19.927	15.659	39.721
TD-1842	5°57'53"N	37°39'19"E	**1.26**	0.703360	0.512867	19.523	15.638	39.412	0.703358	0.512866	4.48	19.519	15.638	39.403
NMER														
Quaternary														
DBDH-4	9°08'58"N	39°57'14"E	**0.20**	0.703949	0.512857	18.757	15.597	38.814	0.703949	0.512857	4.27	18.757	15.597	38.814
DBAG-115	9°08'22"N	39°56'14"E	**0.24**	0.703839	0.512893	18.783	15.595	38.915	0.703839	0.512893	4.98	18.782	15.595	38.914
TG-31	9°08'06"N	39°56'18"E	*0.25*	0.704536	0.512807	18.698	15.592	38.774	0.704536	0.512807	3.30	18.698	15.592	38.773

Afar Stratoid/Nazret series/Bofa/Bishoftu														
DBAG-74	9°58'35"N	40°33'59"E	**6.54**	0.703880	0.512873	18.588	15.576	38.732	0.703872	0.512868	4.64	18.577	15.575	38.712
DBZ-34	9°55'52"N	40°16'10"E	*3.0*	0.703528	0.512924	19.121	15.582	39.041	0.703524	0.512921	5.60	19.113	15.582	39.028
DBAG-77	9°58'23"N	40°11'36"E	**2.95**	0.703630	0.512915	18.647	15.574	38.762	0.703627	0.512912	5.43	18.640	15.574	38.753
DBAG-72A	9°56'26"N	40°04'24"E	**4.20**	0.703906	0.512861	18.508	15.569	38.706	0.703902	0.512857	4.38	18.500	15.569	38.695
DBAG-73	9°58'26"N	40°05'45"E	*4.2*	0.703994	0.512854	18.548	15.595	38.794	0.703991	0.512850	4.25	18.539	15.595	38.782
TG-51	9°02'27"N	40°23'32"E	**4.95**	0.704326	0.512823	18.631	15.585	38.890	0.704325	0.512819	3.65	18.626	15.585	38.883
TG-54	9°07'19"N	40°27'26"E	**5.53**	0.704457	0.512793	19.090	15.641	39.302	0.704454	0.512788	3.07	19.085	15.641	39.295
DBAG-63	9°45'20"N	40°01'51"E	**5.05**	0.703860	0.512843	18.546	15.572	38.715	0.703855	0.512839	4.04	18.534	15.572	38.700
MM-560	9°05'45"N	40°01'01"E	*2.7*	0.703960	0.512866	18.685	15.594	38.715	0.703957	0.512864	4.47	18.678	15.594	38.707
MM-534	9°01'16'N	39°33'00"E	*2.7*	0.704004	0.512779	18.452	15.586	38.540	0.704001	0.512777	2.78	18.446	15.586	38.532
MM-559B	9°01'26"N	39°33'13"E	**2.68**	0.704378	0.512799	18.446	15.546	38.572	0.704376	0.512797	3.16	18.441	15.546	38.566
TG-14	9°00'38"N	39°44'39"E	*2.7*	0.704249	0.512834	18.848	15.608	38.890	0.704248	0.512832	3.84	18.842	15.608	38.883
Tarmaber Megezez Formation														
DBZ-8	9°50'21"N	39°50'51"E	**14.7**	0.703844	0.512844	18.546	15.591	38.570	0.703827	0.512832	4.16	18.509	15.589	38.524
DH-429	9°33'21"N	39°51'40"E	**19.9**	0.706270	0.512559	17.859	15.563	38.837	0.706236	0.512542	-1.38	17.832	15.562	38.789
DH-438	9°32'51"N	39°53'33"E	*20*	0.703806	0.512864	18.681	15.597	38.715	0.703773	0.512848	4.59	18.625	15.594	38.645
TG-24B	9°15'07"N	39°42'53"E	*10*	0.704913	0.512757	18.472	15.593	38.784	0.704877	0.512749	2.42	18.451	15.592	38.755
TG-27C	9°09'44"N	39°43'14"E	*10*	0.704144	0.512818	18.928	15.611	39.022	0.704139	0.512810	3.60	18.908	15.610	38.995
TG-50	9°01'12"N	40°21'53"E	*10*	0.704451	0.512744	17.959	15.555	38.268	0.704431	0.512735	2.15	17.944	15.554	38.249
Alage basalt														
DBZ-22	9°52'51"N	39°48'55"E	**26.7**	0.705188	0.512581	17.909	15.589	38.723	0.705134	0.512559	-0.88	17.877	15.587	38.664
DBZ-30	9°57'57"N	39°51'54"E	**24.6**	0.706864	0.512588	18.624	15.636	39.486	0.706827	0.512570	-0.71	18.556	15.633	39.379
Afar														
Stratoid Series														
DHA-16	12°20'26"N	41°09'57"E	**1.18**	0.703763	0.512912	18.395	15.551	38.389	0.703762	0.512911	5.35	18.391	15.551	38.385
DHA-13	12°04'51"N	41°15'09"E	**1.25**	0.703810	0.512856	–	–	–	0.703808	0.512855	4.26	–	–	–
DHA-12	12°02'42"N	41°15'38"E	*1.3*	0.703701	0.512905	18.562	15.572	38.709	0.703700	0.512904	5.22	18.559	15.572	38.706
DHA-11	11°59'56"N	41°17'25"E	*1.3*	0.703827	0.512905	18.537	15.565	38.669	0.703826	0.512904	5.22	18.535	15.565	38.666
DHA-10	11°58'17"N	41°18'08"E	**1.32**	0.703745	0.512906	18.569	15.573	38.740	0.703739	0.512905	5.24	18.565	15.573	38.735
DHA-4	11°57'46"N	41°22'59"E	**1.65**	0.703843	0.512890	18.743	15.587	38.967	0.703841	0.512889	4.93	18.738	15.587	38.960
DHA-6A	11°55'09"N	41°33'49"E	**1.35**	0.703667	0.512894	18.614	15.566	38.803	0.703664	0.512893	5.00	18.609	15.566	38.797
DHA-31	11°53'27"N	41°38'02"E	**1.66**	0.703489	0.512923	18.669	15.566	38.820	0.703485	0.512922	5.57	18.664	15.566	38.813
DHA-34	11°53'24"N	41°39'18"E	**1.85**	0.703503	0.512911	18.989	15.566	39.034	0.703501	0.512909	5.34	18.982	15.566	39.024

DHA-36A	11°53'26"N	41°42'56"E	**2.87**	0.703510	0.512933	18.995	15.566	39.031	0.703506	0.512931	5.78	18.984	15.565	39.017
DHA-9	11°50'51"N	41°41'11"E	**1.54**	0.703656	0.512887	18.711	15.568	38.840	0.703652	0.512886	4.87	18.706	15.568	38.833
DHA-20	11°42'04"N	40°56'10"E	**1.53**	0.704100	0.512872	18.342	15.573	38.715	0.704099	0.512871	4.58	18.339	15.573	38.710
DHA-24	11°36'01"N	40°56'01"E	**2.00**	0.703573	0.512911	18.990	15.568	39.058	0.703569	0.512909	5.34	18.982	15.568	39.048
DHA-26	11°26'59"N	40°45'10"E	**2.77**	0.703280	0.512982	18.540	15.512	38.523	0.703279	0.512979	6.73	18.532	15.512	38.514
DHA-29	11°25'20"N	40°40'34"E	**4.06**	0.703582	0.512887	18.599	15.573	38.720	0.703580	0.512883	4.88	18.590	15.573	38.708
DHA-30	11°25'29"N	40°38'23"E	**2.95**	0.703503	0.512928	18.434	15.561	38.631	0.703496	0.512925	5.68	18.425	15.561	38.619
DHA-40	11°22'07"N	40°43'57"E	**3.02**	0.703326	0.512957	18.551	15.515	38.539	0.703319	0.512954	6.24	18.540	15.514	38.526
DHA-41	11°12'53"N	40°44'27"E	**2.57**	0.703261	0.512992	18.528	15.506	38.495	0.703259	0.512989	6.92	18.519	15.506	38.486
DHA-45	10°43'33"N	40°40'59"E	**4.50**	0.703556	0.512951	18.640	15.558	38.780	0.703548	0.512947	6.14	18.625	15.557	38.760
DHA-46	10°32'05"N	40°43'49"E	*4.5*	0.703625	0.512914	18.478	15.547	38.699	0.703613	0.512910	5.42	18.465	15.546	38.682
Gulf basalt														
DHA-18	11°37'56"N	41°24'32"E	**0.79**	0.703441	0.512956	18.512	15.560	38.659	0.703440	0.512955	6.21	18.510	15.560	38.657
DHA-17	11°40'04"N	41°22'40"E	*0.79*	0.703460	0.512921	18.502	15.557	38.648	0.703459	0.512920	5.53	18.501	15.557	38.646
Axial Range series														
DHA-43	11°02'08"N	41°11'08"E	*0.12*	0.703482	0.512929	–	–	–	0.703482	0.512929	5.68	–	–	–
DHA-39	11°46'27"N	41°00'22"E	*0.12*	0.703608	0.512897	18.505	15.569	38.657	0.703608	0.512897	5.05	18.505	15.569	38.657
DHA-15	12°11'42"N	40°44'51"E	*0.12*	0.703750	0.512884	18.363	15.552	38.353	0.703750	0.512884	4.80	18.363	15.552	38.353
DHA-3	11°55'30"N	41°12'32"E	*0.12*	0.703683	0.512871	18.432	15.570	38.596	0.703683	0.512871	4.55	18.432	15.570	38.596
DHA-2	11°54'37"N	41°10'46"E	*0.12*	0.703752	0.512896	–	–	–	0.703752	0.512896	5.03	–	–	–
DHA-1	11°48'21"N	41°00'58"E	**0.12**	0.703600	0.512924	18.506	15.567	38.653	0.703600	0.512924	5.58	18.506	15.567	38.653

*Age: bold, dated by K-Ar in this study; italic, inferred from K-Ar ages for the other samples from the adjacent locality or literatures.

Internal precisions ($2\sigma_m$) of $^{87}Sr/^{86}Sr$ and $^{143}Nd/^{144}Nd$ are better than 0.000010 and 0.000009, respectively.

The values are reported relative to the following values for the reference standard materials:

NIST SRM 987 $^{87}Sr/^{86}Sr$=0.710240, La Jolla $^{143}Nd/^{144}Nd$=0.511860, and NIST SRM 981 $^{206}Pb/^{204}Pb$ = 16.9424, $^{207}Pb/^{204}Pb$=15.5003 and $^{208}Pb/^{204}Pb$ = 36.7266, respectively.

Initial isotope ratios of Sr, Nd, and Pb are denoted as $(^{87}Sr/^{86}Sr)_i$, $(^{143}Nd/^{144}Nd)_i$, ε_{Ndi}, $(^{206}Pb/^{204}Pb)_i$, $(^{207}Pb/^{204}Pb)_i$, and $(^{208}Pb/^{204}Pb)_i$, respectively.

Table 2. Results of K-Ar dating for mafic volcanic rocks from NW plateau (Maychew), SMER (Getra-Kele and Tosa-Sucha), NMER and Afar

Sample	Location (section)	[K] (wt%)	[^{36}Ar] (10^{-9} ccSTP·g^{-1})	[^{40}Ar$_{rad}$] (10^{-9} ccSTP·g^{-1})	^{40}Ar/^{36}Ar	age (Ma)	air fraction (%)
NW plateau (Maychew)							
BK01	12°46' N	1.26	2.905 ± 0.049	1359 ± 23	757.7 ± 3.7	27.55 ± 0.72	38.8
(HT2, Seq. 1)	39°31' E		2.198 ± 0.047	1379 ± 23	761.5 ± 3.8	27.95 ± 0.72	38.5
	(Bekura)				mean	**27.8 ± 0.6**	
			2.45 ± 0.03	*1330 ± 23*	*839 ± 6*	*27.0 ± 0.7*	*35.3*
			2.45 ± 0.04	*1355 ± 51*	*849 ± 19*	*27.5 ± 1.2*	*34.9*
					mean	***27.2 ± 0.7***	
MA1905	12°52' N	1.16	0.729 ± 0.012	1279 ± 20	1952 ± 11	28.16 ± 0.71	14.4
(HT2, Seq. 2)	39°33' E		0.639 ± 0.011	1295 ± 21	2186 ± 22	28.52 ± 0.73	12.8
	(Aygi)				mean	**28.3 ± 0.5**	
			0.694 ± 0.018	*1245 ± 36*	*2090 ± 24*	*27.4 ± 1.0*	*14.2*
			0.694 ± 0.017	*1270 ± 39*	*2126 ± 32*	*28.0 ± 1.0*	*13.9*
					mean	***27.7 ± 0.7***	
MA1809	12°50' N	1.12	0.701 ± 0.011	1230 ± 18	1939 ± 7	28.06 ± 0.70	14.4
(HT1, Seq. 2)	39°34' E		0.608 ± 0.010	1237 ± 19	2185 ± 15	28.21 ± 0.71	12.7
	(Bolonta)				mean	**28.1 ± 0.5**	
			0.890 ± 0.017	*1219 ±28*	*1665 ± 18*	*27.8 ± 0.9*	*17.8*
			0.828 ± 0.021	*1219 ± 42*	*1768 ± 36*	*27.8 ± 1.1*	*16.7*
					mean	***27.8 ± 0.7***	
A5	12°52' N	1.20	0.560 ± 0.009	1318 ± 20	2464 ± 18	28.05 ± 0.70	11.2
(HT1, Seq. 3)	39°33' E		0.539 ± 0.009	1307 ± 21	2531 ± 16	27.82 ± 0.70	10.9
	(Aygi)				mean	**27.9 ± 0.5**	
			1.91 ± 0.02	*1266 ± 16*	*959 ± 4*	*26.9 ± 0.6*	*30.9*
			1.85 ± 0.02	*1316 ± 37*	*1008 ± 18*	*28.0 ± 1.0*	*29.4*
					mean	***27.5 ± 0.6***	
BK06	12°50' N	1.15	1.380 ± 0.024	1018 ± 16	1010 ± 15	22.64 ± 0.57	28.6
(HT1, Seq. 3)	39°30' E		1.445 ± 0.023	1029 ± 16	987.4 ± 4.5	22.88 ± 0.58	29.4
	(Debri)				mean	**22.8 ± 0.4**	
			1.24 ± 0.02	*1017 ± 20*	*1116 ± 12*	*22.6 ± 0.6*	*26.5*
			1.24 ± 0.03	*1014 ± 34*	*1134 ± 18*	*22.6 ± 0.9*	*26.1*
					mean	***22.6 ± 0.6***	

MA06A	12°50' N	1.69	0.973 ± 0.016	1862 ± 30	2121 ± 13	28.15 ± 0.71	13.4
(HT1, Seq. 4)	39°34' E		1.271 ± 0.021	1843 ± 30	1697 ± 10	27.86 ± 0.72	17.0
	(Bolonta)				mean	**28.0 ± 0.5**	
			1.67 ± 0.07	*1705 ± 80*	*1317 ± 21*	*25.8 ± 1.3*	*22.5*
			1.67 ± 0.02	*1701 ± 19*	*1315 ± 6*	*25.7 ± 0.6*	*22.5*
					mean	***25.8 ± 0.8***	
TS12	12°52' N	1.02	0.628 ± 0.010	1023 ± 16	1817 ± 10	25.64 ± 0.65	15.4
(HT1, Seq. 4)	39°30' E		0.668 ± 0.011	1031 ± 17	1749 ± 11	25.82 ± 0.66	16.1
	(Tsibet)				mean	**25.7 ± 0.5**	
			0.615 ± 0.015	*1005 ± 37*	*1930 ± 44*	*25.2 ± 1.1*	*15.3*
TS35	12°52' N	1.05	1.594 ± 0.041	890 ± 22	849.5 ± 2.2	21.68 ± 0.63	34.7
(HT1, Seq. 5)	39°30' E		1.634 ± 0.041	877 ± 22	828.7 ± 2.2	21.39 ± 0.62	35.5
	(Tsibet)		1.665 ± 0.042	887 ± 22	824.6 ± 1.8	21.62 ± 0.62	35.7
					mean	**21.6 ± 0.2**	
TS38	12°52' N	0.789	0.862 ± 0.014	879 ± 14	1267 ± 7	28.46 ± 0.72	22.5
(HT1, Seq. 6)	39°30' E		0.791 ± 0.013	866 ± 14	1336 ± 7	28.05 ± 0.71	21.3
	(Tsibet)				mean	**28.3 ± 0.6**	
			1.67 ± 0.05	*866 ± 38*	*815 ± 18*	*28.0 ± 1.3*	*36.3*
			1.67 ± 0.02	*851 ± 35*	*806 ± 20*	*27.6 ± 1.3*	*36.7*
					mean	***27.8 ± 0.9***	
TS43	12°52' N	0.370	1.004 ± 0.026	342.9 ± 8.7	635.1 ± 1.4	23.70 ± 0.70	46.4
(HT1, Seq. 6)	39°30' E		0.998 ± 0.026	345.1 ± 8.8	639.3 ± 1.9	23.85 ± 0.70	46.1
	(Tsibet)		0.961 ± 0.025	344.3 ± 8.9	649.6 ± 1.2	23.80 ± 0.70	45.3
			0.976 ± 0.025	345.2 ± 8.8	645.4 ± 1.5	23.86 ± 0.70	45.5
					mean	**23.8 ± 0.1**	
TS45	12°52' N	0.497	1.119 ± 0.018	405.4 ± 6.6	645.5 ± 2.9	20.88 ± 0.54	45.0
(HT1, Seq. 6)	39°30' E		1.153 ± 0.019	412.5 ± 6.8	641.5 ± 2.9	21.24 ± 0.55	45.3
	(Tsibet)				mean	**21.1 ± 0.4**	
			0.953 ± 0.015	*410 ± 12*	*727 ± 10*	*21.7 ± 0.7*	*40.7*
SMER							
Getra-Kele							
TD-1815	5°00'30" N	1.95	0.489 ± 0.013	837 ± 10	2008 ± 41	11.01 ± 0.25	14.7
	37°45'56" E		0.418 ± 0.008	827 ± 9	2278 ± 14	10.88 ± 0.24	13.1
			0.429 ± 0.006	836 ± 9	2247 ± 14	11.00 ± 0.25	13.2

					mean	**11.0 ± 0.1**	
TD-1817	5°42'56" N	0.765	0.656 ± 0.008	335 ± 4	806.8 ± 9.7	11.24 ± 0.26	36.7
	37°42'56" E		0.295 ± 0.004	337 ± 4	1439 ± 6.0	11.32 ± 0.25	20.6
					mean	**11.3 ± 0.2**	
TD-1825	5°50'32" N	0.789	1.35 ± 0.01	327 ± 5	538.4 ± 3.0	10.64 ± 0.26	55.0
	37°54'04" E		1.13 ± 0.01	334 ± 5	592.1 ± 4.0	10.87 ± 0.27	50.0
					mean	**10.8 ± 0.2**	
TD-1826A	5°50'32" N	1.40	0.459 ± 0.010	893 ± 9	2243 ± 15	16.33 ± 0.37	13.2
	37°54'04" E		0.587 ± 0.008	897 ± 9	1824 ± 9.0	16.40 ± 0.37	16.2
					mean	**16.4 ± 0.3**	
			0.364 ± 0.004	*841 ± 26*	*2607 ± 66*	*15.4 ± 0.6*	*11.4*
			0.364 ± 0.009	*902 ± 39*	*2774 ± 89*	*16.5 ± 0.8*	*10.7*
					mean	***16.0±0.5***	
TD-1826 B	5°50'32" N	1.37	0.959 ± 0.014	883 ± 10	1216 ± 14	16.51 ± 0.38	24.3
	37°54'04" E		0.835 ± 0.012	875 ± 10	1344 ± 17	16.37 ± 0.37	22.0
					mean	**16.4 ± 0.3**	
TD-1833	5°37'58" N	1.22	2.46 ± 0.03	591 ± 8	536.5 ± 2.0	12.39 ± 0.29	55.2
	37°37'26" E		2.38 ± 0.03	573 ± 7	537.3 ± 1.8	12.02 ± 0.28	55.1
					mean	**12.2 ± 0.3**	
Tosa-Sucha							
TD-1836	5°59'32" N	1.33	0.392 ± 0.005	28.7 ± 0.7	369.3 ± 1.0	0.55 ± 0.02	80.2
	37°32'23" E		0.340 ± 0.005	31.7 ± 1.2	389.1 ± 2.5	0.61 ± 0.03	76.1
					mean	**0.58 ± 0.03**	
TD-1837A	5°59'37" N	2.38	1.38 ± 0.02	49.8 ± 1.9	332.0 ± 0.6	0.54 ± 0.02	89.2
	37°32'21" E		1.37 ± 0.03	53 ± 11	334.9 ± 5.8	0.58 ± 0.12	88.4
					mean	**0.56 ± 0.06**	
TD-1839	5°58'06" N	2.03	0.548 ± 0.008	45.0 ± 1.5	378.0 ± 0.6	0.57± 0.02	78.3
	37°36'00" E		0.432 ± 0.011	44.7 ± 4.3	399.4 ± 7.7	0.57 ± 0.06	74.1
					mean	**0.57 ± 0.03**	
TD-1842	5°57'53" N	1.41	0.389 ± 0.005	68.1 ± 1.2	471.0 ± 2.7	1.25 ± 0.03	62.8
	37°39'19" E		0.494 ± 0.006	67.7 ± 1.5	433.1 ± 4.0	1.24 ± 0.04	68.3
			0.457 ± 0.012	69.4 ± 1.8	445.8 ± 1.7	1.27 ± 0.04	66.1
			0.332 ± 0.009	68.3 ± 1.8	497.7 ± 1.8	1.25 ± 0.04	59.0
			0.330 ± 0.009	71.2 ± 1.8	503.6 ± 3.1	1.30 ± 0.04	57.9

					mean	**1.26 ± 0.02**	
NMER							
Quaternary basalt							
DBDH-4	9°08'58" N	0.704	0.834 ± 0.014	5.4 ± 0.5	302.4 ± 0.6	0.20 ± 0.02	97.9
	39°57'14" E		0.705 ± 0.012	5.3 ± 0.4	303.6 ± 0.6	0.20 ± 0.02	97.5
					mean	**0.20 ± 0.01**	
DBAG-115	9°08'22" N	0.540	1.176 ± 0.019	5.0 ± 0.5	300.2 ± 0.4	0.24 ± 0.03	98.6
	39°56'14" E		1.175 ± 0.019	5.3 ± 0.5	300.5 ± 0.4	0.25 ± 0.03	98.5
					mean	**0.24 ± 0.02**	
Afar Stratoid/Nazret series/Bofa/Bishoftu							
DBAG-74	9°58'35" N	0.482	1.312 ± 0.022	123.3 ± 2.3	387.8±1.4	6.57 ± 0.35	75.9
	40°33'59" E		1.314 ± 0.021	122.0 ± 2.2	386.6±1.4	6.51 ± 0.34	76.1
					mean	**6.54 ± 0.25**	
DBAG-77	9°58'23" N	0.432	1.580 ± 0.025	49.8 ± 1.0	327.5 ± 0.4	2.97 ± 0.16	90.4
	40°11'36" E		1.603 ± 0.025	49.2 ± 1.0	326.7 ± 0.5	2.93 ± 0.16	90.6
					mean	**2.95 ± 0.11**	
DBAG-72A	9°56'26" N	0.347	0.902 ± 0.015	56.0 ± 1.1	357.8±0.7	4.16 ± 0.22	82.7
	40°04'24" E		0.603 ± 0.011	57.4 ± 1.0	386.7±1.3	4.25 ± 0.22	75.7
					mean	**4.20 ± 0.16**	
TG-51	9°02'27" N	0.447	1.867 ± 0.032	83.1 ± 3.2	340.2±2.0	4.79 ± 0.30	87.0
	40°23'32" E		1.866 ± 0.031	88.5 ± 4.1	343.0±2.4	5.10 ± 0.35	86.3
					mean	**4.95 ± 0.28**	
TG-54	9°07'19" N	0.606	1.012 ± 0.017	130.4 ± 2.3	420.7±1.7	5.53 ± 0.29	69.7
	40°27'26" E		1.246 ± 0.021	131.4 ± 2.4	398.9±1.6	5.57 ± 0.30	73.7
					mean	**5.53 ± 0.21**	
DBAG-63	9°45'20" N	0.521	0.958 ± 0.016	101.3 ± 1.6	398.4±0.9	5.00 ± 0.26	73.7
	40°01'51" E		0.916 ± 0.015	103.1 ± 1.7	405.1±1.1	5.11 ± 0.27	72.4
					mean	**5.05 ± 0.20**	
MM-559B	9°01'26" N	0.649	1.040 ± 0.017	66.9 ± 1.3	360.0 ± 0.8	2.65 ± 0.14	82.2
	39°33'13" E		0.823 ± 0.014	68.4 ± 1.1	375.9 ± 0.9	2.71 ± 0.14	78.1
					mean	**2.68 ± 0.10**	
Tarmaber Megezez Formation							
DBZ-8	9°50'21" N	0.893	2.452 ± 0.039	510 ± 8	501.0±0.5	14.6 ± 0.8	58.7
	39°50'51" E		2.967 ± 0.047	513 ± 8	467.0±0.5	14.7 ± 0.8	63.1

					mean	**14.7 ± 0.5**	
DH-429	9°33'21" N	0.990	1.695 ± 0.027	766 ± 12	738.2±1.3	19.8 ± 1.0	39.6
	39°51'40" E		1.669 ± 0.027	770 ± 12	747.5±1.2	19.9 ± 1.0	39.1
					mean	**19.9 ± 0.7**	
Alage basalt							
DBZ-22	9°52'51" N	0.725	1.784 ± 0.029	760 ± 12	713.7±2.8	26.8 ± 1.4	41.0
	39°48'55"		1.824 ± 0.029	757 ± 12	701.5±2.4	26.6 ± 1.4	41.7
					mean	**26.7 ± 1.0**	
DBZ-30	9°57'57" N	0.958	1.475 ± 0.024	927 ± 15	910.1±6.5	24.7 ± 1.3	32.0
	39°51'54" E		1.645 ± 0.026	921 ± 15	844.2±5.9	24.6 ± 1.3	34.6
					mean	**24.6 ± 0.9**	
Afar							
Stratoid series							
DHA-16	12°20'26" N	0.979	2.13 ± 0.03	47.2 ± 1.5	318.2 ± 0.7	1.24 ± 0.07	93.0
	41°09'57" E		2.15 ± 0.03	42.8 ± 1.2	315.9 ± 0.5	1.13 ± 0.06	93.7
					mean	**1.18 ± 0.08**	
DHA-13	12°04'51" N	0.698	2.27 ± 0.04	34.0 ± 2.9	310.9 ± 1.3	1.25 ± 0.12	95.2
	41°15'09" E		2.19 ± 0.03	34.1 ± 2.7	311.6 ± 1.3	1.26 ± 0.12	95.0
					mean	**1.25 ± 0.09**	
DHA-10	11°58'17" N	1.52	1.51 ± 0.02	80.1 ± 1.8	349.0 ± 1.0	1.36 ± 0.07	84.8
	41°18'08" E		1.41 ± 0.02	75.6 ± 1.8	349.3 ± 1.1	1.28 ± 0.07	84.7
					mean	**1.32 ± 0.06**	
DHA-4	11°57'46" N	0.556	2.18 ± 0.04	35.2 ± 2.2	312.1 ± 1.0	1.63 ± 0.13	94.8
	41°22'59" E		2.12 ± 0.03	36.2 ± 2.1	313.1 ± 1.0	1.68 ± 0.13	94.5
					mean	**1.65 ± 0.09**	
DHA-6A	11°55'09" N	0.828	2.21 ± 0.04	42.8 ± 4.1	315.3± 2.0	1.33 ± 0.14	93.9
	41°33'49" E		2.36 ± 0.04	43.9 ± 4.4	314.6 ± 2.0	1.37 ± 0.15	94.1
					mean	**1.35 ± 0.10**	
DHA-31	11°53'27" N	1.04	3.37 ± 0.05	67.2 ± 3.8	315.9 ± 1.2	1.67 ± 0.13	93.7
	41°38'02" E		3.32 ± 0.05	66.8 ± 1.2	316.1 ± 1.2	1.66 ± 0.12	93.6
					mean	**1.66 ± 0.09**	
DHA-34	11°53'24" N	0.626	1.47 ± 0.02	46.2 ± 1.9	327.3 ± 1.3	1.90 ± 0.12	90.4
	41°39'18" E		1.37 ± 0.02	43.9 ± 1.6	328.1 ± 1.2	1.81 ± 0.11	90.2

					mean	**1.85 ± 0.10**	
DHA-36A	11°53'26" N	0.463	1.87 ± 0.03	52.1 ± 1.3	333.9 ± 0.6	2.90 ± 0.16	91.4
	41°42'56" E		1.89 ± 0.03	50.9 ± 1.3	322.9 ± 0.6	2.83 ± 0.16	91.7
					mean	**2.87 ± 0.12**	
DHA-9	11°50'51" N	0.823	1.39 ± 0.02	49.2 ± 1.1	331.2 ± 0.7	1.54 ± 0.08	89.4
	41°41'11" E		1.44 ± 0.02	49.2 ± 1.1	333.0 ± 0.7	1.54 ± 0.09	89.7
					mean	**1.54 ± 0.06**	
DHA-20	11°42'04" N	0.694	1.05 ± 0.02	42.0 ± 1.2	336.1 ± 1.0	1.56 ± 0.09	88.1
	40°56'10" E		1.09 ± 0.02	40.3 ± 1.1	333.0 ± 1.1	1.49 ± 0.09	88.9
					mean	**1.53 ± 0.07**	
DHA-24	11°36'01" N	0.695	2.78 ± 0.05	53.5± 2.6	315.2 ± 0.9	1.98 ± 0.14	93.9
	40°56'01" E		2.86 ± 0.04	54.6 ± 2.6	315.1 ± 0.9	2.02 ± 0.14	93.9
					mean	**2.00 ± 0.10**	
DHA-26	11°26'59" N	0.182	1.21 ± 0.02	20.8 ± 1.2	313.1 ± 1.0	2.94 ± 0.22	94.5
	40°45'10" E		1.17 ± 0.02	18.5 ± 1.1	311.8 ± 1.0	2.61 ± 0.22	94.9
					mean	**2.77 ± 0.22**	
DHA-29	11°25'20" N	0.273	1.89 ± 0.03	41.7 ± 1.9	318.0 ± 1.0	3.93 ± 0.27	93.1
	40°40'34" E		2.02 ± 0.03	44.3 ± 2.0	318.0 ± 1.0	4.18 ± 0.28	93.1
					mean	**4.06 ± 0.23**	
DHA-30	11°25'29" N	0.617	2.92 ± 0.05	71.2 ± 3.4	320.4 ± 1.2	2.97 ± 0.21	92.4
	40°38'23" E		2.86 ± 0.05	70.0 ± 1.2	320.5 ± 1.2	2.92 ± 0.20	92.4
					mean	**2.95 ± 0.15**	
DHA-40	11°22'07" N	0.539	2.33 ± 0.04	63.9 ± 2.7	323.4 ± 1.2	3.05 ± 0.20	91.5
	40°43'57" E		2.34 ± 0.04	62.6 ± 2.7	322.7 ± 1.2	2.99 ± 0.20	91.7
					mean	**3.02 ± 0.14**	
DHA-41	11°12'53" N	0.284	1.41 ± 0.02	29.0 ± 1.3	316.6 ± 0.9	2.63 ± 0.18	93.5
	40°44'27" E		1.44 ± 0.02	27.8 ± 1.3	315.2 ± 0.9	2.52 ± 0.17	93.9
					mean	**2.57 ± 0.14**	
DHA-45	10°43'33" N	0.532	1.84 ± 0.03	64.4 ± 1.9	330.9± 1.0	4.51 ± 0.26	89.5
	40°40'59" E		1.77 ± 0.03	64.3 ± 1.9	332.2 ± 1.0	4.50 ± 0.26	89.1
					mean	**4.50 ± 0.19**	
Gulf basalt							
DHA-18	11°37'56" N	0.323	1.16 ± 0.02	8.9 ± 2.9	303.7 ± 2.5	0.71 ± 0.23	97.5
	41°24'32" E		1.10 ± 0.02	10.9 ± 2.0	305.9 ± 1.9	0.87 ± 0.17	96.8

					mean	**0.79 ± 0.16**	
Axial Range series							
DHA-1	11°48'21" N	0.827	1.76 ± 0.03	4.7 ± 1.5	298.7 ± 0.9	0.15 ± 0.05	99.1
	41°00'58" E		1.85 ± 0.03	2.7 ± 1.6	297.5 ± 0.9	0.09 ± 0.05	99.5
					mean	**0.12 ± 0.05**	

$^{40}Ar_{rad}$, radiogenic component in ^{40}Ar

Values expressed in italic are obtained by the unspiked method.

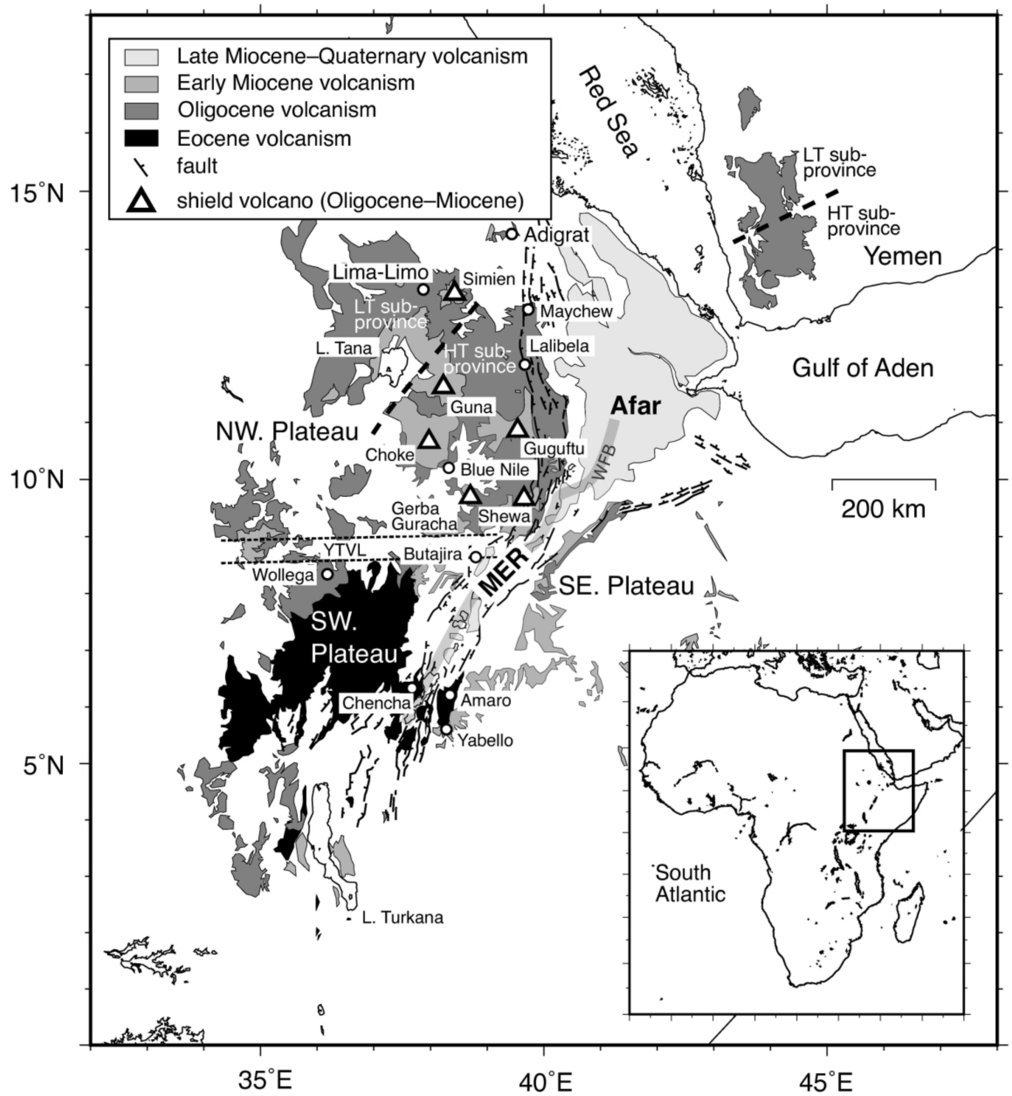

figure 1

163x178mm (300 x 300 DPI)

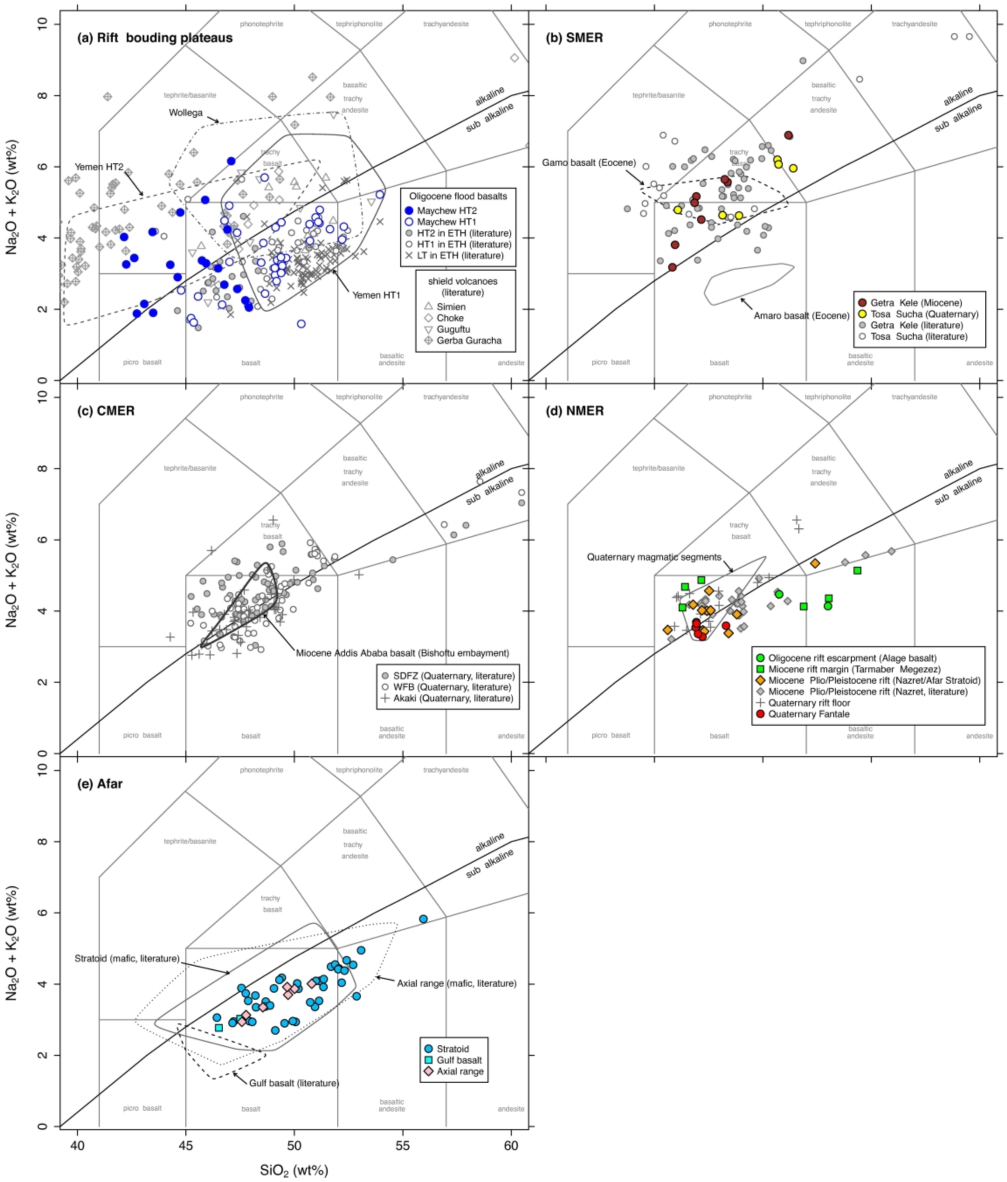

figure 2

300x352mm (300 x 300 DPI)

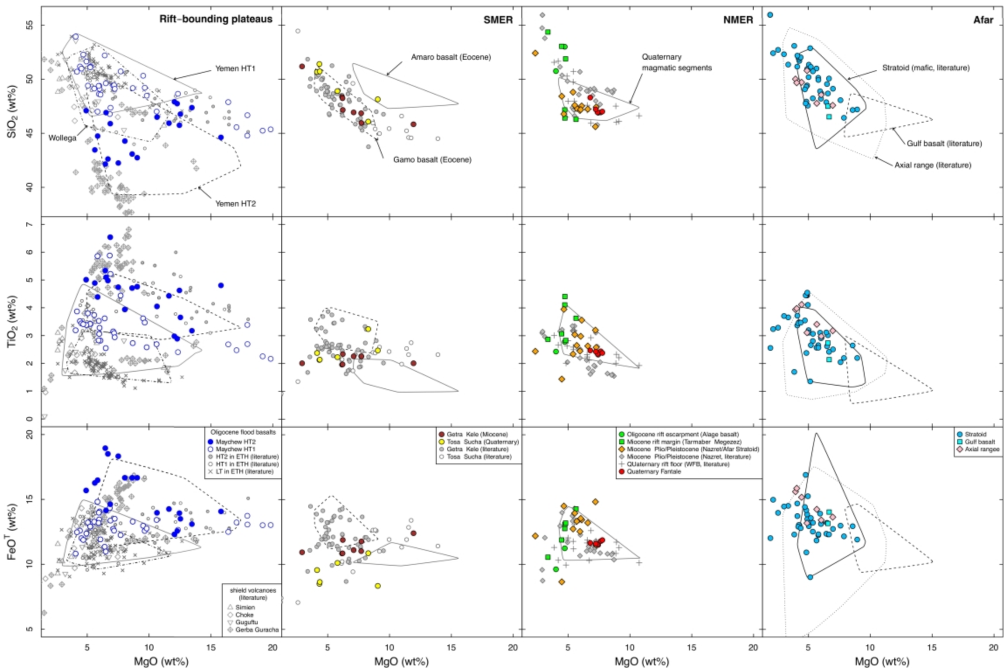

figure 3

451x299mm (300 x 300 DPI)

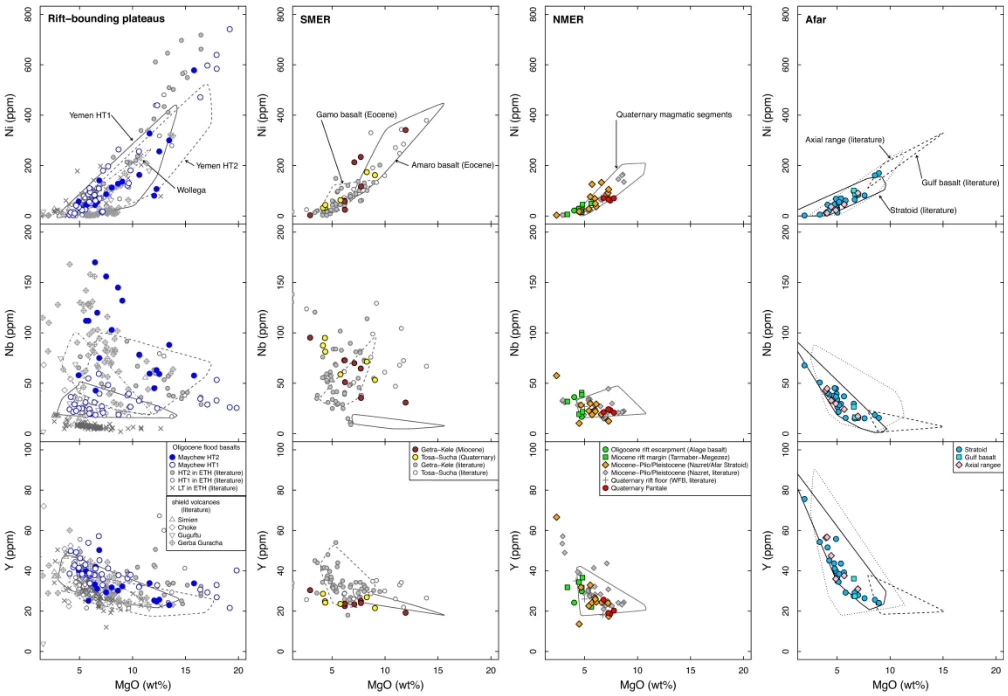

figure 4

435x299mm (300 x 300 DPI)

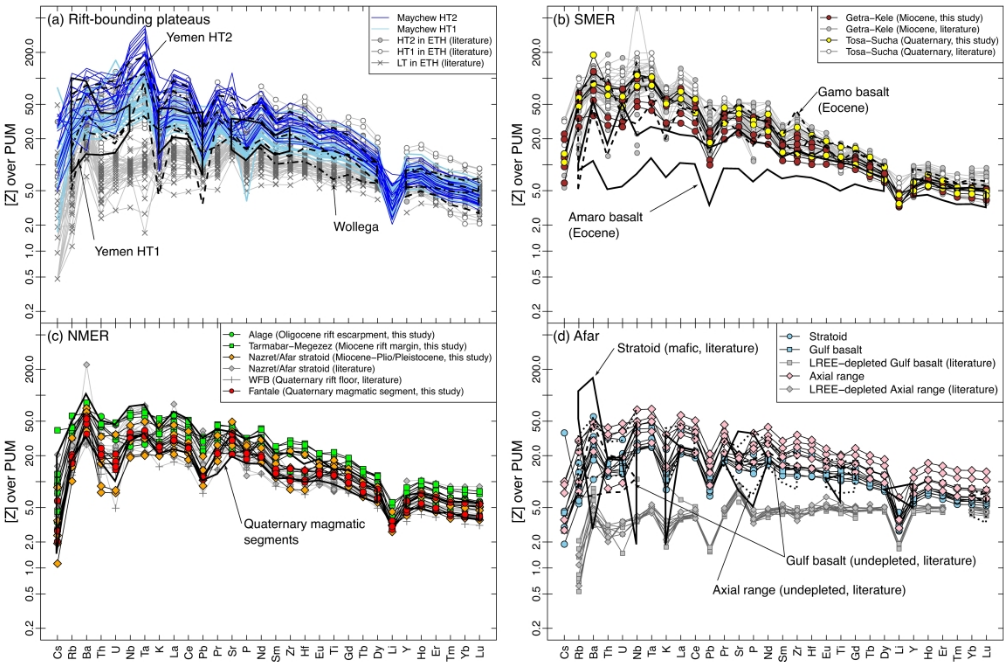

figure 5

447x293mm (300 x 300 DPI)

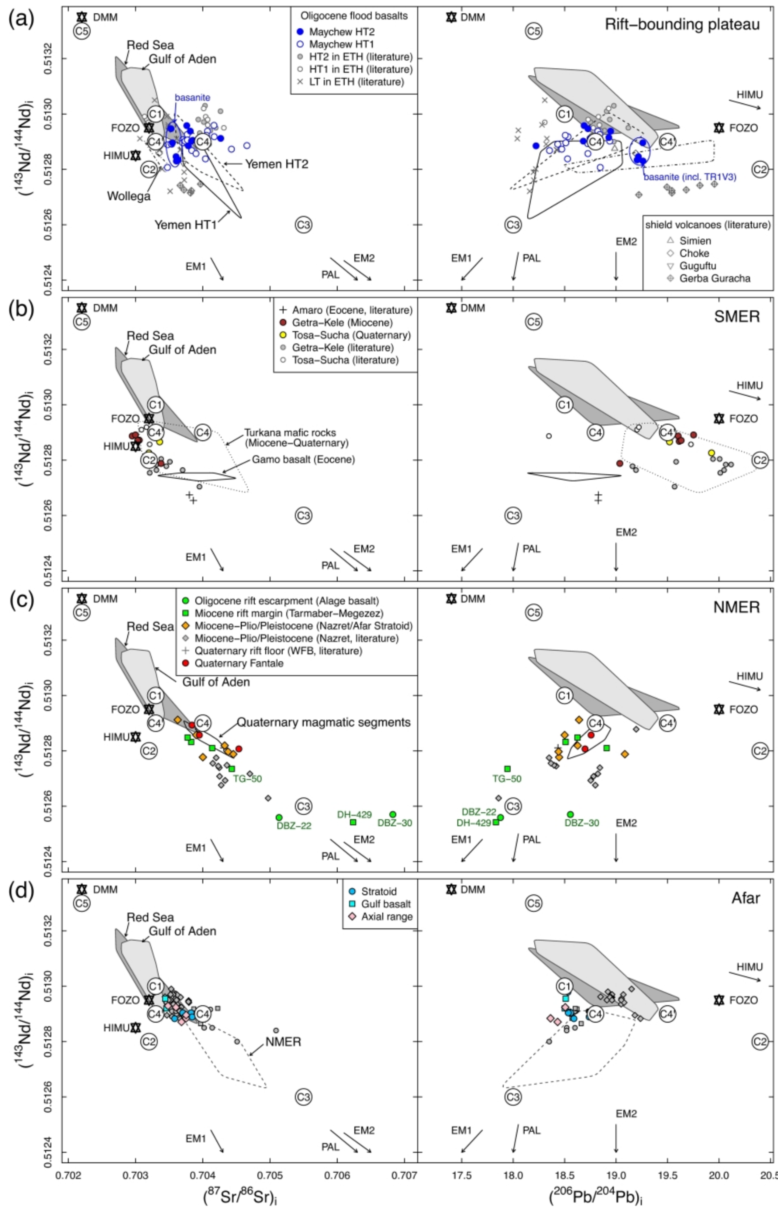

figure 6

290x451mm (300 x 300 DPI)

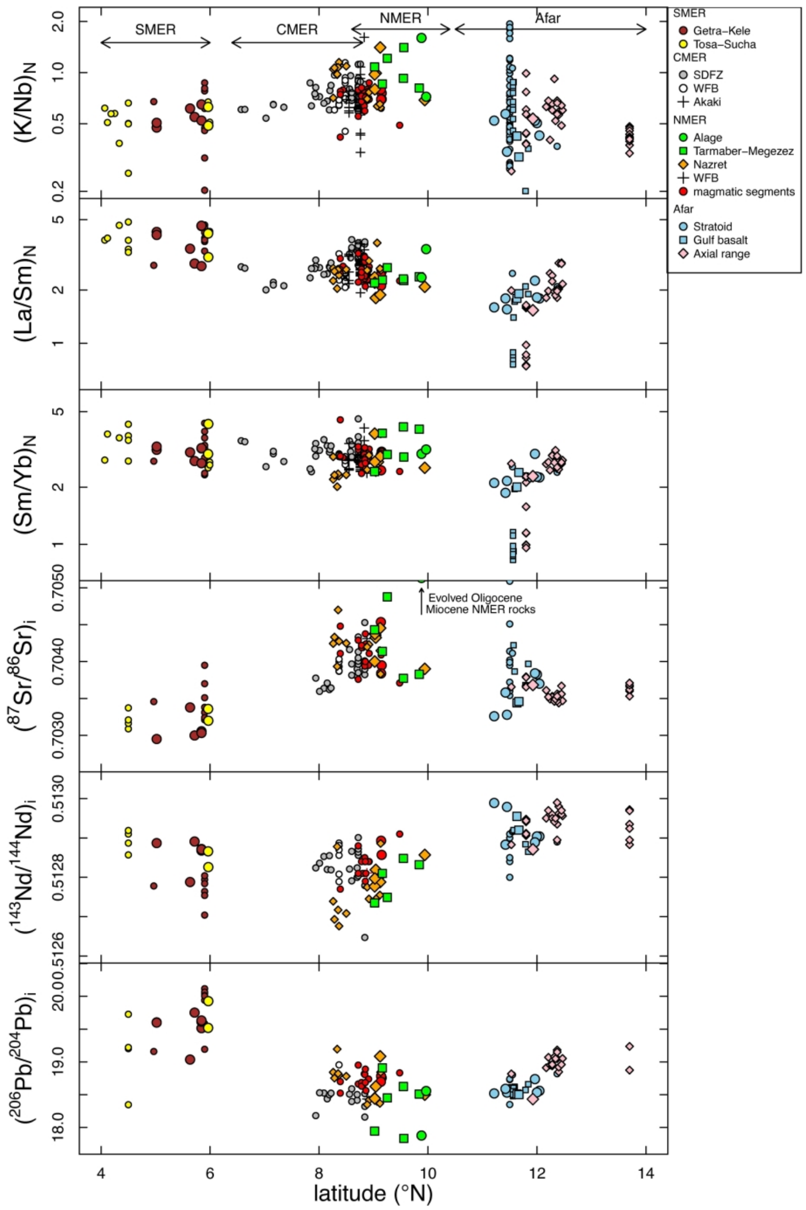

figure 7

197x298mm (300 x 300 DPI)

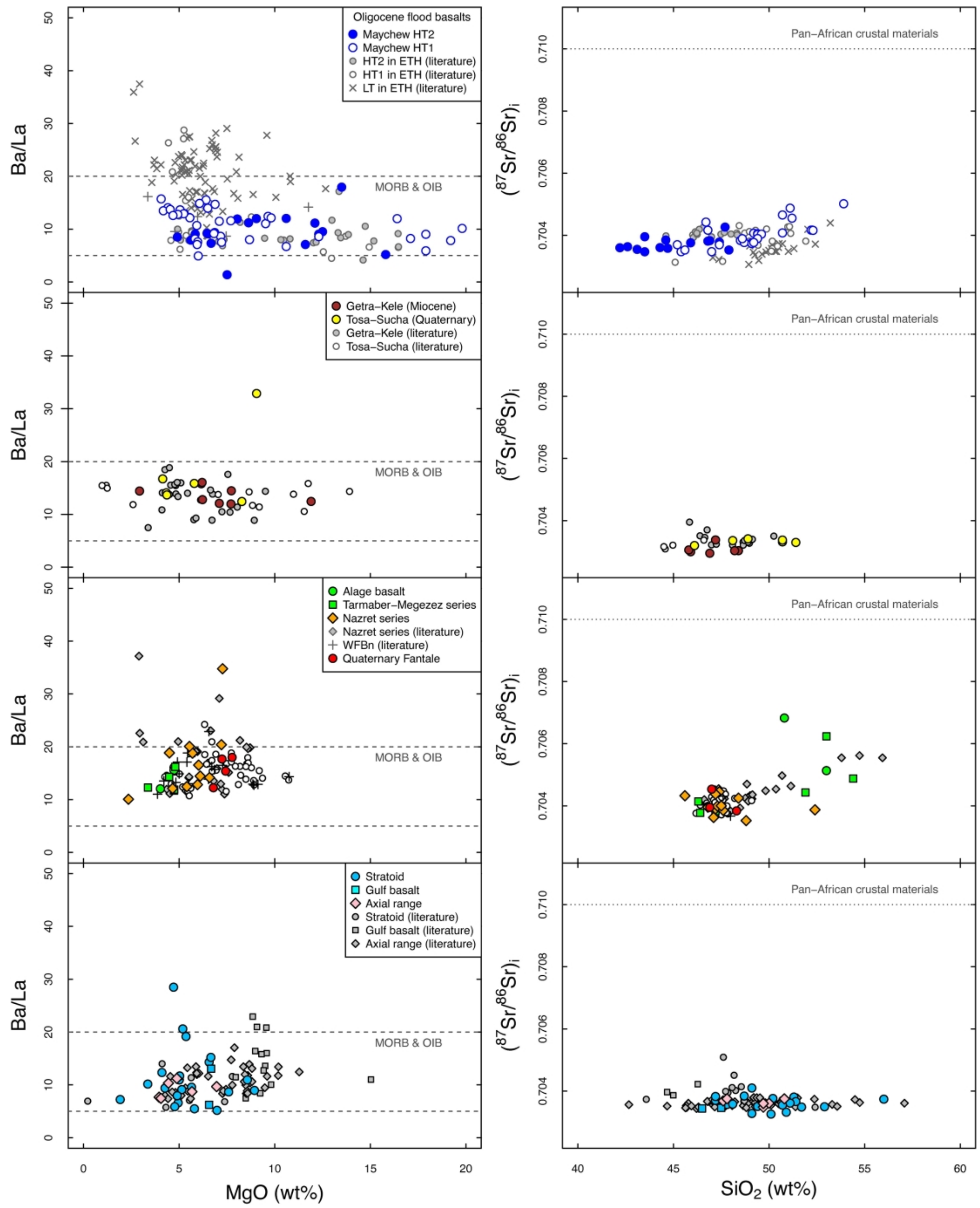

figure 8

241x299mm (300 x 300 DPI)

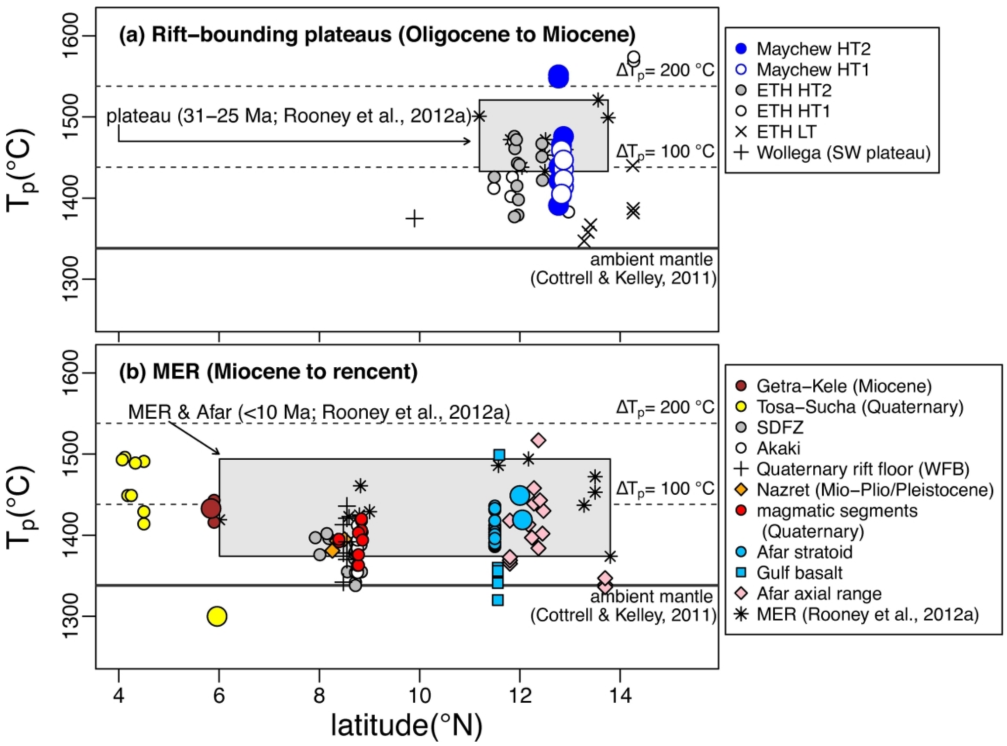

figure 9

195x144mm (300 x 300 DPI)

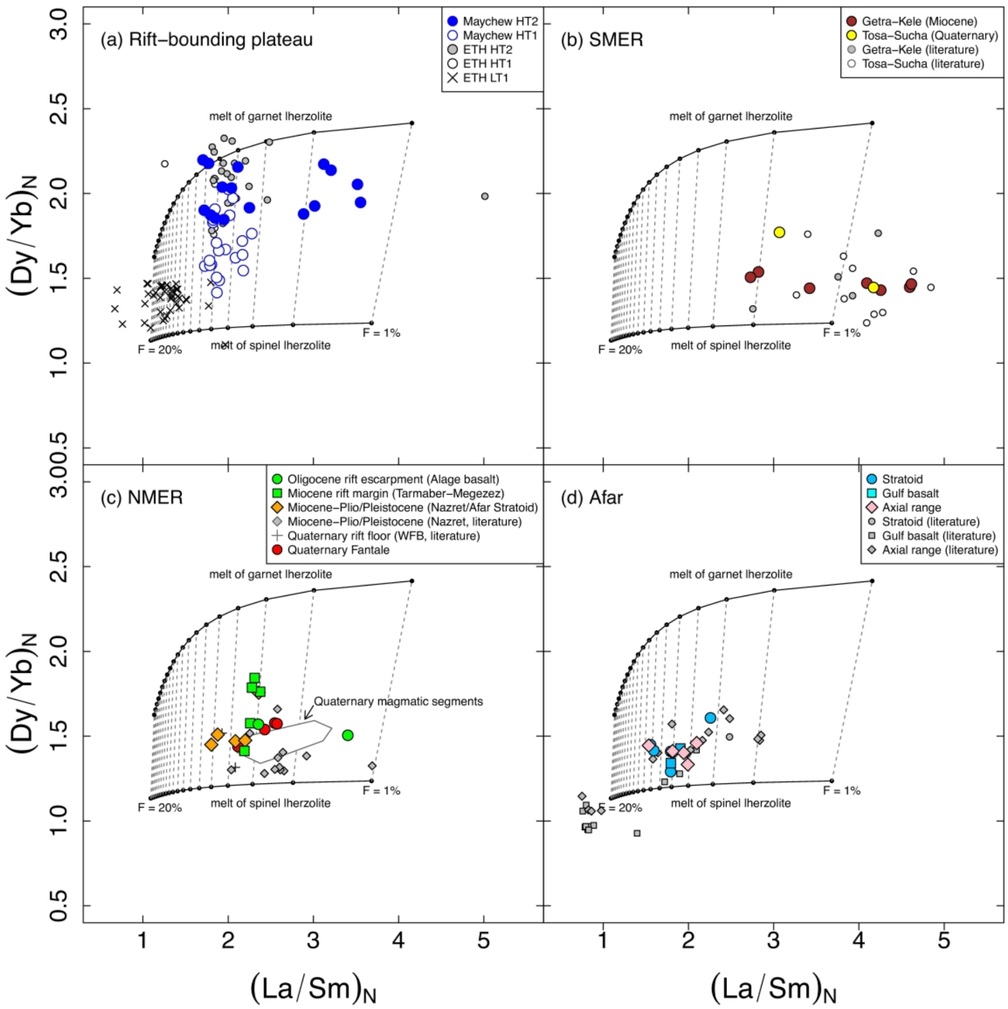

figure 10

298x298mm (300 x 300 DPI)

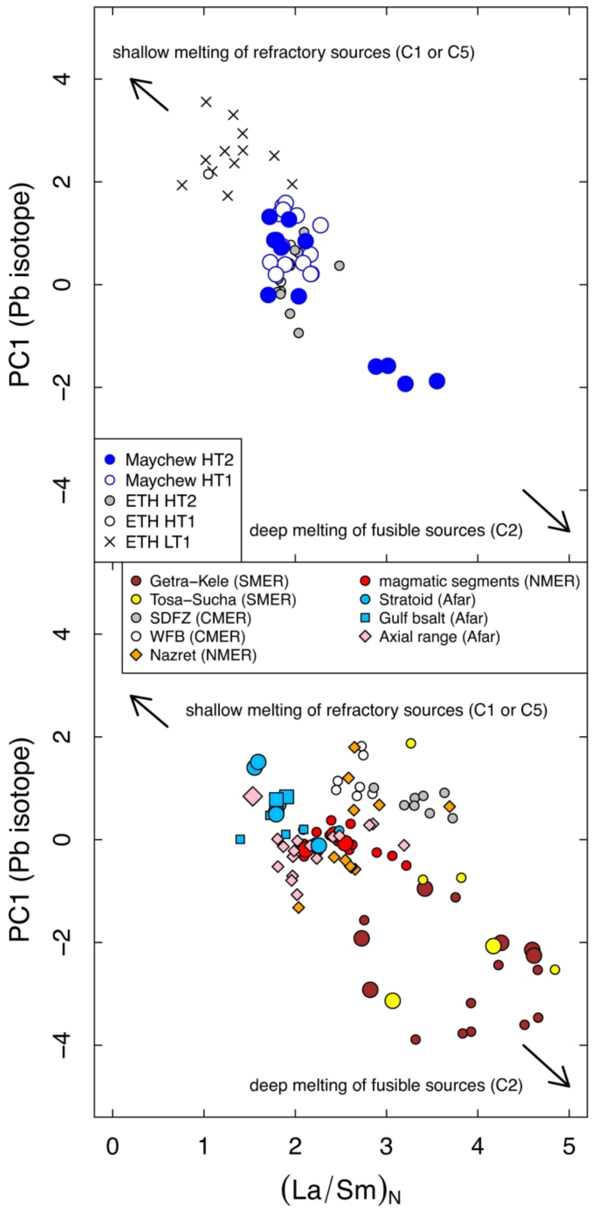

figure 11

143x296mm (300 x 300 DPI)

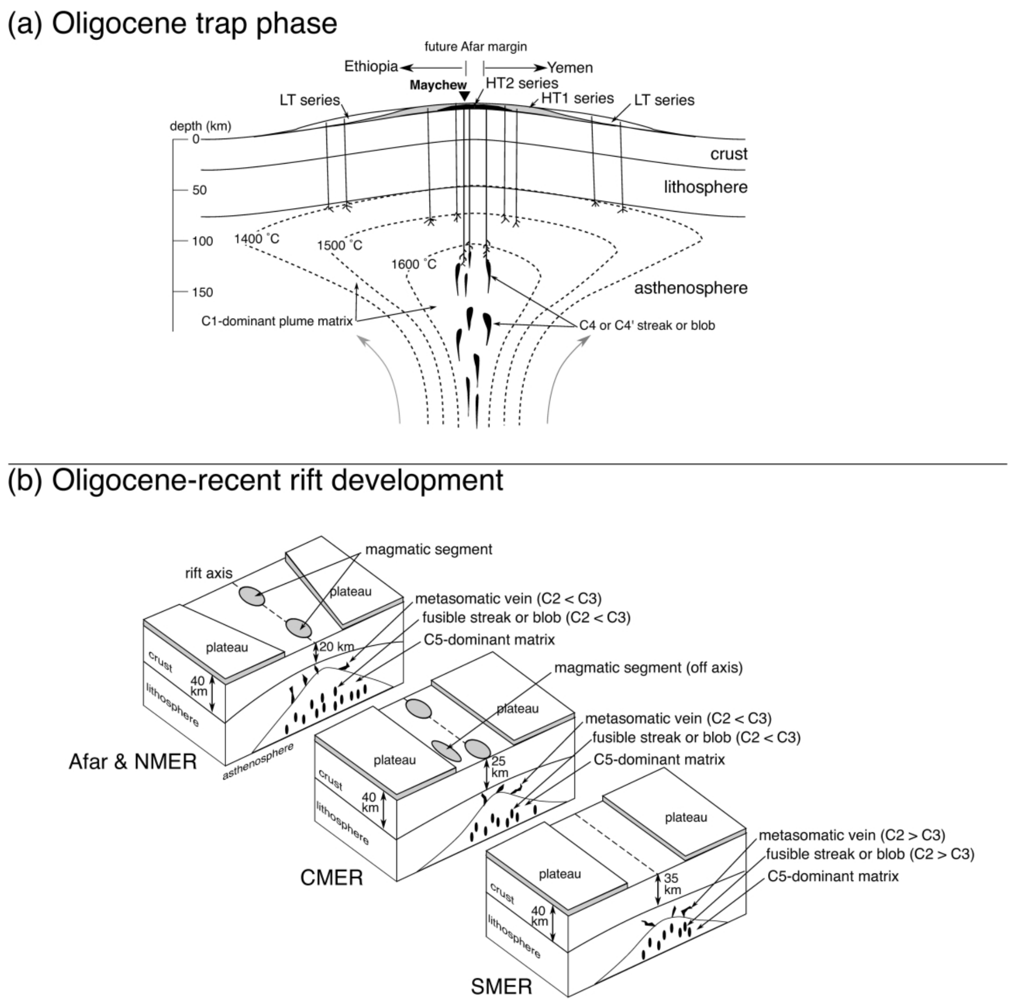

figure 12

328x324mm (300 x 300 DPI)